Investigating alveolar myofibroblasts and alveolar myofibroblast-like cells during lung development and regeneration

Inaugural Dissertation
submitted to the
Faculty of Medicine
in partial fulfillment of the requirements
for the PhD-Degree
of the Faculties of Veterinary Medicine and Medicine
of the Justus Liebig University Giessen

by

Ali Khadim
of
Lahore, Pakistan

Giessen 2025

From the Department of Medicine V and
Institute for Lung Health (ILH)
Director: Prof. Dr. Susanne Herold
Faculty of Medicine of the Justus Liebig University Giessen

First Supervisor and Committee Member: Prof. Dr. Elie El Agha
Second Supervisor and Committee Member: Prof. Dr. Reinhard Dammann
Committee Members (Chair): Prof. Dr. Christine Wrenzycki
Committee Member: Prof. Dr. William Zacharias

Date of Doctoral Defense: 30.07.2025

Ehrenwörtliche Erklärung

„Hiermit erkläre ich, dass ich die vorliegende Arbeit selbständig und ohne unzulässige Hilfe oder Benutzung anderer als der angegebenen Hilfsmittel angefertigt habe. Alle Textstellen, die wörtlich oder sinngemäß aus veröffentlichten oder nichtveröffentlichten Schriften entnommen sind, und alle Angaben, die auf mündlichen Auskünften beruhen, sind als solche kenntlich gemacht. Bei den von mir durchgeführten und in der Dissertation erwähnten Untersuchungen habe ich die Grundsätze guter wissenschaftlicher Praxis, wie sie in der „Satzung der Justus-Liebig-Universität Gießen zur Sicherung guter wissenschaftlicher Praxis“ niedergelegt sind, eingehalten sowie ethische, datenschutzrechtliche und tierschutzrechtliche Grundsätze befolgt. Ich versichere, dass Dritte von mir weder unmittelbar noch mittelbar geldwerte Leistungen für Arbeiten erhalten haben, die im Zusammenhang mit dem Inhalt der vorgelegten Dissertation stehen. Die vorgelegte Arbeit wurde weder im Inland noch im Ausland in gleicher oder ähnlicher Form einer anderen Prüfungsbehörde zum Zweck einer Promotion oder eines anderen Prüfungsverfahrens vorgelegt. Alles aus anderen Quellen und von anderen Personen übernommene Material, das in der Arbeit verwendet wurde oder auf welches direkt Bezug genommen wird, wurde als solches kenntlich gemacht. Insbesondere wurden alle Personen genannt, die direkt und indirekt an der Entstehung der vorliegenden Arbeit beteiligt waren. Mit der Überprüfung meiner Arbeit durch eine Plagiatserkennungssoftware bzw. ein internetbasiertes Softwareprogramm erkläre ich mich einverstanden.“

_____

Ali Khadim

Giessen March, 2025

Table of contents

List of figures

List of tables

Abbreviations and Acronyms

aCap… ..... Aerocytes
ACTA2… .....Actin Alpha 2, Smooth Muscle
ADAMTS4 ..... ADAM metallopeptidase with thrombospondin type 1 motif 4
AMF… ..... Alveolar myofibroblast
AF1… .....Alveolar fibroblast 1 / Lipofibroblasts
AF2… ..... Alveolar fibroblast 2 / Matrix / Adventitial fibroblasts
aMYF… ..... Activated myofibroblast
ARDS… ..... Acute respiratory distress syndrome
ASMCs… ..... Airway smooth muscle cells
AT1.. .....Type I alveolar cells
AT2.. .....Type II alveolar cells
AXIN2 .....Axis Inhibition Protein 2
BCL2 .....Apoptosis Regulator Bcl-2
BMP ..... Bone morphogenetic protein
BPD ..... Bronchopulmonary dysplasia
CD8 .....Cluster of differentiation 8
CLG ..... Compensatory lung growth
COPD ..... Chronic obstructive pulmonary disease
CSE ..... Cigarette smoke exposure
DAPI .....4',6-Diamidino-2-Phenylindole, Dihydrochloride
DASCs ..... Distal airway stem cells
DEGs ..... Differentially expressed genes
DTR ..... Diphtheria toxin receptor
DTX ..... Diphtheria toxin
ECM .....Extracellular matrix
EGF ..... Epidermal growth factor
EMT .....Epithelial-mesenchymal transition
EpiSPC .....Epithelial stem/progenitor cells
FAM ..... Fibrosis associated myofibroblasts
FGF9 .....Fibroblast growth factor 9
FGF10 .....Fibroblast growth factor 10
FGF18 .....Fibroblast growth factor 18

FGFR2b ..... Fibroblast growth factor receptor 2
FOX ..... Forkhead Box
FOX3P ..... Forkhead Box P3
FOXF1 ..... Forkhead Box F1
gCap ..... General capillary cells
GLI1 ..... Glioma-associated oncogene family zinc finger 1
GLI3 ..... Glioma-associated oncogene family zinc finger 3
GM-CSF ..... Granulocyte-macrophage colony-stimulating factor
GO ..... Gene ontology
H1N1 ..... Influenza A virus subtype H1N1
HA ..... Haemagglutinin
HGF ..... Hepatocyte growth factor
HHIP ..... Hedgehog interacting inhibitory protein
IAV ..... Influenza A virus
IDTR ..... Inducible diphtheria toxin receptor
IFNs ..... Type I interferons
IFN-γ ..... Interferon gamma
IGF ..... Insulin-like growth factor
IF ..... Immunofluorescence
IL-22 ..... Interleukin-22
ITGB4 ..... Integrin Subunit Beta 4
i.p. ..... Intraperitoneal
KGF ..... Keratinocyte growth factor
KRT5 ..... Keratin-5
LEF1 ..... Lymphoid enhancer binding factor 1
L-Nil ..... L-N6-(1-Iminoethyl)lysine
maEC ..... Macrovascular arterial endothelium
MHC II ..... Major histocompatibility complex class II
MyoFBs ..... Myofibroblasts
NA ..... Neuraminidase
OCT ..... Optimal cutting temperature
RSV ..... Respiratory syncytial virus
PAMPs ..... Pathogen-associated molecular patterns
PBS ..... Phosphate-buffered saline
PDGF ..... Platelet-derived growth factor

PDGFRα.....Platelet-derived growth factor receptor alpha
PeriFBs.....Peribronchial fibroblasts
PD-L1.....Programmed Cell Death 1 Ligand 1
PFA.....Paraformaldehyde
PNX.....Pneumonectomy
PR8.....A/Puerto Rico/8/34 H1N1
PRRs.....Pattern recognition receptors
SARS-CoV-2..... severe acute respiratory syndrome coronavirus 2
scRNA-seq.....single-cell RNA sequencing
s.c......Subcutaneous
SMCs.....Smooth muscle cells
SFTPC.....Surfactant Protein C
SHH.....Sonic hedgehog
SOX2.....SRY-Box Transcription Factor 2
ssRNA..... single stranded RNA
Tam.....Tamoxifen
TBX.....T-Box transcription factor
TH17.....T-helper 17
TGFβR2.....Transforming growth factor-beta receptor 2
TNF-α.....Tumor Necrosis Factor Alpha
TTF1.....Thyroid transcription factor 1
vRNPs.....Viral ribonucleoproteins
VSMCs…..Vascular smooth muscle cells
WNT.....Wingless-related integration site
YAP.....Yes-associated protein

1. Introduction

1.1. Lung development

The murine lung like other mammals is a highly complex, branched organ characterized by a tree-like architecture. Lung development is mediated by cellular rearrangment, pattern formation and coordinated signaling between multiple cellular compartments with much of this development being fullfiled postnataly [1–3]. The lung arises from the ventral forgut endoderm and a tightly regulated interaction between the mesenchyme and epithelium, mediated by intricate cellular communication, is essential for the proper patterning of the foregut along the proximal-distal axis [4]. The branching mechanism during lung development is initiated in the embryonic stage and is driven by a sophisticated network of signaling pathways. Central to this process are Fibroblast Growth Factor 10 (FGF10), Sonic Hedgehog (SHH), and Wingless-related integration site (WNT) signaling. FGF10, secreted by the mesenchyme, promotes epithelial cell proliferation and branching by activating its receptor FGFR2b on the epithelial cells [5,6]. SHH, produced by the epithelium, functions as a morphogen that regulates the growth and patterning of the

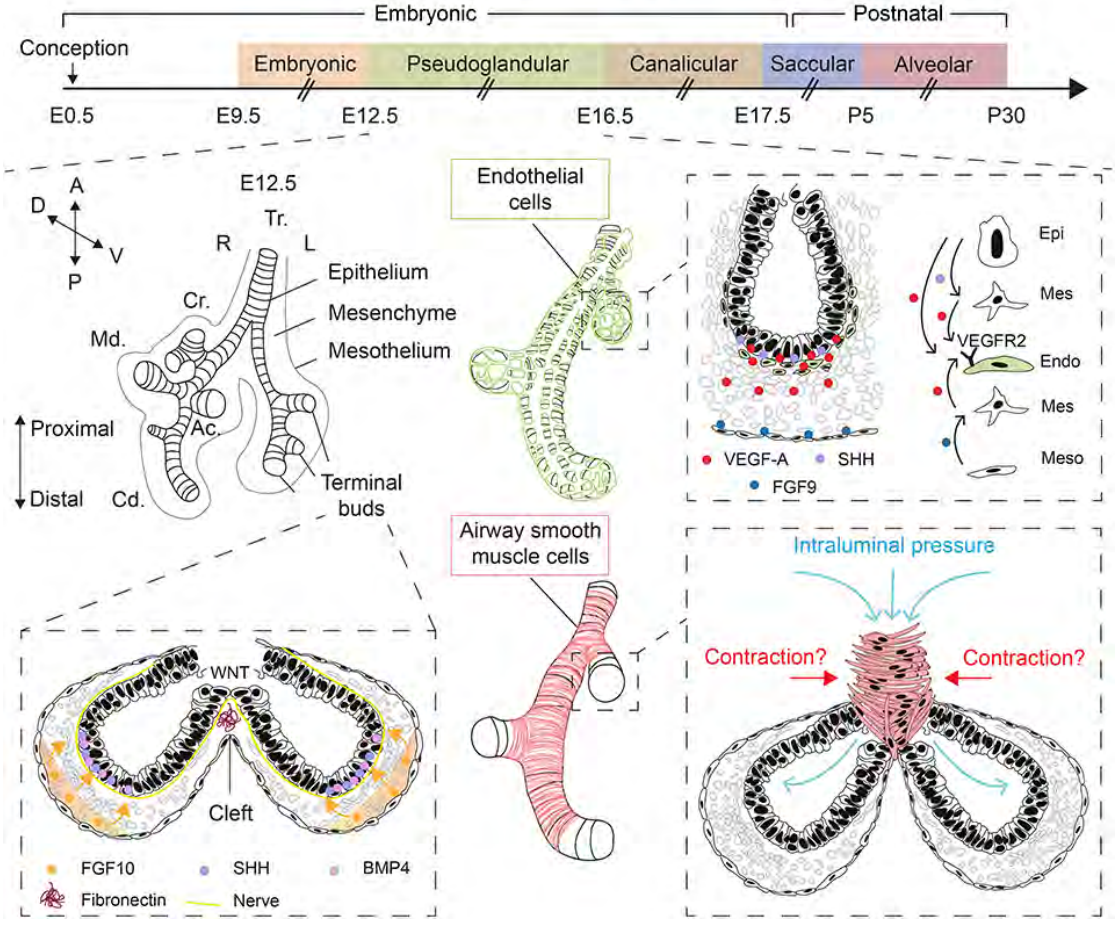

Timeline of murine lung development [1]

surrounding mesenchyme by modulating the expression of downstream targets in the mesenchymal compartment [7]. The WNT signaling pathway, encompassing both canonical and non-canonical routes, influences cell fate decisions and maintains the balance between epithelial proliferation and differentiation. Canonical WNT signaling, through β-catenin, impacts the transcription of genes involved in cell growth and patterning, while non-canonical WNT pathways affect cellular orientation and movement [8]. The interplay among these signaling pathways ensures the precise regulation of lung branching morphogenesis and the establishment of a functional respiratory architecture in parallel to the progression of lung development.

1.1.1. Stages of lung development

At embryonic day 8.5 (E8.5), the initiation of lung development is marked by the expression of NK2 homeobox 1 (*Nkx2.1*), a transcription factor essential for the specification of the foregut endoderm along the ventral anterior axis [9]. *Nkx2.1* orchestrates the early differentiation of endodermal epithelial cells into lung progenitor cells. Following the differentiation of germ layers and gastrulation, the initial endodermal tube that will eventually give rise to the anterior and posterior foregut is formed. By E9.5, primary bronchi formation is evident, and the specification of the endoderm is further influenced by signaling factors from the adjacent mesenchyme. The commitment of cells to the endoderm lineage relies on the expression of transcription factors such as FOX, GLI, WNT, BMP, TBX, and FGF family members playing pivotal roles in regulating cell proliferation and differentiation [10–14]. By E11.5, extensive branching of the conducting airways results in the formation of secondary and tertiary bronchi. Concurrently, at this stage cartilage formation provides structural support, and the development of terminal bronchioles is underway [15]. Paracrine signaling from the mesenchyme induces further differentiation of epithelial cells, preparing them for more specialized functions [16].

As shown above in the murine lung development timeline, the pseudoglandular stage occurring from E12.5 to E16.5, is characterized by the development of a complex network of airways and the formation of a initial lung buds [17,18]. During this stage, epithelial cells differentiate further into ciliated and secretory cells, while the

mesenchyme bound *Fgf10*, expressed in the distal mesoderm, regulates lung development by promoting epithelial cell proliferation and branching morphogenesis through interaction with *Fgfr2b*, possibly via various downstream signaling pathways such as WNT ligand/Frizzled 2 receptor signaling and HIPPO/YAP signaling, which regulates myosin light chain kinase activity, creating mechanical forces influencing cell shape required for branching morphogenesis [19,20].

It is also worth noting that *Fgf10* expression is negatively regulated by transforming growth factor-beta receptor 2 (*Tgfβr2*) signaling in the mesoderm and retinoic acid (RA), which is more prevalent proximally [21]. Additionally, *Fgf9*, produced in both the mesothelium and epithelium, stimulates *Fgf10*-expressing mesenchymal cell proliferation and inhibits bone morphogenetic protein 4 (BMP4) and noggin in response to Sonic Hedgehog (SHH) signaling [22]. *Shh* enhances mesenchymal proliferation and *Bmp4* expression while suppressing *Fgf10* and increasing the expression of the Hedgehog-interacting inhibitory protein (*Hhip*). The partial rescue of the *Shh*-null lung phenotype by *Gli3* deletion indicates that the repressor form of *Gli3* modulates mesenchymal proliferation and *Foxf1* expression [23]. Although *Wnt7b* promotes mesodermal proliferation through *Axin2* and *Lef1*, loss of Wnt2 leads to significant lung hypoplasia due to decreased cell proliferation [24,25]. The effects of BMP signaling on cellular responses are influenced by ligand levels, signaling interactions, and cell types, indicating its multifaceted roles in lung development and postnatal maturation [26].

The canalicular and saccular stages, spanning from E16.5 to postnatal day 4 (P4), constitute a critical period in lung development characterized by the formation of respiratory bronchioles and the differentiation of epithelial cells into type I and type II alveolar epithelial cells (AT1 and AT2). Type I alveolar epithelial cells, which are thin and specialized for efficient gas exchange, and AT2, which secrete surfactant to reduce surface tension within the alveoli, are both vital for establishing functional respiration [27,28]. During this stage, the mesenchyme undergoes significant vascularization, with the development of a complex pulmonary capillary network that is essential for effective gas exchange [29]. Key regulatory genes such as *Sftpb* and *Sftpc* drive surfactant production, while VEGF is crucial for vascular development in the developing lung [30]. The structural maturation of the lung includes the formation

of alveolar sacs, which are precursors for mature alveoli, facilitated by interactions between epithelial cells expressing *Nkx2-1* and *Sox2* and mesenchymal cells. The transition from the canalicular to the saccular stage of lung development is characterized by ongoing and refined epithelial-mesenchymal interactions that are crucial for the proper maturation of the lung. During this period, the terminal (acinar) airways undergo significant growth, both in length and in diameter, resulting in the formation of increasingly larger airspaces. This growth is marked by the expansion of the terminal ends of the airways, which develop into larger, sac-like structures known as sacculi. These sacculi are pivotal in this stage as they represent the precursors to the mature alveoli, facilitating the preparation of the lung for its primary function of gas exchange postnatally. Exposure to hyperoxia and inflammation during this critical period of lung development in preterm infants can lead to enduring alterations in lung maturation, often resulting in irreversible structural damage and chronic respiratory issues [31]. The development and maturation of these structures are driven by complex signaling pathways involving epithelial and mesenchymal cell interactions, ensuring that the lung's architecture and functionality are fully established by birth [32].

1.1.2. Alveolar maturation and emergence of alveolar myofibroblasts

The alveolar stage of lung development in mice, spanning from postnatal day 4 (P4) to the end of the second postnatal week, is characterized by significant maturation and expansion of alveoli, the primary sites for gas exchange. During this period, alveolar type II cells (AT2s) further differentiate into alveolar type I cells (AT1s), facilitating efficient gas exchange. This differentiation is crucial as AT1 cells cover a large surface area and are thin enough to allow for the rapid diffusion of gases. Simultaneously, the surrounding mesenchyme undergoes extensive vascularization, leading to the formation of a dense pulmonary capillary network that is essential for gas exchange [33,34]. This vascularization is driven by various growth factors and signaling pathways, including VEGF and fibroblast growth factor FGF, which are crucial for the development of the pulmonary vasculature[1].

A key feature of this stage is the emergence of a specific mesenchymal cell population known as alveolar myofibroblasts (AMFs). These cells share

characteristics with both fibroblasts and smooth muscle cells and are identified by their expression of markers such as alpha smooth muscle actin (*Acta2*), platelet-derived growth factor receptor alpha (*Pdgfrα*), and glioma-associated oncogene homolog 1 (*Gli1*). AMFs play a pivotal role in promoting alveologenesis, contributing to the structural integrity and functionality of the developing alveoli [35–37]. AMFs are also believed to promote alveologenesis as during the alveolar stage, the lung undergoes a series of morphological changes that are essential for the formation of functional alveoli. The process of alveologenesis involves the subdivision of primitive alveolar sacs into smaller units, increasing the surface area available for gas exchange. This is achieved through the formation of secondary septa, which are thin walls that protrude into the alveolar sacs. AMFs are instrumental in this process as they produce and organize the extracellular matrix components necessary for septation. The extracellular matrix provides the structural framework that supports the alveolar walls and maintains the integrity of the alveolar architecture. Additionally, AMFs secrete growth factors and cytokines that influence the behavior of other cell types within the lung, further promoting alveolar development [38–40].

The differentiation and function of AMFs are tightly regulated by a complex network of key signaling pathways, including the insulin-like growth factor (IGF), WNT, prenatal FGFR2, SHH, PDGF, and TGF-β pathways [41–46]. These pathways are crucial for the differentiation and maintenance of AMFs during the alveolar stage. For instance, the WNT signaling pathway is known to regulate the proliferation and differentiation of mesenchymal cells, while the TGF-β pathway is involved in the production of extracellular matrix components that provide structural support to the alveoli. The IGF signaling pathway, for example, plays a critical role in the proliferation and survival of AMFs. IGF signaling is mediated through the activation of the IGF-1 receptor, which triggers downstream signaling cascades that promote cell growth and prevent apoptosis. Similarly, SHH signaling is essential for the maintenance of the mesenchymal progenitor cell population from which AMFs are derived[47]. Disruptions in these signaling pathways can lead to defects in alveolar development and are associated with various lung diseases, such as bronchopulmonary dysplasia (BPD) and pulmonary fibrosis [46]. However, once the process of developmental alveologenesis is complete, it is widely believed that

AMFs are eliminated from the lung through apoptotic mechanisms mediated by CD11+ alveolar macrophages, ensuring that the lung maintains its proper structure and function into adulthood [48–50].

1.1.3. Human lung development

Human lung development, akin to that of the murine lung, is also delineated into five key morphological stages: embryonic, pseudoglandular, canalicular, saccular, and alveolar [51]. These stages represent critical developmental transitions and are marked by overlapping timelines, reflecting the non-synchronous nature of lung development [52]. This overlap is attributed to the inherent variability in developmental processes, influenced by both genetic and environmental factors [53,54]. The embryonic stage, occurring between 3-6 post-conception weeks (pcw), involves the formation of the lung bud from the foregut endoderm, which then bifurcates to form the primary bronchi [55]. The pseudoglandular stage, spanning pcw 6-16, is characterized by the branching morphogenesis that forms the bronchial tree. During this period, the airways continue to branch extensively, forming the conducting airways [56]. The canalicular stage, from pcw 16-26, sees the differentiation of the epithelium and the formation of the respiratory bronchioles and alveolar ducts. This stage is crucial for the development of the air-blood barrier, as the capillary network becomes closely associated with the developing alveoli. Additionally, the canalicular stage is marked by the appearance of type I and type II alveolar cells, which are essential for gas exchange and surfactant production, respectively. While the saccular stage in human lung development, occurring between pcw 26-36, involves the formation of terminal sacs or primitive alveoli, which are lined by type I and type II alveolar cells. The final alveolar stage, from pcw 32 to 8 years of age, is marked by the maturation and multiplication of alveoli, significantly increasing the surface area for gas exchange [57,58]. This coordinated development ensures the proper formation and function of the lung, enabling efficient gas exchange and respiratory function essential for life.

1.2. Chronic incurable lung diseases

Lung injuries encompass a broad spectrum of conditions that can severely impair respiratory function. These injuries may result from various causes, including infections, mechanical trauma, chemical exposure, and inflammatory diseases. For instance, acute respiratory distress syndrome (ARDS) is a severe form of lung injury often triggered by infections such as pneumonia or sepsis. ARDS is characterized by widespread inflammation and increased permeability of the alveolar-capillary barrier, leading to fluid accumulation in the lungs and impaired gas exchange [59]. Lung injuries can also occur due to autoimmune conditions like rheumatoid arthritis or systemic lupus erythematosus, where the immune system mistakenly attacks lung tissue [60]. Additionally, lung injuries leading to ARDS may result from direct physical damage, such as that caused by blunt force trauma or inhalation of harmful substances, including smoke or toxic chemicals [61,62].

Chronic lung injuries, such as those seen in chronic obstructive pulmonary disease (COPD) or pulmonary fibrosis, involve long-term damage to lung tissue, resulting in progressive loss of lung function. These conditions are often exacerbated by environmental factors like smoking or prolonged exposure to pollutants. In COPD, for example, the inhalation of toxic substances leads to persistent inflammation and remodeling of the airways [63], while pulmonary fibrosis is characterized by excessive deposition of extracellular matrix proteins, leading to stiffening and scarring of lung tissue [64,65].

The response to lung injury often involves a complex interplay of cellular and molecular mechanisms aimed at repairing damaged tissue. A recent study has shown in bleomycin-induced lung fibrosis model that activated myofibroblast (aMYF) are heterogeneous, with a significant potential for shift toward a LIF-like phenotype [66]. However, in many cases, these reparative processes can become dysregulated, leading to chronic inflammation, fibrosis, or other pathological changes that further compromise lung function. Understanding the underlying mechanisms of lung injuries and the factors that influence their progression is crucial for developing effective therapeutic strategies to mitigate these conditions.

1.2.1. Mouse models of injury, repair and regeneration

Mouse models are invaluable tools in studying injury, repair, and regeneration processes due to their genetic similarities to humans and the ability to manipulate their genomes [67,68]. These models replicate various types of lung injuries seen in humans, such as acute lung injury (ALI), COPD, and pulmonary fibrosis [69–71]. The significance of these models lies in their ability to mimic human lung diseases at a molecular and cellular level, providing insights into disease mechanisms and potential therapeutic targets.

1.2.2. The pneumonectomy model

Compensatory lung growth (CLG) in mice is a vital model for studying regrowth and regeneration, as it effectively mimics the lung's inherent regenerative capacity following partial resection [72,73]. In this model, the remaining lung tissue undergoes compensatory growth to restore overall pulmonary function by proliferation of alveolar epithelial cells and the expansion of the gas exchange area, facilitated by increased blood flow and mechanical stretch [74]. Proliferation and expansion of various cell types in the epithelial, endothelial, mesenchymal, and myeloid compartments are some of the hallmark features of CLG [75–77]. Mesenchymal cells, located at the interface between the epithelial lining and the stroma, act as a signalling hub among diverse cellular compartments of the lung [78]. Mesenchymal contraction is critical for re-septation, which is essential for the structural and functional maturation of the lung [79]. Key paracrine signalling pathways, including those involving growth factors such as keratinocyte growth factor (KGF), IGF1, Hippo and TGF-β, play crucial roles in mediating CLG after partial pneumonectomy [80–82]. This model has also recently been proposed to study pulmonary hypertension [83,84].

Previous studies have also highlighted the role of various epithelial lineages, particularly SFTPC+ AT2 cells, in driving AT1 regeneration after lung resection. Additionally, quiescent and immature AT2 progenitor cells in mice, which expand following pneumonectomy, suggest the presence of a similar population in human

lungs, characterized by low differentiation marker expression, distinct chromatin accessibility, and overexpression of PD-L1 [85,86].

In the context of lung cancer, CLG can have both beneficial and detrimental effects. On one hand, the regenerative capacity of the lung can help restore lung function and improve the quality of life for patients who have undergone surgical resection of lung tumours [72]. On the other hand, the hyperplastic environment created during CLG can potentially enhance tumorigenesis. Studies have shown that in mice treated with carcinogens, such as 3-methylcholanthrene, the incidence of lung tumours is significantly higher in those that have undergone PNX [87]. This suggests that the regenerative processes involved in CLG may inadvertently promote the growth of residual cancer cells or the development of new tumours, while minimizing the risks associated with cancer recurrence or progression [88,89].

1.2.3. Chronic obstructive pulmonary disease and cigarette smoke-induced emphysema

Chronic Obstructive Pulmonary Disease (COPD) is a debilitating condition characterized by persistent airflow limitation and chronic inflammation. This condition is primarily caused by long-term exposure to harmful particles or gases, with cigarette smoke exposure (CSE) being the most significant contributor. COPD encompasses several respiratory disorders, including chronic bronchitis and emphysema, which together lead to a progressive decline in lung function and quality of life [90,91]. One of the key pathological features of COPD is emphysema [92], a condition marked by the destruction of alveolar walls and the loss of lung elasticity. In emphysema, the walls between the alveoli are damaged, leading to larger but fewer alveoli. This reduces the surface area available for gas exchange, resulting in impaired oxygen and carbon dioxide transfer. The loss of lung elasticity further exacerbates this problem, making it difficult for the lungs to expand and contract effectively during breathing. As a result, individuals with emphysema often experience shortness of breath, chronic cough, and a decreased ability to perform physical activities [93]. Previous research has shown that CSE-induced emphysema is driven by a complex interplay of inflammatory responses, oxidative stress, and an imbalance between proteases and antiproteases, ultimately resulting in the

breakdown of the lung extracellular matrix. Similarly, studies utilizing cigarette smoke-induced emphysema in experimental models have provided evidence for epithelial cell death as well as onset of vascular remodelling leading to pulmonary hypertension [94–97].

1.2.4. Pathogen-induced lung injuries

Pathogen-induced lung injuries are a significant cause of morbidity and mortality worldwide, resulting from the invasion of various microorganisms, including viruses, bacteria, and fungi. These pathogens trigger a range of immune responses that, while intended to eliminate the invading organisms, often lead to extensive tissue damage. Viral pathogens like Influenza A virus (IAV) [98], respiratory syncytial virus (RSV) [99], and severe acute respiratory syndrome coronavirus 2 (SARS-CoV-2) initiate lung injuries by infecting respiratory epithelial cells, leading to cell death and disruption of the epithelial barrier [100]. This disruption allows pathogens to invade deeper lung tissues and triggers a robust inflammatory response. The resulting cytokine storm, characterized by excessive production of pro-inflammatory cytokines, can cause widespread alveolar damage, increased vascular permeability, and the formation of pulmonary edema [101]. Such immune responses, while critical for controlling infection, can lead to ARDS characterized by diffuse alveolar damage and impaired gas exchange.

Bacterial pathogens, such as *Streptococcus pneumoniae* and *Pseudomonas aeruginosa*, can also induce lung injuries primarily through the release of toxins and the activation of inflammatory pathways [102–104]. These bacteria can cause direct injury to lung tissue through the secretion of exotoxins and endotoxins, which disrupt cellular functions and provoke a strong neutrophilic response [105]. The recruitment and activation of neutrophils, although essential for bacterial clearance, can lead to the release of reactive oxygen species (ROS) and proteases, further damaging the lung parenchyma. Additionally, pathogen-associated molecular patterns (PAMPs) from both bacterial and viral sources activate pattern recognition receptors (PRRs) on immune cells, leading to the amplification of the inflammatory response [106,107]. The excessive inflammation and tissue injury caused by these pathogens not only

compromise lung function but can also predispose the lung to secondary infections and chronic conditions, such as bronchiectasis or even fibrosis [108,109].

1.2.5. Influenza A virus

Influenza A virus (IAV) is a member of the Orthomyxoviridae family, a zoonotic pathogen responsible for causing respiratory diseases in humans and animals [110]. Structurally, IAV is characterized by an envelope surrounding eight segments of anti-sense single-stranded RNA (ssRNA), each tightly associated with nucleoproteins. The viral capsid features major glycoproteins, haemagglutinin (HA) and neuraminidase (NA), which are critical for the virus's infectivity and antigenicity, as they are the primary targets for host antibodies and determine the viral subtype [111,112]. IAV is notorious for its high mutation rate, particularly in its structural genes, facilitating the emergence of novel strains to which the human population has little pre-existing immunity. Upon entry into the host through the oral or nasal cavities, IAV first encounters the mucus layer covering the respiratory epithelium. Successful penetration of this barrier allows the virus to attach to and invade respiratory epithelial cells, subsequently spreading to both non-immune and immune cells, such as macrophages and dendritic cells within the respiratory tract [113,114]. IAV entry is facilitated by its binding to sialic acid (SA)–terminating glycan receptors, with avian influenza strains typically recognizing α2,3-linked sialylated glycans and mammalian strains preferring α2,6-linked sialylated glycans. This receptor specificity plays a crucial role in the interspecies transmission of IAV, contributing to its persistent threat to public health [115].

1.2.6. Influenza-induced lung Injury

IAV infections in humans typically begin in the respiratory tract and are usually confined to this region. IAV can infect both the upper and lower respiratory tracts, often leading to severe outcomes. In the United States, influenza causes approximately 200,000 hospitalizations and 36,000 deaths annually. These numbers can surge during pandemics, such as the 1918 Spanish influenza, which resulted in 600,000 deaths in the U.S. alone and around 40 million deaths worldwide [116–118]. A major factor contributing to the severity of IAV infections is the potential

development of ARDS, defined as "*acute onset of noncardiogenic pulmonary oedema, hypoxaemia and the need for mechanical ventilation*" and is characterized by rapid-onset pneumonia, diffuse alveolar damage, hypoxemia and a significant rise in inflammatory cytokines. The mortality rate for ARDS is approximately 40%, and there is no specific conventional therapy available. Current treatment is primarily supportive, involving mechanical ventilation, fluid management, and prone positioning [59,119].

IAV relies heavily on HA for host cell recognition and attachment. Once recognized, the virus exploits the host cell machinery to transfer its genome to the nucleus, where transcription, translation and replication commence. The innate immune system provides a robust defence against the influenza virus, primarily through pro-inflammatory cytokines, interferons, and chemokines [120,121]. The initial step in IAV infection involves the virus binding to surface glycoconjugates containing terminal SA residues, mediated by its HA molecules [122,123]. This HA-mediated binding leads to endocytosis of the virion, which can occur via clathrin-dependent pathways involving dynamin and the adaptor protein Epsin-1, or through micropinocytosis. Once inside the host cell, the virus is transported to the endosome, where the low pH activates the M2 ion channel, triggering significant structural changes in HA and exposing the fusion peptides. This process acidifies the viral protein and releases viral ribonucleoproteins (vRNPs) into the host cytoplasm after their dissociation from the M1 protein [124–126]. Following the release of vRNPs into the cytoplasm, the virus utilizes the host cell transport machinery to move these complexes into the nucleus [127]. Studies have shown that vRNPs use the importin-α/importin-β nuclear import pathway to enter the nucleus [128,129].

1.2.7. Resolution of IAV-induced lung Injury

IAV infection results in significant damage to the basement membrane across the upper and lower airways, leading to a loss of lung architecture [130,131]. To restore effective gas exchange, a robust regenerative response is essential. This response encompasses the resolution of inflammation, deposition of extracellular matrix, proliferation of progenitor cells, and re-establishment of the alveolar-capillary barrier. The production of antibodies targeting the NA and HA proteins on the viral surface

is critical for viral clearance and prevention of reinfection by the same IAV strain [132]. Clearance of the viral load is closely associated with the resolution of acute inflammation, a process involving various T-cell populations.

CD8+ T-cells play a pivotal role in this process by producing the anti-inflammatory cytokine IL-10. Activated macrophages express the co-stimulatory molecule CD86, which facilitates the expansion of FOXP3+ regulatory T-cells (Tregs). These Tregs are crucial for suppressing cytokine release by neutrophils. Studies have demonstrated that the transfer of Tregs into immunodeficient mice effectively controls the otherwise lethal inflammation mediated by immune cells during IAV infection [133–135].

Type I interferons (IFNs) inhibit T-helper 17 (Th17) responses and reduce neutrophil recruitment, while Interferon Gamma (IFN-γ) suppresses the expression of the scavenger receptor MARCO on alveolar macrophages. Interleukin-22 (IL-22), a tissue-protective cytokine produced by lymphoid tissue inducer cells and innate lymphoid cells, plays a key role in lung regeneration [136,137]. IL-22 enhances the expression of genes involved in tissue repair and promotes the upregulation of anti-apoptotic proteins such as BCL2 and BCL2l1 [138–140].

IL-33, also secreted by lymphoid cells, induces the production of amphiregulin—a member of the epidermal growth factor (EGF) family—that is essential for maintaining epithelial integrity and proper airway remodelling [141]. Additionally, monocyte-derived alveolar macrophages secrete hepatocyte growth factor (HGF), a potent lung epithelial mitogen, which drives the proliferation of AT2s in IAV-infected mice [142]. Tissue-resident alveolar macrophages further support the regeneration of type II alveolar epithelial cells through a mechanism dependent on tumor necrosis factor-alpha (TNF-α) and granulocyte-macrophage colony-stimulating factor (GM-CSF) [143–145].

1.2.8. IAV-induced injury and epithelial repair

The regeneration of lung tissue following influenza-induced damage involves several specialized progenitor cells, each contributing to the repair of specific areas.

In the trachea and bronchus, basal cells with dual expression of *Trp63* and *Krt5* are essential for restoring the epithelial barrier [146]. These cells are capable of proliferating and differentiating to replace damaged tissue. Distal airway stem cells (DASCs) [147], which also express TRP63 and KRT5, are key players in the repair process. Unlike tracheal basal cells, DASCs derive from a distinct lineage and are crucial for the regeneration of the distal lung regions. These cells require Notch signalling to become activated and can differentiate into alveolar epithelial cells, thus contributing to the repair of alveolar structures that have been compromised by viral infection [148]. In this regard, a subset of airway secretory cells marked by *Il22ra1* have recently been shown to populate inflamed lung parenchyma after IAV-induced injury driving epithelial re-differentiation falling short of restoring normal alveolar epithelium [149].

In the distal airways, two main progenitor cell populations play a crucial role in lung repair. First, AT2 cells, which express surfactant protein C (SFTPC), are vital for both producing surfactant and serving as progenitors for alveolar regeneration. After influenza infection, AT2 cells actively proliferate to repair the damaged alveolar epithelium [150]. Importantly, AT2 cells also express high levels of major histocompatibility complex class II (MHCII) molecules, contributing to host defence by supporting adaptive immune responses while minimizing excessive inflammation, as shown in recent studies [151,152].

Additionally, a unique subset of club cells, characterized by ITGB4+ and $CD24^{low}$ expression, assists in repairing the distal airway epithelium. These cells, located in the bronchiolar regions, contribute to the restoration of epithelial integrity by proliferating and differentiating into various cell types necessary for lung regeneration [153–155]. In this regard, previously bronchioalveolar stem cells (BASC) and BASC-derived cells have been shown to also moderately expand following IAV-induced injury [156]. Epithelial stem/progenitor cells (EpiSPC) responsive to Fgfr2b signalling have also have been to expand, renew and regenerate lung, and administering exogenous FGF10 enhanced the regenerative potential of non-infected EpiSPC, improving lung repair and survival after IAV-induced injury [157]. Collectively, these progenitor cells are integral to the lung ability to recover from

influenza-induced injury, working in concert to restore both the structure and function of the airways and alveoli.

1.2.9. Influenza and mesenchyme: A fibrosis-like response to infection and injury

During IAV infection, lung fibroblasts undergo distinct activation states, including extracellular matrix (ECM)-synthesizing and damage-responsive states. This activation is characterized by the production of ECM components and remodelling enzymes, such as ADAMTS4 [158], which lead to the deposition of fibrotic tissue. Excessive ECM remodelling contributes to lung stiffness and disrupts alveolar architecture, significantly impairing gas exchange and overall lung function. The pathological role of these fibroblasts in driving fibrosis highlights the dual nature of mesenchymal responses in lung injury.

Lung mesenchymal cells, particularly fibroblasts, play a crucial role in modulating the inflammatory response during IAV infection. Upon activation, these cells secrete a variety of cytokines and chemokines, which attract immune cells to the site of infection[159]. While this process is essential for effective viral clearance, the intense immune response can lead to collateral damage in the lung, thus exacerbating injury. The balance between necessary inflammation and harmful overactivation is a critical aspect of mesenchymal involvement in IAV-induced lung pathology [157,160]. IAV infection triggers epithelial-mesenchymal transition (EMT) in lung tissues, a process driven by the activation of TGF-β signalling within the mesenchyme. EMT involves the transformation of epithelial cells into a mesenchymal phenotype, contributing to the development of fibrosis. This transition not only exacerbates the fibrotic response but also leads to long-term structural changes in the lung, which can result in chronic lung disease. The role of mesenchymal cells in facilitating EMT underscores their contribution to the fibrotic remodelling seen in severe IAV infections [161] .

Some of the fibroblast growth factors (FGFs) produced by lung mesenchyme are important regulators of viral replication and spread during IAV infection. Previously, *Fgfr1* has been shown to suppress IAV replication, silencing the *Fgfr1* leads to

increased viral replication, whereas overexpression of *Fgfr1* reduces IAV levels. This suggests that mesenchymal *Fgfr1* is a protective factor, limiting the severity of infection by directly interfering with the virus's ability to replicate within the host cells [162,163]. Intra-tracheal application of recombinant FGF10 have been shown to counteract the impaired *Fgfr2b*-mediated renewal response in IAV-infected mice by increasing the recruitment of non-infected *Fgfr2b*^{high} EpiSPCs. FGF10 treatment significantly enhanced EpiSPC proliferation, improved lung architecture, re-established epithelial structures, and increased survival rates compared to PBS-treated controls, highlighting FGF10 therapeutic potential for epithelial regeneration [157]

2. Objectives

Understanding the role of mesenchymal cells in lung regeneration is critical for openning novel research avenues for future therapy. This is because such cells form the in vivo niche that instruct epithelial progenitor cell activation and subsequent behavior during physiological repair and regeneration. This project aims to address this knowledge gap by focusing on AMFs, a key mesenchymal cell type, and their dynamic contributions to lung development, homeostasis, repair, and regeneration. Investigating AMFs across different stages of life and in response to various lung injuries will provide essential insights into their functional roles and interactions with epithelial progenitors within the lung, ultimately advancing our understanding of lung tissue repair mechanisms and identifying potential therapeutic targets and candidates. The aims can be summarized as follows:

2.1. Characterize AMFs during developmental alveologenesis, homeostasis and aging in mice

Using a mouse model, this study aimed to comprehensively characterize the spatio-temporal distribution and validate the transcriptomic signature of AMFs during key phases of lung development, maintenance, and aging. By utilizing single-cell RNA sequencing (scRNA-seq), lineage tracing, and 3D confocal imaging, this research seeks to achieve a detailed understanding of AMF dynamics throughout the mouse's lifespan. Specifically, AMFs will be profiled at various life stages to identify changes in gene expression and cellular states, revealing distinct transcriptomic signatures associated with developmental and aging processes. Additionally, 3D confocal imaging will provide spatially resolved information on AMF distribution and their interactions within the lung tissue. This integrated approach will map the spatial organization of AMFs and elucidate their relationships with other lung cell types, offering a comprehensive view of their location across different stages of lung development and aging.

2.2. Investigate the contribution of AMF-like cells to alveolar regeneration after lung injury

To determine the contribution of AMF-like cells to alveolar regeneration, this study will examine their role during the repair and recovery phases following various injury models. Using a mouse model of IAV-induced lung injury, along with additional models for compensatory lung growth following partial pneumonectomy (PNX) and chronic cigarette smoke exposure (CSE), the project will assess how AMF-like cells contribute to the restoration of alveolar structures and lung function. Transcriptomic and spatial changes in response to various lung injuries will be investigated.

2.3. Test functional requirement of AMFs and AMF-like cells for lung regeneration

To test the functional requirement of AMFs and AMF-like cells for the regeneration of the lung, a combination of IAV-induced lung injury and selective ablation of AMF-like cells using the inducible diphtheria toxin receptor (IDTR) system will be utilized. The impact of cell ablation on the regeneration processe will be determined by comparing lung recovery in mice with and without the ablation. Key endpoints will include the histological evaluation of alveolar structure restoration, and the overall effectiveness of regeneration using ex vivo organoids and scRNA-seq with surviving cell populations. This approach will provide critical insights into the functional contributions of AMFs and AMF-like cells to the regeneration process following IAV-induced injury, helping to elucidate the role of such cells. The status of AMF-like cells will also be investigated in human patient-derived lung materials.

3. Materials and Methods

3.1. Mice and tamoxifen administration

All animal studies were performed according to protocols approved by the Animal Ethics Committee of Justus Liebig University Giessen and by the local authorities (Regierungspraesidium Giessen). Mice were housed in a specific pathogen-free (SPF) environment with unrestricted access to food and water. *Acta2-Cre-ERT2* mice (STOCK Tg(Acta2-cre/ERT2)12Pcn) were generously provided by Dr. Pierre Chambon from the University of Strasbourg, France. *Gli1*$^{Cre\text{-}ERT2}$ mice (STOCK Gli1$^{tm3(cre/ERT2)Alj}$/J, JAX stock number 007913), *tdTomato*^{flox} mice (B6;129S6-Gt(ROSA)26Sor$^{tm9(CAG\text{-}tdTomato)Hze}$/J) (JAX stock number 007905) and *iDTR*^{flox} mice (C57BL/6-Gt(ROSA)26Sor$^{tm1(HBEGF)Awai}$/J) were purchased from the Jackson Laboratory. To induce Cre-ERT2-mediated genetic recombination, mice were exposed to tamoxifen as described in the corresponding figure legends. For subcutaneous (s.c.) or intraperitoneal (i.p.) injections, tamoxifen stock (20 mg/mL) was prepared by dissolving tamoxifen powder in corn oil (both from Sigma) and administered at a dose of 0.5 mg per pup at postnatal day 4 (P4) (approval number G83/2017) or 0.1 mg/g body weight in the adult stage (approval numbers G57/2021 and G75/2022), respectively. Tamoxifen-containing pellets (0.4 g tamoxifen per kg pellets) were purchased from Altromin and was administered for one week whenever indicated (approval number G06/2017).

3.2. Mouse genotyping

Table Primer sequences and protocols for genotyping.

Mouse Line	Primer sequence	PCR Protocol		
		Step	Temp.(°C)	Time
Acta2-CreERT2	**F:** ATT TGC CTG CAT TAC CGG TC **R:** ATC AAC GTT TTG TTT TCG GA	1	94	30sec
		2	94	30 sec
		3	51,7	1 min
		4 (repeat	72	1 min

		Step 2-4 35 times total)		
		5	72	2 min
		6	12	hold

Gli1^{CreERT2} (Mutant + WT)	**F:** GCG GTC TGG CAG TAA AAA CTA TC **R:** GTG AAA CAG CAT TGC TGT CAC TT **F(WT):** GGG ATC TGT GCC TGA AAC TG **R(WT):** CTT GTG GTG GAG TCA TTG GA	1	94	30 sec
		2	94	30 sec
		3	51,7	1 min
		4 (repeat Step 2-4 35 times total)	72	1 min
		5	72	2 min
		6	12	hold

iDTR	**F:** GCG AAG AGT TTG TCC TCA ACC **R:** AAA GTC GCT CTG AGT TGT TAT **WT:** GGA GCG GGA GAA ATG GAT ATG	1	94	30 sec
		2	94	30 sec
		3	65	1 min
		4 (repeat Step 2-4 35 times total)	72	1 min
		5	72	2 min
		6	10	hold

tdTomato	**F:** CTG TTC CTG TAC GGC ATG G **R:** GGC ATT AAA GCA GCG TAT CC **F(WT):** CCG AAA ATC TGT GGG AAG TC **R(WT):** AAG GGA GCT GCA GTG GAG TA	1	94	30 sec
		2	94	30 sec
		3	61	1 min
		4 (repeat Step 2-4 40 times total)	72	1 min
		5	72	2 min
		6	4	hold

3.3. Pneumonectomy

The samples used to analyze AMFs in sham and pneumonectomized mice were generated in a previous study [86]. Briefly, C57BL6 mice were subjected to surgery (sham or pneumonectomy (PNX)) at 8-12 weeks of age. In the PNX group, the left lung lobe was resected while in the sham control group, thoracotomy was performed without lung removal. At days 7 and 14 post-surgery, mice were euthanized, and lungs were isolated. The left lobe was excluded from the analysis in the sham group to maintain consistency with the PNX group, which had the left lobe removed.

3.4. Cigarette smoke-induced emphysema

For cigarette smoke (CS) exposure, adult *Gli1$^{Cre\text{-}ERT2}$; tdTomato^{flox}* mice were exposed to mainstream smoke from 3R4F cigarettes (Lexington, KY) for a duration of 8 months. Such exposure occurred five days a week for 6 h each day, resulting in an exposure level of 200 mg of particulate matter per m^3. Cigarette smoke was generated using a Burghart cigarette smoke generator from Wedel, Germany. Age-matched control mice were kept under identical conditions but were not exposed to cigarette smoke (referred to as room air (RA) controls). During the last week of the 8-month exposure period, mice were fed tamoxifen-containing pellets to label GLI1+ cells. To promote regeneration following emphysema, mice were administered with L-NIL, an inducible nitric oxide synthase (iNOS) inhibitor, through drinking water for a period of 3 months. L-NIL treatment has already been shown to reverse emphysema in various models [164,165]. At the end of the 3-month L-NIL regimen, mice were sacrificed, and lungs were isolated for further analysis. These experiments were approved by the local authorities (approval number G06/2017).

3.5. Influenza-A virus-induced lung injury

Mice were anesthetized and intratracheally inoculated with 400 focus forming units (FFU) of influenza A/PR/8/34 (PR8; a mouse adapted H1N1 influenza virus). The virus was diluted in sterile PBS to a total volume of 70 μL. These experiments were approved by the local authorities (approval number G57/2021). For ablating GLI1+ cells, adult *Gli1$^{Cre\text{-}ERT2}$; tdTomato^{flox}; iDTR^{flox}* mice (8-12 weeks old) received i.p. injections of 100 ng diphtheria toxin (DTX) (Sigma, D0564-1MG) dissolved in sterile phosphate-buffered saline (PBS) solution at days 10, 11 and 12 after PR8 infection.

The ablation experiments were approved by the local authorities (approval number G75/2022).

3.6. Tissue sectioning

To prepare tissue samples for histological analysis, lungs were flushed by transcardiac perfusion with sterile PBS. Subsequently, different protocols were followed based on the intended analysis. For paraffin embedding, the lungs were first fixed in 4% paraformaldehyde, dehydrated through a series of ethanol solutions, cleared in xylene, and then embedded in paraffin wax. Once embedded, the tissue blocks were sectioned using a rotary microtome (Leica), typically at a thickness of 5 µm, and the sections were mounted on Superfrost Plus microscope slides (#03-0060, R. Langenbrinck GmbH). For cryosectioning, the lungs are embedded in compound Tissue-Tek optimal cutting temperature (OCT) compound (#4583, Sakura) and rapidly frozen. The frozen tissue blocks are then sectioned using a cryotome (Leica) at a thickness of 7 µm, allowing for the preservation of reporter (tdTomato), enzyme activity and antigenicity. Thicker sections of 200 µm were generated using vibrotome (Leica) by first inflating perfused lungs with 1.5% ultra-low melting point agarose (Sigma) and then embedding in 4% agarose, tissues were sliced into precision-cut lung slices (PCLS). These thicker sections were used for whole mount immunofluorescence stainings and three-dimensional imaging.

3.7. Hematoxylin and eosin staining

To prepare mouse lung tissues slides for staining, deparaffinization was performed. Slides were treated with hematoxylin (Roth) stain for a duration of 2 min. Following this, slides were washed with running tap water for 10 min. Subsequently, they were stained with eosin (Thermo Fisher Scientific) for 2 min.

3.8. Aniline blue staining and collagen quantification

Mouse lungs slides were deparaffinized and rehydrated, incubated in Bouin’s Solution (Sigma) for 15 min at 56°C and cooled down (18-26°C) in tap water. Afterwards, they were incubated in phosphotungstic/phosphomolybdic acid solution (Sigma) for 5 min and stained with aniline blue solution (Sigma) for 5 min. After the staining, slides were first treated with 1% acetic acid for 2 min and then washed in

distilled water. For collagen quantification, Orbit image analysis software (Idorsia Pharmaceuticals Ltd) was used. Using machine learning, collagen fibers were identified on the sections and their coverage was quantified.

3.9. Immunofluorescence

Immunofluorescence (IF) was performed using monoclonal anti-ACTA2 (Sigma, 1:100 or Santa Cruz 1:200), polyclonal anti-PDGFRα (Abcam, 1:200), monoclonal anti-KI-67 (Cell Signaling Technology, 1:200), polyclonal anti-KI-67 (Thermo Fisher Scientific, 1:200), polyclonal anti-CTHRC1 (R&D System 1:100), monoclonal anti-RAGE (R&D System 1:400), monoclonal anti-KRT8 (DSHB 1:200), polyclonal anti-SFTPC (Seven Hills, 1:1000), polyclonal anti-KRT5 (Biolegend 1:200), monoclonal anti-CD45 (Biolegend 1:200) and polyclonal anti-RFP antibodies (Thermo Fisher Scientific, 1:200; used only in combination with KI-67 staining, which requires antigen retrieval). Neutral lipids were stained using LipidTOX (Thermo Fisher Scientific, 1:200) and nuclei were stained using DAPI (Life Technologies). The catalogue numbers of the antibodies and other key reagents are provided in Table 2. Fluorescent images were acquired using either a Leica DM550 B fluorescence microscope or an SP8 confocal microscope, or MICA widefield live cell equipped with a white-light laser and hybrid detectors (Leica Microsystems). When applicable, three-dimensional (3D) reconstruction of z-stacks was performed using LAS X software (version 3.5; Leica Microsystems). Image quantification was conducted using Fiji and Imaris software (Oxford Instruments). For quantification, sections from at least 3 independent lungs were analyzed, and multiple images were used ($n > 8$) for stained control and experimental lungs.

3.10. In situ hybridization

Cthrc1 and *Piezo2* transcripts were detected using specific probes (Mm-Cthrc1 Cat. # 413341 and Mm-Piezo2-C3 Cat. # 400191-C3, respectively), and the RNAscope Multiplex Fluorescent Reagent Kit v2 assay (document Nr:323100-USM, Advanced Cell Diagnostic) was employed according to the manufacturer's instructions. Upon completion of the RNAscope protocol, slides were washed with PBST buffer at room temperature for 5 min. ACTA2 immunofluorescence staining was performed using

monoclonal anti-ACTA2 antibodies (Sigma) for 3 h at room temperature. After staining, samples were counterstained with DAPI (Life Technologies). Finally, the samples were mounted with Flouromount (SouthernBiotech), and images were acquired using Mica (Leica).

Table 2: List of antibodies used

Mouse monoclonal anti-Actin, α-Smooth Muscle - FITC antibody produced in mouse	Sigma	F3777-.2ML	1:200
α-Actin Antibody (1A4) Alexa Fluor® 647	Santa Cruz Biotechnology	sc-32251 AF647	1:200
Rabbit monoclonal anti-PDGFR alpha antibody [EPR22059-270]	Abcam	ab203491	1:200
Mouse monoclonal anti-KI67 antibody	Cell signaling Technology	9449s	1:200
Rabbit polyclonal anti-KI67 antibody	Thermo Fisher Scientific	PA5-19462	1:200
Rat monoclonal anti-RAGE	R&D System	MAB1179	1:400
Sheep polyclonal anti-CTHRC1	R&D System	AF5960	1:100
Rat monoclonal anti-CD45	Biolegend	103102	1:100
Rat monoclonal anti-RAGE	R&D System	MAB1179	1:400
Chicken Polyclonal anti-Keratin 5 Antibody	Biolegend	905904	1:200
Rabbit polyclonal anti-Pro-SP-C antibody	Seven Hills	WRAB-9337	1:1000
Goat anti-Mouse IgG (H+L) Cross-Adsorbed Secondary Antibody, Alexa Fluor 488	Thermo Fisher Scientific	A-11001	1:1000
Donkey anti-Mouse IgG (H+L) Highly Cross-Adsorbed Secondary Antibody, Alexa Fluor 647	Thermo Fisher Scientific	A-31571	1:1000
Goat anti-Rabbit IgG (H+L) Cross-Adsorbed Secondary Antibody, Alexa Fluor 488	Thermo Fisher Scientific	A-11008	1:1000
Goat anti-Rabbit IgG (H+L) Highly Cross-Adsorbed Secondary Antibody, Alexa Fluor 647	Thermo Fisher Scientific	A-21245	1:1000
Donkey anti-Rabbit IgG (H+L) Highly Cross-Adsorbed Secondary Antibody, Alexa Fluor Plus 488	Thermo Fisher Scientific	A32790	1:1000
Donkey anti-Rabbit IgG (H+L) Highly Cross-Adsorbed Secondary Antibody, Alexa Fluor 647	Thermo Fisher Scientific	A-31573	1:1000

Chicken anti-Rat IgG (H+L) Cross-Adsorbed Secondary Antibody, Alexa Fluor 488	Thermo Fisher Scientific	A-21470	1:1000
Goat anti-Rat IgG (H+L) Cross-Adsorbed Secondary Antibody, Alexa Fluor™ 647	Thermo Fisher Scientific	A-21247	1:1000
Donkey anti-Sheep IgG (H+L) Cross-Adsorbed Secondary Antibody, Alexa Fluor™ 488	Thermo Fisher Scientific	A-11015	1:1000
Donkey anti-Sheep IgG (H+L) Cross-Adsorbed Secondary Antibody, Alexa Fluor™ 647	Thermo Fisher Scientific	A-21448	1:1000
Pacific Blue™ anti-mouse Ly-6A/E (Sca-1) Antibody	Biolegend	108120	1:50
APC/Cy7 anti-mouse CD326 (Ep-CAM) Antibody	Biolegend	118218	1:50
APC anti-mouse CD140a Antibody	Biolegend	135908	1:50
Alexa Fluor® 488 anti-mouse CD45 Antibody	BioLegend	103122	1:100
Alexa Fluor® 488 anti-mouse CD31 Antibody	BioLegend	102514	1:100
APC anti-mouse Sca-1 Antibody	Biolegend	108112	1:50

3.11. Flow cytometry analysis and cell sorting

Flow cytometry and cell sorting procedures were performed according to standard procedures. Briefly, lungs were isolated and placed in Hank's Balanced Salt Solution (HBSS, Gibco). They were then minced into small pieces and incubated with 0.5% collagenase type IV in HBSS (Life Technologies) at 37 °C for 45 min. Subsequently, lung homogenates were filtered through 70 µm and 40 µm cell strainers (BD Biosciences) to obtain single-cell suspensions. Cells were then centrifuged at 4 °C at 1000 rpm for 5 min and resuspended in MACS buffer. Following that, cells were stained with anti-Ly6a (APC-conjugated, 1:50), anti-EpCAM (APC-Cy7-conjugated, 1:50), anti-CD31 (FITC-conjugated, 1:100), and anti-CD45 (FITC-conjugated, 1:100) antibodies (all from Biolegend) for 25 min on ice in the dark. Subsequently, cells were washed with MACS buffer. Flow cytometry and cell sorting were performed using a FACSAria III cell sorter (BD Biosciences), and live cells were gated using SyTOX (1:1000). Data were analyzed using FlowJo software (FlowJo LLC).

3.12. Bulk RNA sequencing

For analyzing gene expression following sham or PNX, FACS-sorted mesenchymal cells defined as $CD45^{neg}$ $CD31^{neg}$ $EpCAM^{neg}$ (non-leukocytic, non-endothelial, non-

epithelial) cells were centrifuged at 300G for 10 min and subjected to RNA extraction using the RNeasy Microkit (Qiagen). Bulk RNA sequencing (Bulk RNA-seq) was carried out according to standard procedures. For genome-wide analysis of gene expression, RNA sequencing libraries from polyadenylated mRNA were generated and sequenced by the Institute for Lung Health (ILH) – Genomics and Bioinformatics – at the Justus-Liebig-University (JLU) Giessen (Germany). A total amount of 2-10 ng of RNA per sample was used for cDNA sequencing library preparation utilizing the NEBNext® Single Cell/Low Input RNA Library Prep Kit for Illumina® (New England BioLabs) according to the manufacturer's instructions. After library quality control by capillary electrophoresis (4200 TapeStation, Agilent), cDNA libraries were sequenced on the Illumina NovaSeq 6000 platform generating 50 bp paired-end reads. For demultiplexing and the subsequent FASTQ file generation, Illumina's bcl2fastq (2.19.0.316) was used. Primary processing of the sequencing reads, i.e., quality control, filtering, trimming, read alignment and generation of gene specific count tables was performed using the nf-core 46 RNA-seq v3.7 bioinformatics pipeline (NEXTFLOW version 23.04.03). The mus musculus mm10 genome and gene annotation was used as downloaded from Illumina's iGenome repository (https://support.illumina.com/sequencing/sequencing_software/igenome.html). The pipeline run was performed with standard parameters in docker mode. The resulting tables with raw read counts were imported into R where all down-stream processing was performed (R Core Team (2022) R: A Language and Environment for Statistical Computing. R Foundation for Statistical Computing, Vienna. URL https://www.R-project.org/). Normalization and detection of differentially expressed genes was determined using DESeq2. Gene set enrichment analysis was done using clusterProfiler and fgsea packages in R [166] using GO and KEGG annotations.

3.13. Single-cell RNA sequencing

Single-cell RNA-seq (scRNA-seq) of tdTomato+ (tdTom+) cells FACS-sorted from *Gli1*$^{Cre\text{-}ERT2}$*; tdTomato*^{flox} lungs was carried out using the Chromium Next GEM Single-Cell 3' Reagent Kit v3.1 (10x Genomics). After following the 10x Genomics library preparation protocol, all samples were sequenced on an Illumina NovaSeq 6000 sequencer. For demultiplexing and the subsequent FASTQ file generation Illumina's bcl2fastq was used (2.19.0.316). Sequencing reads were aligned to the

mouse mm10 reference genome (refdata-gex-mm10-2020-A downloaded from 10xGenomics) using STAR solo (2.7.9a) resulting in three UMI count matrices for spliced, unspliced ambiguous counts per cell per gene to enable subsequent velocity analysis. During the alignment step UMI deduplication was performed by STAR. Droplet filtering was done using the EmptyDrops_CR parameter setting.

After quality control, resulting UMI count matrices from the raw output folder of the STAR solo results were pre-processed for further analyses using Scanpy (1.9.3) in a Python (3.9.12) environment [167]. To filter out low quality cells, doublets, cell debris or ambient RNA the following filter criteria were applied to the data. Scrublet was used with standard parameters to identify doublets. Cells were selected to contain a maximum of 15,000 and a minimum of 1,200 UMI counts. Less than 20 % of all UMI counts are allowed to map to a mitochondrial origin. Finally, at least 600 different genes must be detectable (at least one read mapped to the gene) for each cell. To reduce the gene set size, only those genes were kept, which were expressed in at least 20 cells (function filter_cells with min_cells paramter set to 20). UMI counts underwent normalization in respect to the library size and such that each cell contains 10,000 reads using Scanpy's normalize_per_cell function. The resulting counts were log transformed using the log1p function. For dimensionality reduction and for data integration with Harmony PCAs were calculated. For that purpose, 500 genes were selected as highly variable using the highly_variable_genes function. 20 principal components were identified using the pca function based on these highly variable genes. Harmony integration was performed using the harmony_integrate function using default parameters. A k-nearest-neighbor approach was applied to calculate a neighborhood graph using the neighbors function using default paramter setting (15 neighbors) on which Leiden clustering was performed with resolutions of 0.4, 0.6, 1.0 and 1.4. A two-dimensional visualization of the cells was achieved by calculating UMAPs. Next, automatic cell-type annotation was performed by calculating the average gene expression of all clusters individually. Data were compared to the Mouse Cell Atlas (MCA) using the scMCA R package (https://github.com/ggjlab/scMCA) and later corrected by additional manual annotation according to LungMAP's CellCards classification (https://lungmap.net/research/cell-cards/)[168]. Differentially expressed genes (DEGs)

were identified by the Scanpy rank_gene_groups function. The method parameter for the statistical testing procedure was selected as t-test. For gene set enrichment analysis (GSEA) the genes were ranked for the negative decadic logarithm of the corresponding p-value multiplied by the sign of the log2-transformed fold change. GSEA was performed within R (version 4.3.1) using the GSEA function of the clusterProfiler (version 4.10) package 60 using default settings and a gene signature extracted from the scRNA-seq data by comparing the gene expression in p7 AMF versus all that of all other cells.

Velocity analysis was done using scVelo[169] using standard setting. The number of highly variable genes was set to 500. First and second order moments were calculated with the moments function with parameters n_pcs=30 and n_neighbors=30.

The data were exported in H5AD format and subsequently loaded into cellxgene v1.1.1 extended by the VIP plugin (v3.1). UMAP plots were generated with the Embedding Plot function of cellxgene. The gene specificity function was used to generate specificity heat maps indicating the ratio of the expression of a given gene in a specific cell type compared to the gene's expression across all cell types.

With cellxgene, DEGs were calculated using the DEG function comparing selection of cells per cluster versus all other cells using Welch's t-test in cellxgene. FDR significance was defined as > 0.05 with an absolute $\log_2$(Fold change) of 1. Gene enrichment and KEGG analysis were performed using and ShinyGO (version 0.80) [170]. Mus musculus assembly with STRING-db ID mmusculus_gene_ensembl was used with mouse genes GRCm39 assembly (taxonomy ID 10090). Visualization was performed using GO Biological Process with FDR cutoff set at 0,05 and with 10 genes as minimum pathway requirement. Pathways were sorted by -log10(FDR) and colored with fold enrichment, and chart type was selected as either lollipop or barplot_inside. For the cell-cell interaction analysis, the single-cell atlas of mouse lung development [2] and the AMF & AMF-like cluster (Fig. S7C) were integrated using Seurat (v4.3.0) [171]. The single-cell atlas of mouse lung development raw read counts (GSE165063) was extracted from the final processed data (obtained by

personal correspondence) as were AMF & AMF-like raw read counts. Therefore, both datasets were only subjected to normalization with SCTransform prior to a dimensional reduction and followed by the integration using Seurat's Harmony algorithm implementation. Clustered data were annotated by label transfer from the pre-existing information. The cell-cell interaction analysis was performed using CellChat 64 (v2.1.1) [172]. Integrated data were subset for the time points "P7", "P28", "Mock" and "Tam-PR8" (Fig. S7C). Each subset was analyzed individually with the CellChat pipeline as described in the vignette using standard parameters. CellChatDB.mouse was used as database. Circle plots were created using CellChat's netVisual_circle function. For the heatmap depicting ligand-receptor interaction between AMF/AMF-like cells and AT2 cells, probability values were first calculated by CellChat's netVisual_bubble and subsequently plotted with ComplexHeatmap (v2.6.2). The heatmap depicts the top 20 ligand-receptor interactions identified in P7 AMF to AT2 cells for all four time points. Gene specificity was calculated as the ratio between cumulative expression across all cells in a cluster (normalized to cell count) and the cumulative expression across all cells (also normalized).

3.14. Alveolosphere assay

FACS-sorted tdTom+ cells from *Gli1*$^{Cre\text{-}ERT2}$*;tdTomato*^{flox} lungs were centrifuged and then resuspended in Dulbecco's Modified Eagle Medium (Life Technologies). 17,000 tdTom+ cells were mixed with 5,000 alveolar epithelial cells (AECs; defined as CD45^{neg} CD31^{neg} EpCAM^{low}) and mixed at a ratio of 1:1 with cold growth factor-reduced phenol red-free Matrigel (Corning) as previously described [173]. Cultures were maintained under air-liquid conditions at a temperature of 37 °C with 5% CO2 for a duration of 3 weeks to allow the formation of alveolar organoids (alveolospheres). The culture medium was changed every other day to provide optimal conditions for steady growth and development. Alveolospheres were imaged using EVOS M7000 (Thermo Fisher Scientific) and quantified using Fiji.

3.15. Human Samples

Human donor and COPD biospecimen were provided by the UGMLC Giessen Biobank, member of the DZL Platform Biobanking. These samples were subjected

to RNA extraction followed by bulk RNA-seq and qPCR as well as immunofluorescence. Human ARDS biospecimen were obtained from the CPC-M bioArchive at the Comprehensive Pneumology Center (CPC), Munich in collaboration with Prof. Herbert B. Schiller & Prof. Jürgen Behr, and were subjected to immunofluorescence.

Table 2: List of primer sequences for qPCR.

Gene name (human)	Forward-primer sequence	Reverse-primer sequence
GLI1	AGCCTTCAGCAATGCCAGTGAC	GTCAGGACCATGCACTGTCTTG
CTHRC1	CAGGACCTCTTCCCATTGAAGC	GCAACATCCACTAATCCAGCACC
18s rRNA	ACCCGTTGAACCCCATTCGTGA	GCCTCACTAAACCATCCAATCGG

3.16. Statistical analyses and figure assembly

Quantitative data were assembled and analyzed using GraphPad Prism software (GraphPad Software). Results are presented as mean ± standard error of the mean (SEM). Statistical comparisons between two groups were performed using Student's t-test while one-way ANOVA was used for comparisons involving three or more groups with a single variable. Two-way ANOVA was employed for comparisons involving multiple groups with two variables. Statistical significance was defined as $P < 0.05$. The number of biological replicates is indicated in the corresponding figure legends. Figures were created using Adobe Illustrator (Adobe).

3.17. Data availability

The bulk and scRNA-seq data generated in this study were deposited on gene expression omnibus (GEO) under the accession number GSE248798. Uninjured mock control for adult *Gli1*$^{Cre\text{-}ERT2}$*;tdTomato*^{flox} mice was obtained from publicly available dataset GSE215094 [174].

4. Results

4.1. Characterization during developmental alveologenesis, homeostasis and whole lifespan in mouse model

4.1.1. Characterization of AMFs and their fate during developmental alveologenesis and adulthood

To characterize AMFs [175], two independent genetic approaches were employed: *Acta2-Cre-ERT2; tdTomato^{flox}* to label ACTA2+ cells and *Gli1$^{Cre-ERT2}$; tdTomato^{flox}* to label GLI1+ cells **(Fig. 1, Fig. 2**). Cells were labeled by a single subcutaneous (s.c.) injection of tamoxifen at postnatal day 4 (P4), a timepoint that precedes alveolarization that starts at P5, and lungs were harvested at various time points corresponding to developmental alveologenesis (P7 and P14) and maturation (P28), adulthood (P56) and beyond (P182) **(Fig. 1A, Fig. 2A)**. Histological analysis of thick sections revealed high abundance of parenchymal *Acta2* and *Gli1*-traced tdTom+ at P7 and P14, with gradual decline through P28 to P182 **(Fig. 1B, Fig. 2B)**. These cells were mostly ACTA2+ at P7 but not at later timepoints **(Fig. 1C, E, Fig. 2B, E)**. As expected, the majority of parenchymal tdTom+ cells that were initially ACTA2+ were predominantly PDGFRα+ **(Fig. 1D, 1E)**. Thus, they were identified as AMFs at P7. The tdTom+ lineage maintained *Pdgfra* expression throughout all analyzed timepoints **(Fig. 1D, E)**. Analysis of Ki-67 immunostaining revealed massive proliferation at P7 but not at later timepoints **(Fig. 1D, E, Fig. 2C, E)**. Over the course of aging, tdTom+ cells showed locality of lipid accumulation stained with LipidTOX preferentially at later timepoints **(Fig. 1D, E, Fig. 2D, E)**.

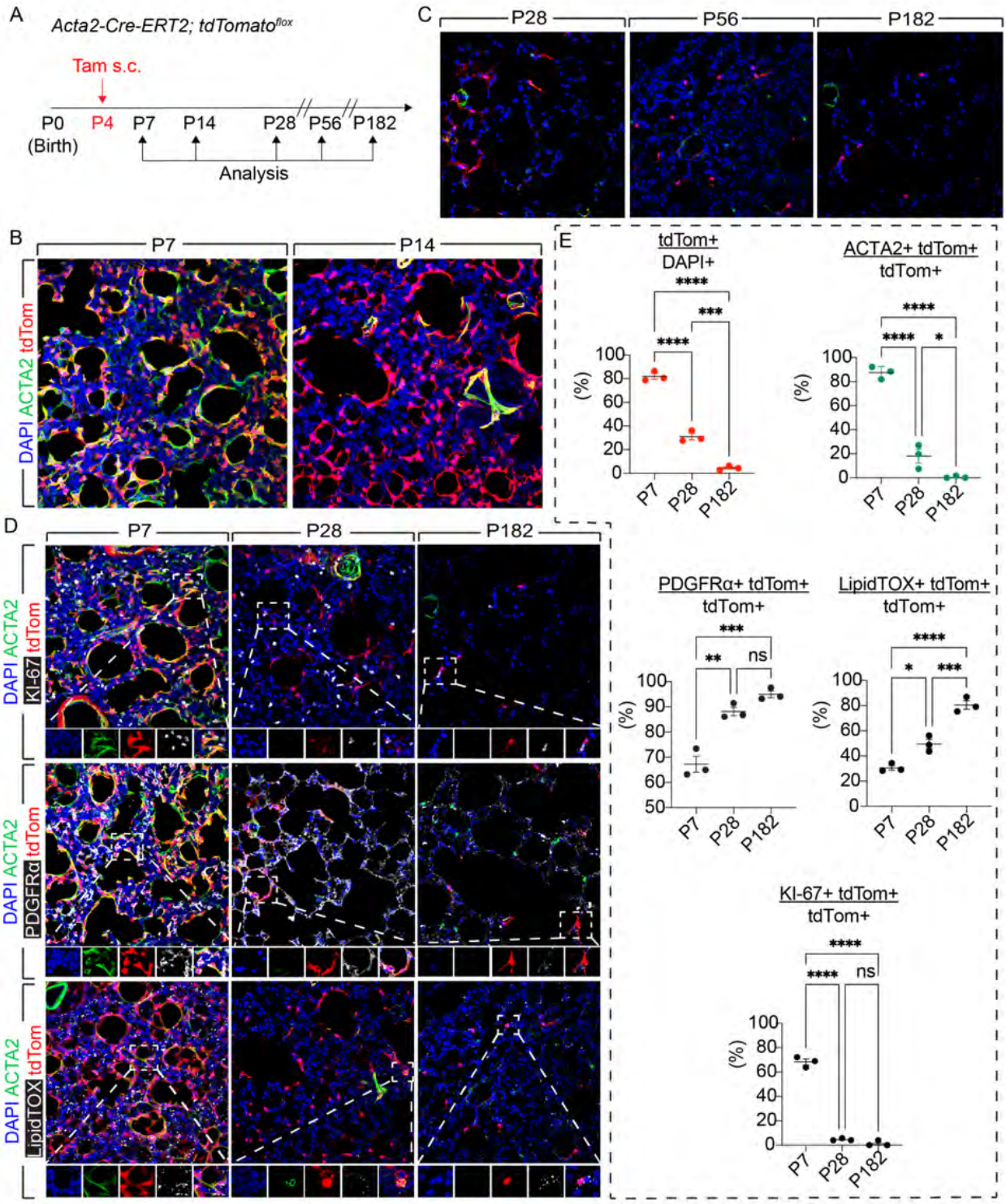
A
Acta2-Cre-ERT2; tdTomato^flox
Tam s.c.
P0 (Birth)
P4
P7
P14
P28
P56
P182
Analysis
B
P7
P14
DAPI ACTA2 tdTom
C
P28
P56
P182
D
P7
P28
P182
DAPI ACTA2 tdTom
KI-67
DAPI ACTA2 tdTom
PDGFRα
DAPI ACTA2 tdTom
LipidTOX
E
tdTom+ DAPI+
ACTA2+ tdTom+ tdTom+
PDGFRα+ tdTom+ tdTom+
LipidTOX+ tdTom+ tdTom+
KI-67+ tdTom+ tdTom+
(%)
ns

Fig.1 *Acta2*+ lineage tracing shows that the alveolar myofibroblast lineage is not completely cleared following the completion of developmental alveologenesis.

(A) Timeline and experimental design. **(B-D)** Immunofluorescence using indicated antibodies at various timepoints. **(E)** Quantification of the different cell populations shown by immunofluorescence. IF: Immunofluorescence; ns: Not significant; s.c.: Subcutaneous injection. Tam: Tamoxifen. n = 3 per group. Data are represented as mean +/- SEM. * $P < 0.05$; ** $P < 0.01$; *** $P < 0.001$; **** $P < 0.0001$. Scale bars: 100 µm.

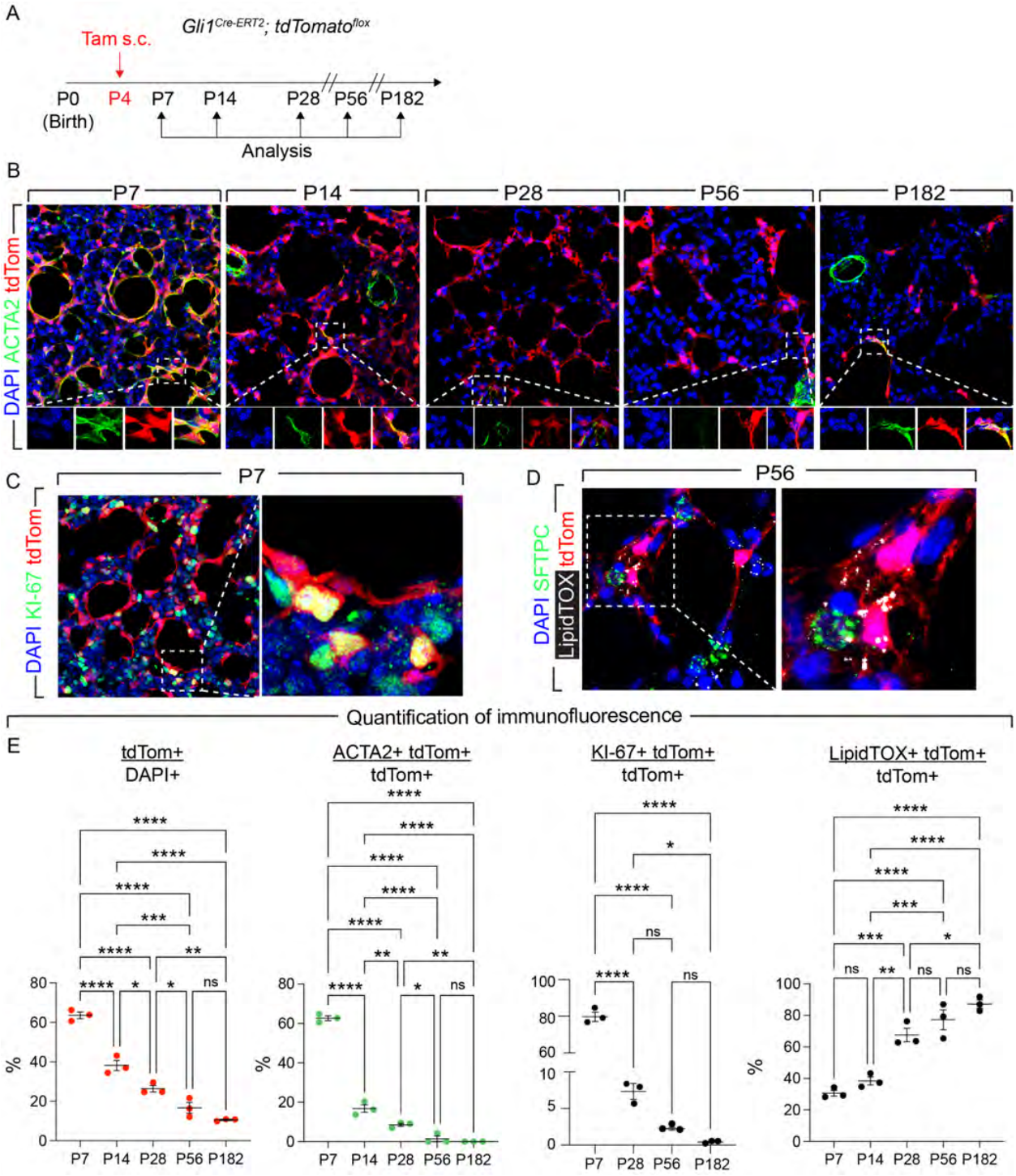
A
Tam s.c.
Gli1Cre-ERT2; tdTomatoflox
P0 (Birth)
P4
P7
P14
P28
P56
P182
Analysis
B
P7
P14
P28
P56
P182
DAPI ACTA2 tdTom
C
P7
DAPI KI-67 tdTom
D
P56
DAPI SFTPC tdTom
LipidTOX
Quantification of immunofluorescence
E
tdTom+ DAPI+
ACTA2+ tdTom+ tdTom+
KI-67+ tdTom+ tdTom+
LipidTOX+ tdTom+ tdTom+
%
P7 P14 P28 P56 P182
P7 P28 P56 P182

Fig.2 *Gli1+* lineage tracing also confirms the non-clearance of alveolar myofibroblast lineage following the completion of developmental alveologenesis. **(A)** Timeline and experimental design. **(B-D)** Immunofluorescence using indicated antibodies at various timepoints. **(E)** Quantification of the different cell populations shown by immunofluorescence. IF: Immunofluorescence; ns: Not significant; s.c.: Subcutaneous injection; Tam: Tamoxifen. n = 3 per group. Data are represented as mean +/- SEM. * $P < 0.05$; ** $P < 0.01$; *** $P < 0.001$; **** $P < 0.0001$. Scale bars: 100 µm.

4.1.2. Single cell RNA-seq profiling on the fate of AMFs

RNA-seq survey was carried out on tdTom+ cells that were FACS-sorted from *Acta2-Cre-ERT2; tdTomato^{flox}* or *Gli1$^{Cre-ERT2}$; tdTomato^{flox}* lungs **(Fig. 3)**. FACS analysis confirmed the decline in cell abundance over time **(Fig. 3B, K)**, thus agreeing with histological quantifications, and ACTA2+ PDGFRα+ cells were detected at P7 **(Fig. 3D, F, M)**. Other cellular clusters included alveolar fibroblasts 1 and 2 (AF1/2s), peribronchial fibroblasts (PeriFBs), and smooth muscle cells (SMCs) **(Fig. 3C, G, H, N-P)**. It was also verified that analyzed cells express *Wpre* (tdTom) but not epithelial or endothelial markers **(Data not shown)**. Interestingly, *Acta2*-lineage traced cells seemed to be more significantly cleared compared to *Gli1*-lineage traced cells over time **(Fig. 3B, K)**, indicating that cells responding to hedgehog signaling neonatally represent a more stable cell population and therefore retained more than cells that express *Acta2*. Notably, both datasets showed that the remaining cells were largely AF1/2s at later stages **(Fig. 3G and Fig. 3P)**, indicating that they may regulate alveolar homeostasis during adulthood and aging. Both datasets were integrated **(Fig. 3Q, R)**. Integrative analysis of the two datasets at P7 identified the AMF cluster defined as ACTA2+ PDGFRα+ **(Fig. 4A-D, I)**, which accounted for around 40-45% of total labeled cells at P7 **(Fig. 4E)**. The AMF cluster was also the most proliferative compared to other clusters (*Mki67* UMAP plot in **Fig. 4C**). Other clusters were identified as airway and vascular smooth muscle cells (ASMCs and VSMCs, respectively), pericytes, and PeriFBs **(Fig. 4C, F)**, and to a lesser extent AF1/2s **(Fig. 4C, G)**. Using this P7 timepoint where AMFs are most abundant, a gene signature for these cells was established**.** GO analysis of the P7 AMF signature (top 500 differentially expressed genes; DEGs) showed that the top enriched pathways were dominated by processes related to morphogenesis and development such as anatomical structure morphogenesis, tissue development, tube morphogenesis, animal organ development, mesenchyme development, and others **(Fig. 4H)**.

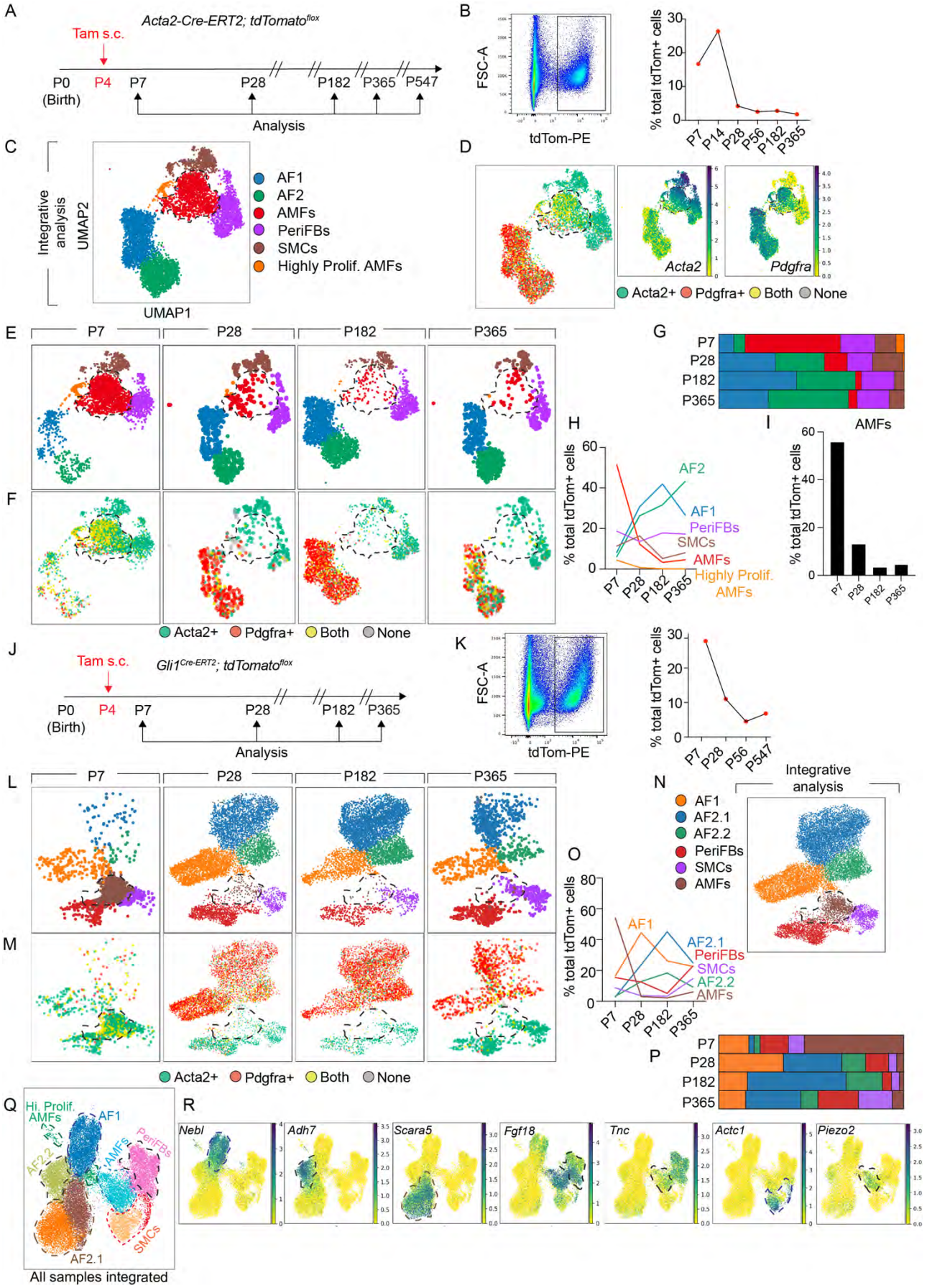
A
Acta2-Cre-ERT2; tdTomatoflox
Tam s.c.
P0 (Birth)
P4
P7
P28
P182
P365
P547
Analysis
B
FSC-A
tdTom-PE
% total tdTom+ cells
P7
P14
P28
P56
P182
P365
C
Integrative analysis
UMAP2
UMAP1
AF1
AF2
AMFs
PeriFBs
SMCs
Highly Prolif. AMFs
D
Acta2
Pdgfra
Acta2+ Pdgfra+ Both None
E
P7
P28
P182
P365
F
Acta2+ Pdgfra+ Both None
G
H
% total tdTom+ cells
AF2
AF1
PeriFBs
SMCs
AMFs
Highly Prolif. AMFs
I
AMFs
J
Tam s.c.
Gli1Cre-ERT2; tdTomatoflox
P0 (Birth)
P4
P7
P28
P182
P365
Analysis
K
FSC-A
tdTom-PE
% total tdTom+ cells
P7
P28
P56
P547
L
P7
P28
P182
P365
M
Acta2+ Pdgfra+ Both None
N
Integrative analysis
AF1
AF2.1
AF2.2
PeriFBs
SMCs
AMFs
O
% total tdTom+ cells
AF1
AF2.1
PeriFBs
SMCs
AF2.2
AMFs
P
P7
P28
P182
P365
Q
Hi. Prolif. AMFs
AF1
AF2.2
AMFs
PeriFBs
SMCs
AF2.1
All samples integrated
R
Nebl
Adh7
Scara5
Fgf18
Tnc
Actc1
Piezo2

Fig. 3 Longitudinal single-cell RNA sequencing deconvolutes the heterogeneity of the ACTA2+ and GLI1+ lineages.

(A) Timeline and experimental design. **(B)** Gating strategy and quantification of lineage-labeled cells. **(C)** Integrative analysis of all timepoints highlighting the AMF cluster using the *Acta2-Cre-ERT2; tdTomato^{flox}* approach. **(D)** Integrative UMAP showing single- and double-positive cells for *Acta2* and *Pdgfra*. **(E)** UMAPs for the individual timepoints highlighting the AMF lineage. **(F)** UMAPs from different timepoints showing single- and double-positive cells for *Acta2* and *Pdgfra*. **(G-I)** Quantification of the AMF cluster as well as other clusters across different timepoints using the *Acta2-Cre-ERT2; tdTomato^{flox}* approach. **(J)** Timeline and experimental design. **(K)** Gating strategy and quantification of lineage-labeled cells. **(L)** UMAPs for the individual timepoints highlighting the AMF cluster using the *Gli1$^{Cre-ERT2}$; tdTomato^{flox}* approach. **(M)** UMAPs for the individual timepoints showing single- and double-positive cells for *Acta2* and *Pdgfra*. **(N)** Integrative analysis of all timepoints highlighting the AMF cluster using the *Gli1$^{Cre-ERT2}$; tdTomato^{flox}* approach. **(O, P)** Quantification of the AMF cluster as well as other clusters across different timepoints using the *Gli1$^{Cre-ERT2}$; tdTomato^{flox}* approach. **(Q, R)** Integrative analysis of both *Acta2-Cre-ERT2; tdTomato^{flox}* and *Gli1$^{Cre-ERT2}$; tdTomato^{flox}* approaches highlighting markers of the constituent clusters. AF1: Alveolar fibroblasts 1; AF2: Alveolar fibroblasts 2/Matrix fibroblasts 2/Adventitial fibroblasts; AMFs: Alveolar myofibroblasts; PeriFBs: Peribronchial fibroblasts; s.c.: Subcutaneous injection; SMCs: Smooth muscle cells. n = 3 for all timepoints for *Acta2-Cre-ERT2; tdTomato^{flox}* and *Gli1$^{Cre-ERT2}$; tdTomato^{flox}* expect for *Gli1$^{Cre-ERT2}$; tdTomato^{flox}* P28 (n = 2). (C-I) For the integrative analysis of the *Acta2-Cre-ERT2; tdTomato^{flox}* dataset, the initial number of cells sequenced at P7, P28, P182 and P365 was 2,812, 1,901, 3,011 and 988, respectively. Clusters 0, 11, 14, 15 and 16 (leiden 0.4) were identified as contaminants and therefore removed. The final number of cells analyzed after removal of contaminants for P7, P28, P182 and P365 is 2,798, 795, 2,996 and 955, respectively. (L-P) For the integrative analysis of the *Gli1$^{Cre-ERT2}$; tdTomato^{flox}* dataset, the initial number of cells sequenced at P7, P28, P182 and P365 was 1,474, 8,097, 6,275 and 2,154. Clusters 5, 9, 10 and 11 (leiden 0.4) were identified as contaminants and therefore removed.

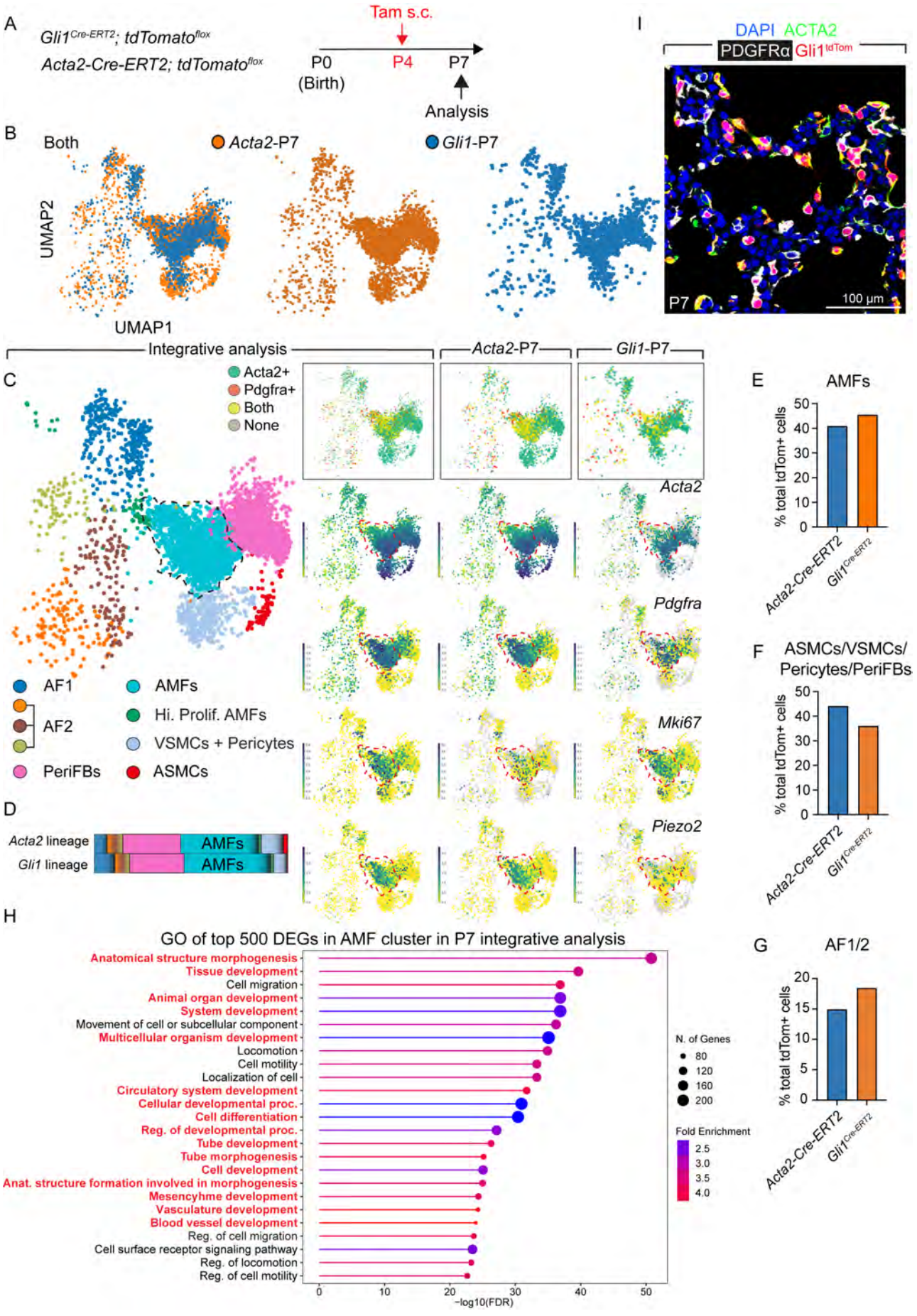
A
Gli1Cre-ERT2; tdTomatoflox
Acta2-Cre-ERT2; tdTomatoflox
Tam s.c.
P0 (Birth)
P4
P7
Analysis
B
Both
Acta2-P7
Gli1-P7
UMAP2
UMAP1
I
DAPI ACTA2
PDGFRα Gli1tdTom
P7
100 μm
Integrative analysis
Acta2-P7
Gli1-P7
C
Acta2+
Pdgfra+
Both
None
Acta2
Pdgfra
Mki67
Piezo2
AF1
AF2
PeriFBs
AMFs
Hi. Prolif. AMFs
VSMCs + Pericytes
ASMCs
D
Acta2 lineage
Gli1 lineage
AMFs
AMFs
E
AMFs
% total tdTom+ cells
Acta2-Cre-ERT2
Gli1Cre-ERT2
F
ASMCs/VSMCs/ Pericytes/PeriFBs
% total tdTom+ cells
Acta2-Cre-ERT2
Gli1Cre-ERT2
G
AF1/2
% total tdTom+ cells
Acta2-Cre-ERT2
Gli1Cre-ERT2
H
GO of top 500 DEGs in AMF cluster in P7 integrative analysis
Anatomical structure morphogenesis
Tissue development
Cell migration
Animal organ development
System development
Movement of cell or subcellular component
Multicellular organism development
Locomotion
Cell motility
Localization of cell
Circulatory system development
Cellular developmental proc.
Cell differentiation
Reg. of developmental proc.
Tube development
Tube morphogenesis
Cell development
Anat. structure formation involved in morphogenesis
Mesenchyme development
Vasculature development
Blood vessel development
Reg. of cell migration
Cell surface receptor signaling pathway
Reg. of locomotion
Reg. of cell motility
−log10(FDR)
N. of Genes
Fold Enrichment

Fig. 4 Identification of the alveolar myofibroblast cluster at postnatal day 7. **(A)** Timeline and experimental design. The P7 datasets were extracted from the integrative analysis for all timepoints shown in **Fig. 3. (B)** Integrative and single UMAPs at P7. **(C)** Integrative UMAP highlighting the AMF cluster at P7 and showing selected markers. **(D-G)** Quantification of the AMF cluster as well as other clusters at P7. **(H)** Gene ontology (GO) analysis of the top 500 differentially regulated genes (DEGs) in the AMF cluster. **(I)** Immunofluorescence using indicated antibodies. AF1: Alveolar fibroblasts 1; AF2: Alveolar fibroblasts 2/Matrix fibroblasts 2/Adventitial fibroblasts; AMFs: Alveolar myofibroblasts; ASMCs: Airway smooth muscle cells; Hi. Prolif. AMFs: Highly proliferative AMFs; PeriFBs: Peribronchial fibroblasts; VSMCs: Vascular smooth muscle cells. n =3 animals per group. Scale bar: 100 µm. (C) For the integrative analysis of the *Acta2-Cre-ERT2; tdTomato*^{flox} and *Gli1*$^{Cre\text{-}ERT2}$*; tdTomato*^{flox} datasets, the initial number of cells sequenced was 2,813 and 1,474, respectively. After removal of contaminants, 2,799 and 1,462 cells were used for the analysis. Clusters 6, 7, 16, 18, 19 and 20 (leiden 1.0) were identified as contaminants and therefore removed.

4.2. Determine the contribution of AMF-like cells to alveolar regeneration after lung injury

4.2.1. Mesenchymal cells display a transcriptomic signature that closely mimics that of developmental AMFs during lung regrowth following pneumonectomy

There is a consensus that developmental mechanisms are often mimicked during regrowth or regeneration of the adult lung. As AMFs are regarded as main drivers of developmental alveologenesis, we sought to determine whether their transcriptomic signature is enriched in mesenchymal cells during compensatory lung growth following unilateral partial pneumonectomy (PNX) **(Fig. 5)**. Histological analysis of sham and PNX lungs following surgery showed an emergence of proliferative ACTA2+ CTHRC1+ (myofibroblastic) cells in the lung parenchyma at day 7 in PNX mice **(Fig. 5A-H)**. In another set of animals, lungs were digested, and mesenchymal cells were FACS-sorted and subjected to bulk RNA-seq **(Fig. 5I)**. Myofibroblast (MyoFB) genes were among the top enriched genes in mesenchymal cells isolated from PNX versus sham, including *Cthrc1*, *Calca*, *Npl*, *Adam12*, *Timp1*, *Sparc*, *Spp1*, and *Wisp1* **(Fig. 5J, K)**. GO analysis showed that such mesenchymal cells were enriched for processes that are related to ECM biology, development, and cell motility such as ECM organization, structure organization, system development, animal organ development, cell migration, cell motility, supramolecular fiber organization, collagen fibril organization, and others **(Fig. 5L)**. Importantly, gene set enrichment analysis (GSEA) revealed that the AMF signature, defined as the top 200 DEGs at P7 **(Fig.** 4**)**, was significantly upregulated (Adj. $P = 3 \times 10^{-10}$) in mesenchymal cells derived from PNX lungs **(Fig. 5M)**. These results show that the developmental AMF signature is enriched in mesenchymal cells during compensatory lung regrowth **(Fig. 5N)**.

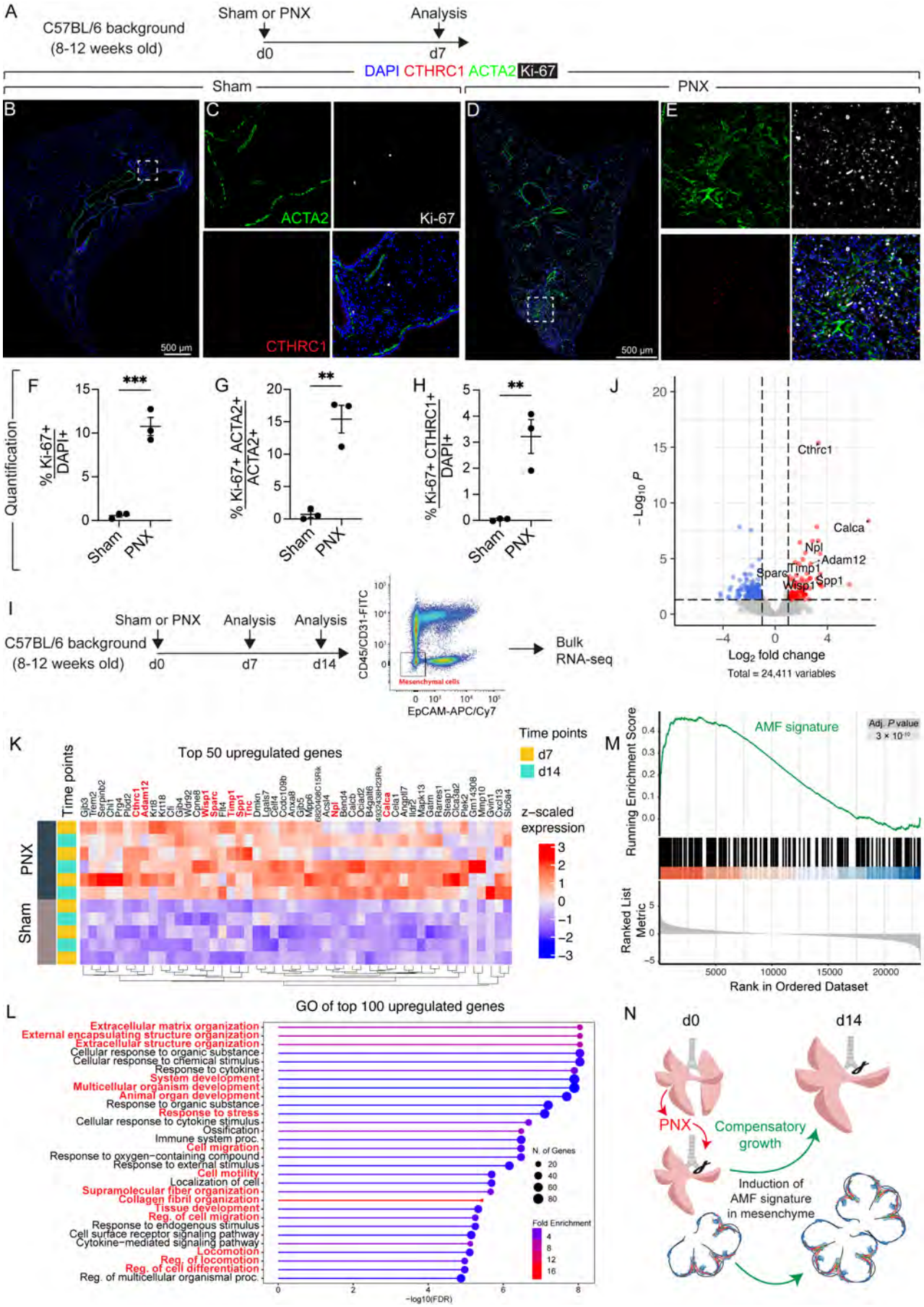
A
C57BL/6 background
(8-12 weeks old)
Sham or PNX
Analysis
d0
d7
DAPI CTHRC1 ACTA2 Ki-67
Sham
PNX
B
C
D
E
ACTA2
Ki-67
CTHRC1
500 µm
Quantification
F
% Ki-67+ DAPI+
G
% Ki-67+ ACTA2+ ACTA2+
H
% Ki-67+ CTHRC1+ DAPI+
Sham
PNX
J
Cthrc1
Calca
Npl
Adam12
Timp1
Spare
Wisp1
Spp1
−Log10 P
Log2 fold change
Total = 24,411 variables
I
Sham or PNX
Analysis
Analysis
C57BL/6 background
(8-12 weeks old)
d0
d7
d14
CD45/CD31-FITC
Mesenchymal cells
EpCAM-APC/Cy7
Bulk
RNA-seq
K
Top 50 upregulated genes
Time points
d7
d14
z-scaled
expression
PNX
Sham
M
AMF signature
Adj. P value
3 × 10⁻¹⁰
Running Enrichment Score
Ranked List
Metric
Rank in Ordered Dataset
L
GO of top 100 upregulated genes
Extracellular matrix organization
External encapsulating structure organization
Extracellular structure organization
Cellular response to organic substance
Cellular response to chemical stimulus
Response to cytokine
System development
Multicellular organism development
Animal organ development
Response to organic substance
Response to stress
Cellular response to cytokine stimulus
Ossification
Immune system proc.
Cell migration
Response to oxygen−containing compound
Response to external stimulus
Cell motility
Localization of cell
Supramolecular fiber organization
Collagen fibril organization
Tissue development
Reg. of cell migration
Response to endogenous stimulus
Cell surface receptor signaling pathway
Cytokine−mediated signaling pathway
Locomotion
Reg. of locomotion
Reg. of cell differentiation
Reg. of multicellular organismal proc.
N. of Genes
Fold Enrichment
−log10(FDR)
N
d0
d14
PNX
Compensatory
growth
Induction of
AMF signature
in mesenchyme

Fig. 5 Mesenchymal cells upregulate the AMF gene signature after pneumonectomy.

(A) Timeline and experimental design. **(B, D)** Immunofluorescence using indicated antibodies. The regions marked with dashed boxes are magnified in **(C, E). (F-H)** Quantification of the immunofluorescence shown in (B-E). **(I)** Timeline and experimental design. **(J)** Volcano plot showing upregulation of AMF signature genes in PNX versus sham. **(K)** Heatmap showing the top 50 upregulated genes in PNX versus sham. Selected myofibroblast markers are marked in red font. **(L)** Gene ontology (GO) analysis of the top 100 upregulated genes in PNX versus sham. AMF-related pathways are marked by red font. **(M)** Gene set enrichment analysis (GSEA) showing enrichment of the AMF signature (top 200 DEGs extracted from P7 scRNA-seq dataset in Fig. 1 and Supplementary file 1 in PNX versus sham. **(N)** Model showing upregulation of the AMF signature in mesenchymal cells during regeneration following PNX. AMF: Alveolar myofibroblast; PNX: Pneumonectomy. (A-H) n = 3 per group; (K-M) Sham d7 n = 3, PNX d7 n = 3, Sham d14 n = 2, PNX d14 n = 3. Data are represented as mean +/- SEM. ** $P < 0.01$; *** $P < 0.001$. Scale bars: 500 µm.

4.2.2. GLI1+ cells are amplified during alveolar regeneration following chronic exposure to cigarette smoke

To show that adult GLI1+ are mobilized during alveolar regeneration, *Gli1*$^{Cre\text{-}ERT2}$*; tdTomato*^{flox} mice were subjected to 8 months of room air (RA) or cigarette smoke (CS) exposure, and GLI1+ cells were labeled during the last week of exposure **(Fig. 6A)**. It has been shown that lung emphysema can be reversed by returning the mice to RA in parallel to treatment with the inducible nitric oxide synthase (iNOS) inhibitor L-N-1-iminoethyl-lysine (L-NIL)[165]. Histological examination showed a dramatic increase in tdTom+ cell abundance during alveolar regeneration **(Fig. 6E versus B-D; H)**. The data also showed significant upregulation of *Acta2* in the parenchyma of these L-NIL-treated regenerating lungs **(Fig. 6E, I)**, particularly in GLI1+ cells **(Fig. 6J)**. Further immunostaining revealed that these cells also express the MyoFB marker *Cthrc1* **(Fig. 6G, K)**. These data indicate that GLI1+ are amplified and display a myoFB-like phenotype during alveolar regeneration following emphysema development (**Fig. 6L**).

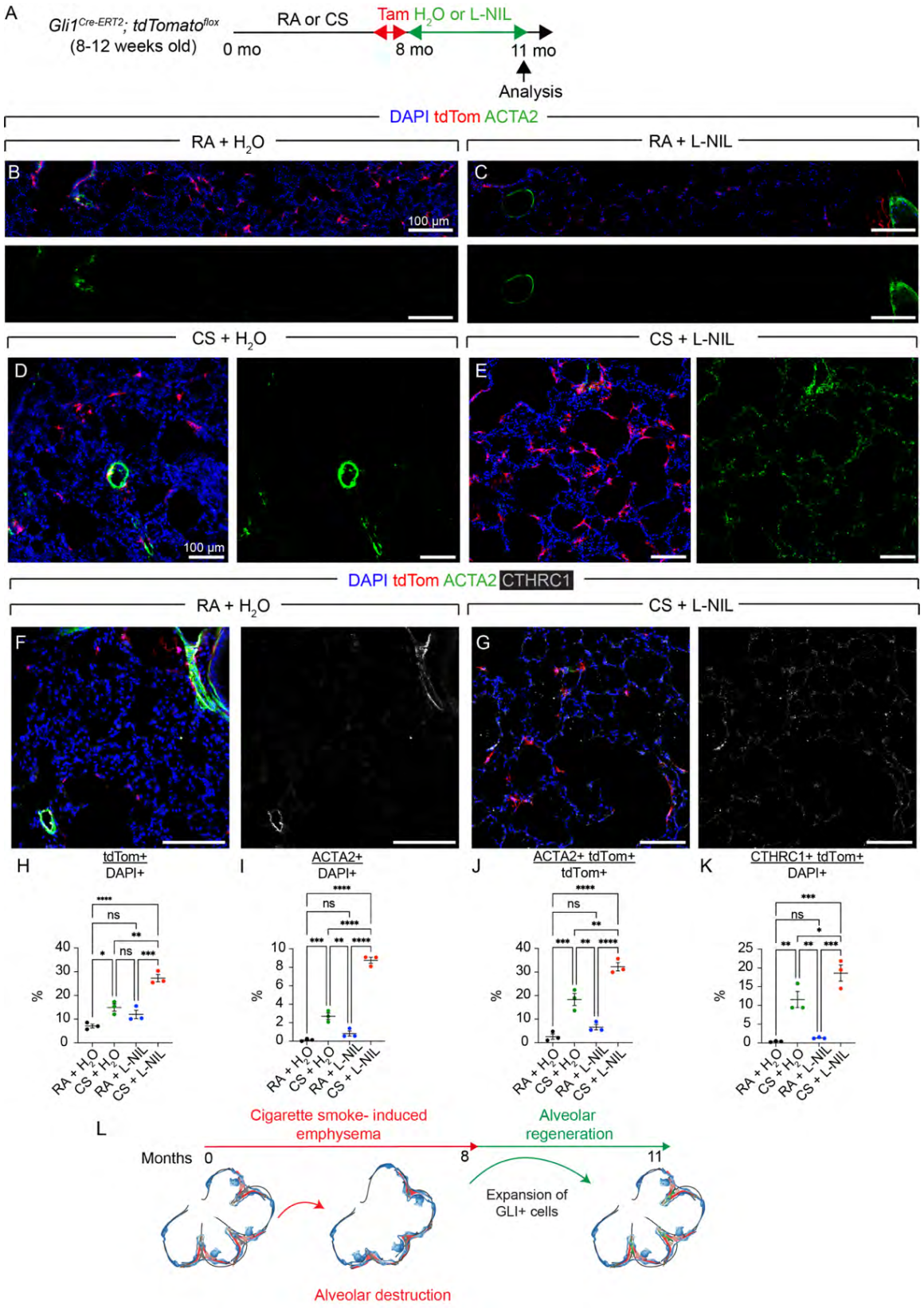
A
Gli1Cre-ERT2; tdTomatoflox
(8-12 weeks old)
RA or CS
Tam H2O or L-NIL
0 mo
8 mo
11 mo
Analysis
DAPI tdTom ACTA2
RA + H2O
RA + L-NIL
CS + H2O
CS + L-NIL
B
C
D
E
100 µm
DAPI tdTom ACTA2 CTHRC1
F
G
H tdTom+ DAPI+
I ACTA2+ DAPI+
J ACTA2+ tdTom+ tdTom+
K CTHRC1+ tdTom+ DAPI+
%
ns
RA + H2O
CS + H2O
RA + L-NIL
CS + L-NIL
L
Cigarette smoke- induced emphysema
Alveolar regeneration
Months 0
8
11
Expansion of GLI+ cells
Alveolar destruction

Fig. 6 GLI1+ cells expand during alveolar regeneration following cigarette smoke exposure.

(A) Timeline and experimental design. (B-G) Immunofluorescence using indicated antibodies in different experimental groups. (H-K) Quantification of immunofluorescence shown in (B-G). (L) Model showing the expansion of AMF-like cells during alveolar regeneration following cigarette smoke exposure. AMF: Alveolar myofibroblast; CS: Cigarette smoke; L-NIL: L-N-1-iminoethyl-lysine; RA: Room air. n = 3 per group. Data are represented as mean +/- SEM. * $P < 0.05$; ** $P < 0.01$; *** $P < 0.001$; **** $P < 0.0001$. Scale bars: 100 μm.

4.2.3. AMF-like cells emerge in response to influenza virus infection

To determine whether AMF-like MyoFBs contribute to alveolar regeneration following influenza virus-induced lung injury, 8–12-week-old *Gli1*$^{Cre\text{-}ERT2}$*; tdTomato*^{flox} mice were treated with tamoxifen before being infected with influenza A/Puerto Rico/8/34 H1N1 (PR8) or mock, and FACS-sorted tdTom+ cells were subjected to scRNA-seq at day 14, a timepoint corresponding to active regeneration **(Fig. 7A)**. The data showed a clear emergence of MyoFBs in response to PR8 infection **(Fig. 7B-G)**. These cells were enriched for *Mki67* as well as typical MyoFB markers including *Tnc* and *Cthrc1* **(Fig. 7H)**. These cells also expressed *Piezo2* **(Fig. 7H)**. To confirm the scRNA-seq data, we carried out RNAscope for *Cthrc1* and *Piezo2*, and the results revealed, in addition to an increase in the abundance of tdTom+ cells, a striking increase in the expression of *Cthrc1* and *Piezo2* upon infection, particularly in tdTom+ cells **(Fig. 7I-R)**. Interestingly, *Piezzo2* showed a wider expression pattern compared to *Cthrc1* where more than 70% of tdTom+ cells expressed *Piezo2* (**Fig. 7Q**) and *Piezo2*+ tdTom+ (double-positive) cells represented 20% of total DAPI+ cells in PR8-infected lungs (**Fig. 7R**). To investigate whether adult GLI1+ cell-derived MyoFBs resemble developmental P7 AMFs, we carried out GSEA for the top 200 DEGs constituting the P7 AMF signature identified in **Fig. 3** in the MyoFB cluster of mock and PR8-infected samples. The results showed significant upregulation for this signature in the PR8 sample.

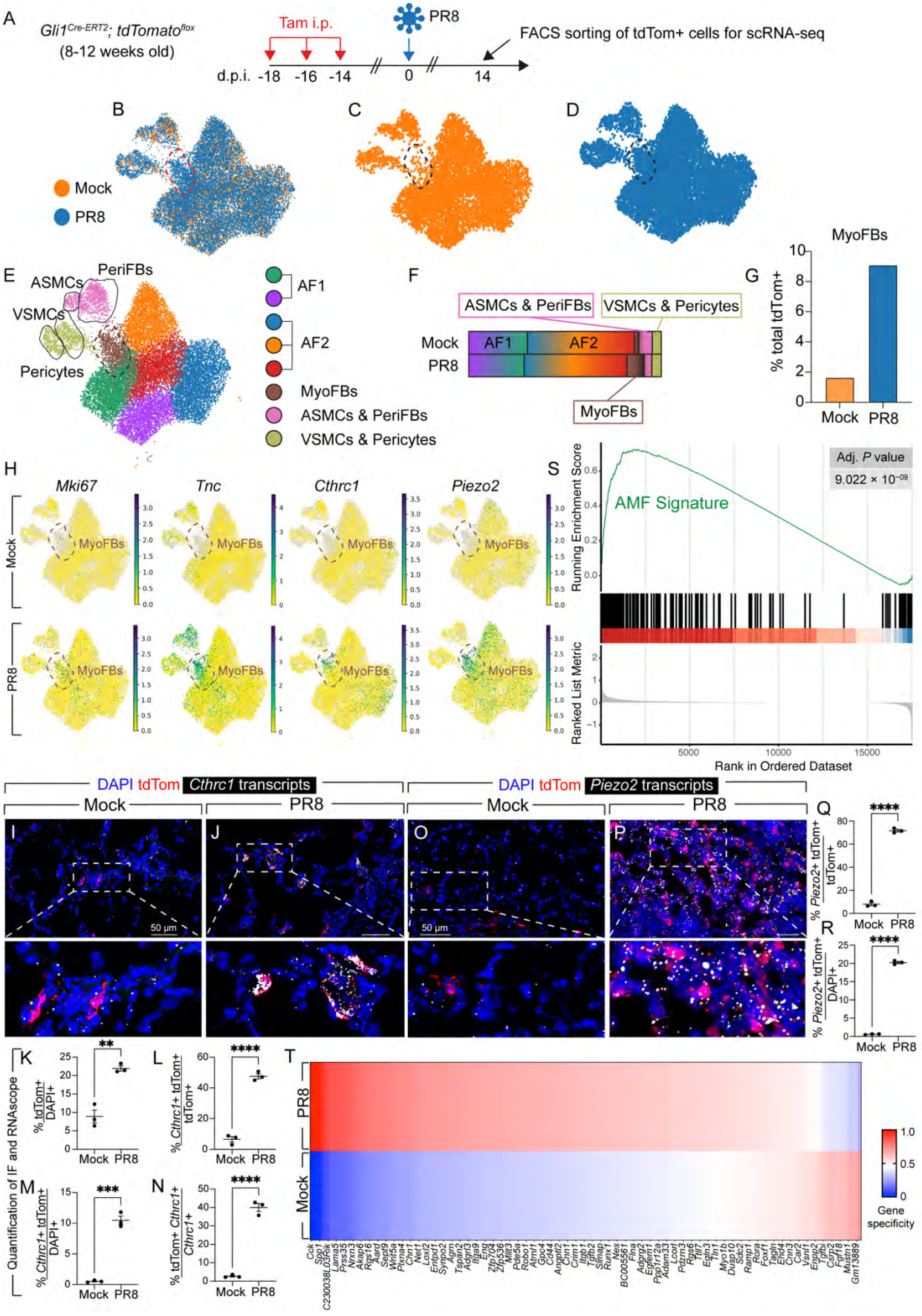
A
Gli1Cre-ERT2; tdTomatoflox
(8-12 weeks old)
Tam i.p.
PR8
FACS sorting of tdTom+ cells for scRNA-seq
d.p.i. -18 -16 -14 0 14
B
Mock
PR8
C
D
E
ASMCs
PeriFBs
VSMCs
Pericytes
AF1
AF2
MyoFBs
ASMCs & PeriFBs
VSMCs & Pericytes
F
ASMCs & PeriFBs
VSMCs & Pericytes
Mock
PR8
AF1
AF2
MyoFBs
G
MyoFBs
% total tdTom+
Mock PR8
H
Mki67
Tnc
Cthrc1
Piezo2
Mock
PR8
MyoFBs
S
Adj. P value
9.022 × 10-09
AMF Signature
Running Enrichment Score
Ranked List Metric
Rank in Ordered Dataset
DAPI tdTom Cthrc1 transcripts
DAPI tdTom Piezo2 transcripts
Mock
PR8
I
J
O
P
50 µm
Q
% Piezo2+ tdTom+ tdTom+
R
% Piezo2+ tdTom+ DAPI+
Quantification of IF and RNAscope
K
% tdTom+ DAPI+
L
% Cthrc1+ tdTom+
M
% Cthrc1+ tdTom+ DAPI+
N
% tdTom+ Cthrc1+ Cthrc1+
T
Gene specificity

Fig. 7 Adult GLI1+ cells give rise to myofibroblasts during regeneration following influenza A virus infection.

(A) Timeline and experimental design. **(B-D)** Integrative and single UMAP plots for mock and PR8-infected samples. **(E)** Integrative analysis revealing the different cellular clusters within the GLI1+ lineage. **(F)** Quantification of constituent cellular clusters in each condition. **(G)** Quantification of myofibroblasts in each condition. **(H)** UMAP plots for selected proliferation and myofibroblast markers. **(I, J)** RNAscope for *Cthrc1* counterstained with DAPI. **(K-N)** Quantification of *Cthrc1* RNAscope. **(O, P)** RNAscope for *Piezo2* counterstained with DAPI. **(Q, R)** Quantification of *Piezo2* RNAscope. **(S)** Gene set enrichment analysis (GSEA) showing highly significant upregulation of the AMF signature (top 200 differentially expressed genes (DEGs) of the AMF cluster extracted from P7 scRNA-seq dataset in Fig. 1 and Supplementary file 1) in the MyoFB cluster in the PR8 sample compared to mock. **(T)** Heatmap showing the genes used in (S). Every third gene is shown. AF1: Alveolar fibroblasts 1; AF2: Alveolar fibroblasts 2/Matrix fibroblasts 2/Adventitial fibroblasts; ASMCs: Airway smooth muscle cells i.p.: Intraperitoneal injection; MyoFBs: Myofibroblasts; PeriFBs: Peribronchial fibroblasts; PR8: A/Puerto Rico/8/34 H1N1; VSMCs: Vascular smooth muscle cells; Tam: Tamoxifen. n =3 animals per group. The initial number of cells sequenced for mock and PR8 was 7,630 and 13,675 respectively. Clusters 8, 9, 10, 11, 12 and 13 (leiden 0.6) were identified as contaminants and therefore removed. The final number of cells analyzed for mock and PR8 are 7,264 and 11,828, respectively. Data are represented as mean +/- SEM. ** $P < 0.01$; *** $P < 0.001$; **** $P < 0.0001$. Scale bars: 50 µm.

4.2.4. AMF-like cells emerge in response to influenza virus infection share conserved transcriptomic signature with that of developmental AMFs

The scRNA-seq datasets from adult mock and PR8-infected mice were also integrated with the P7 and P28 (both labeled at P4) datasets **(Fig. 8A, B)**. Integrative analysis showed that the MyoFBs emerging after infection cluster with developmental AMFs; thus, dubbed them AMF-like cells. Similarly to AMFs, these cells are proliferative **(Fig. 8F)** and express typical MyoFB markers such as *Acta2* **(Fig. 8E)**, *Cthrc1* **(Fig. 8G)**, and *Tnc* **(Fig. 8H)**. GO analysis of the AMF & AMF-like cluster in PR8-infected mice showed enrichment for proliferative, ECM, and developmental/morphogenic pathways such as cell division, ECM organization, tissue development, and others **(Fig. 8I)**.

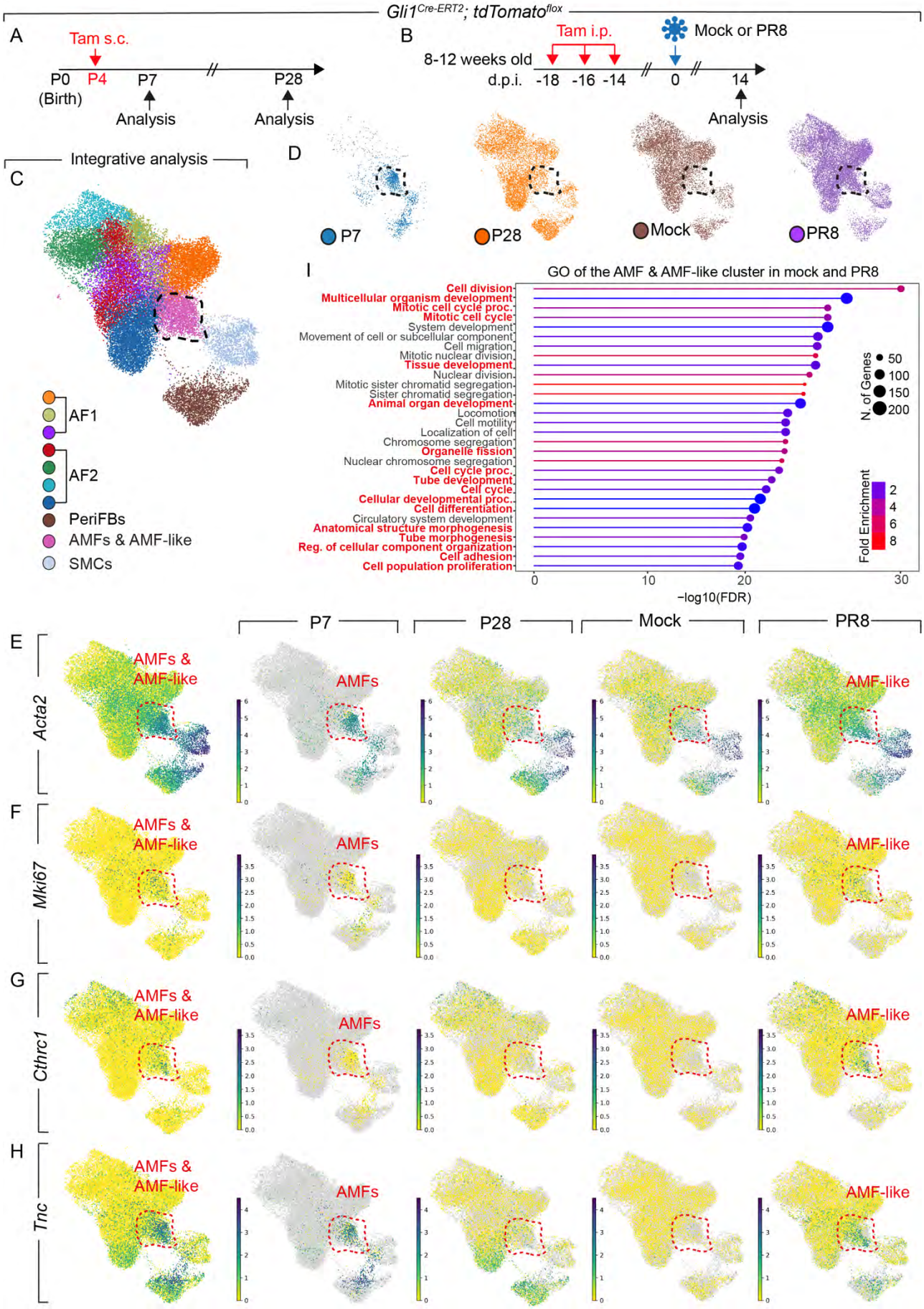
Gli1Cre-ERT2; tdTomatoflox
A
Tam s.c.
P0 (Birth)
P4
P7
Analysis
P28
Analysis
B
Tam i.p.
Mock or PR8
8-12 weeks old
d.p.i. -18 -16 -14
0
14
Analysis
C
Integrative analysis
AF1
AF2
PeriFBs
AMFs & AMF-like
SMCs
D
P7
P28
Mock
PR8
I
GO of the AMF & AMF-like cluster in mock and PR8
Cell division
Multicellular organism development
Mitotic cell cycle proc.
Mitotic cell cycle
System development
Movement of cell or subcellular component
Cell migration
Mitotic nuclear division
Tissue development
Nuclear division
Mitotic sister chromatid segregation
Sister chromatid segregation
Animal organ development
Locomotion
Cell motility
Localization of cell
Chromosome segregation
Organelle fission
Nuclear chromosome segregation
Cell cycle proc.
Tube development
Cell cycle
Cellular developmental proc.
Cell differentiation
Circulatory system development
Anatomical structure morphogenesis
Tube morphogenesis
Reg. of cellular component organization
Cell adhesion
Cell population proliferation
0
10
20
30
−log10(FDR)
N of Genes
50
100
150
200
Fold Enrichment
2
4
6
8
P7
P28
Mock
PR8
E
Acta2
F
Mki67
G
Cthrc1
H
Tnc
AMFs & AMF-like
AMFs
AMF-like

Fig. 8 AMF-like cells expand following influenza A virus infection.
(A, B) Timeline and experimental design. The P7 and P28 datasets were extracted from the integrative analysis for all time points shown in fig. S1J-P. **(C)** Integrative UMAP showing various cellular clusters. **(D)** Single UMAPs for the different experimental conditions highlighting the AMF and AMF-like cluster. **(E-H)** Integrative UMAPs showing selected myofibroblast marker genes in different experimental conditions. AMFs and AMF-like cells are highlighted. **(I)** Gene ontology analysis of the top 500 DEGs in AMFs and AMF-like cells in mock and PR8 infection. AF1: Alveolar fibroblasts 1; AF2: Alveolar fibroblasts 2/Matrix fibroblasts 2/Adventitial fibroblasts; AMFs: Alveolar myofibroblasts; i.p.: Intraperitoneal injection; PeriFBs: Peribronchial fibroblasts; PR8: A/Puerto Rico/8/34 H1N1; s.c.: Subcutaneous injection; SMCs: Smooth muscle cells. n =3 per group. The initial number of cells sequenced for mock and PR8 was 7,630 and 13,675, respectively. For P7 and P28, 1,474 and 8,087 cells were sequenced, respectively. In the integrative analysis, clusters 10, 11, 12, 16, 17 and 19 (leiden 1.0) were identified as contaminants and therefore removed. The final number of cells included in the analysis is 1,458, 7,917, 7,614 and 12,563 for P7, P28, mock and PR8, respectively.

4.2.5. AMF-like cells unlike fibrosis-associated MyoFBs (FAMs) are pro-regenerative and support AT2 growth ex vivo

To determine if these AMF-like MyoFBs are pathological or regenerative, first step was to compare their transcriptomic signature to bona fide fibrosis-associated MyoFBs (hereafter referred to FAMs) that are known to drive aberrant repair and remodeling in response to bleomycin injury. In next step, this dataset was integrated with the *Col1a1-EGFP* dataset where CTHRC1 was identified as a marker for such pathological FAMs [176](**Fig. 9**). Strikingly, AMFs and AMF-like cells formed a single cluster with FAMs (**Fig. 9B-E**). GO analysis revealed that the top pathways relate to ECM biology and development/morphogenesis such as tube development, tube morphogenesis, ECM organization, extracellular structure organization, regulation of cell differentiation, tissue morphogenesis, cell morphogenesis and others (**Fig. 9I**). Therefore, it is concluded that AMFs and AMF-like cells share a similar transcriptomic signature with pathological FAMs. To investigate further, the *Gli1*$^{Cre\text{-}ERT2}$ dataset from P7, P28, (adult) mock, and (adult) PR8 was integrated with the single-cell atlas of mouse lung development [2] and we carried out CellChat [172] analysis to reveal cell-cell interactions (**Fig. 10A-F**). While the P7 AMF cluster revealed strong interactions with AT1s and AT2s (**Fig. 10C**), these interactions were weaker at P28 (**Fig. 10D**). In the adult stage and in the absence of injury (mock), weak interactions were observed between the AMF-like cluster with AT1s and AT2s (**Fig. 10F**) while strong interactions were observed after PR8 infection (**Fig. 10E**). These data demonstrate that AMFs and AMF-like cells strongly interact with AT1s and AT2. The top targets included collagen-syndecan interactions (**Fig. 10G**). In line with the bioinformatic prediction, organoid cultures showed that tdTom+ cells isolated from PR8-infected lungs showed superior ability to support AT2 growth ex vivo compared to their mock-derived counterparts (**Fig. 10H-J**). Although the AT2-supportive ability after infection might not be directly attributable to the AMF-like cluster, these data hint to an important in vivo role for GLI1+ cells in promoting alveolar regeneration following influenza virus-induced lung injury in vivo.

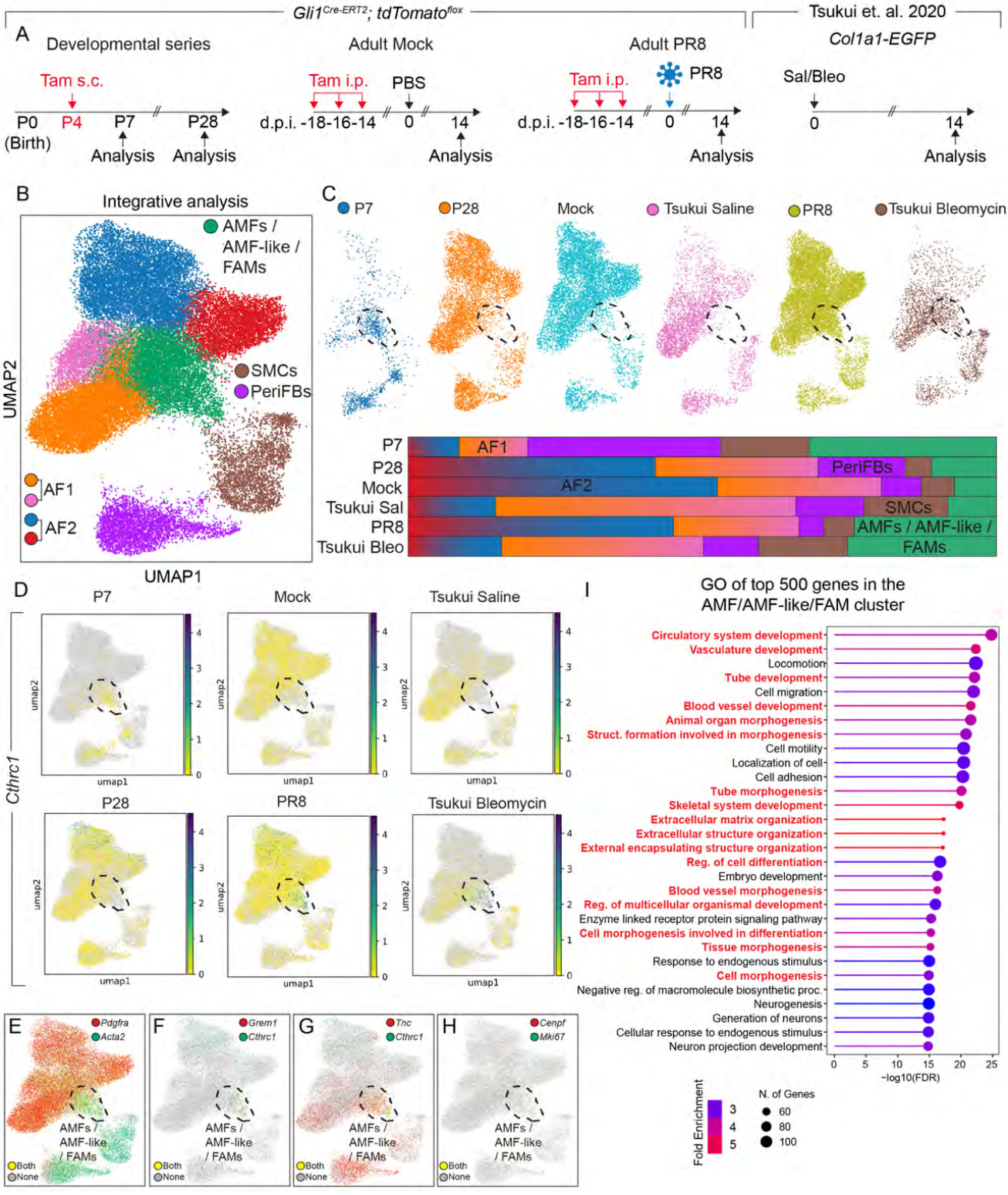
Gli1Cre-ERT2; tdTomatoflox
Tsukui et. al. 2020
Col1a1-EGFP
A
Developmental series
Adult Mock
Adult PR8
Tam s.c.
Tam i.p.
PBS
PR8
Sal/Bleo
P0 (Birth)
P4
P7
P28
d.p.i. -18-16-14
0
14
Analysis
B
Integrative analysis
AMFs / AMF-like / FAMs
SMCs
PeriFBs
AF1
AF2
UMAP1
UMAP2
C
P7
P28
Mock
Tsukui Saline
PR8
Tsukui Bleomycin
P7
P28
Mock
Tsukui Sal
PR8
Tsukui Bleo
AF1
AF2
PeriFBs
SMCs
AMFs / AMF-like / FAMs
D
Cthrc1
P7
Mock
Tsukui Saline
P28
PR8
Tsukui Bleomycin
umap1
umap2
I
GO of top 500 genes in the AMF/AMF-like/FAM cluster
Circulatory system development
Vasculature development
Locomotion
Tube development
Cell migration
Blood vessel development
Animal organ morphogenesis
Struct. formation involved in morphogenesis
Cell motility
Localization of cell
Cell adhesion
Tube morphogenesis
Skeletal system development
Extracellular matrix organization
Extracellular structure organization
External encapsulating structure organization
Reg. of cell differentiation
Embryo development
Blood vessel morphogenesis
Reg. of multicellular organismal development
Enzyme linked receptor protein signaling pathway
Cell morphogenesis involved in differentiation
Tissue morphogenesis
Response to endogenous stimulus
Cell morphogenesis
Negative reg. of macromolecule biosynthetic proc.
Neurogenesis
Generation of neurons
Cellular response to endogenous stimulus
Neuron projection development
−log10(FDR)
Fold Enrichment
N. of Genes
E
Pdgfra
Acta2
F
Grem1
Cthrc1
G
Tnc
Cthrc1
H
Cenpf
Mki67
AMFs / AMF-like / FAMs
Both
None

Fig. 9 AMFs and AMF-like cells show high resemblance to fibrosis-associated myofibroblasts that arise during aberrant repair.

(A) Timeline and experimental design for the integration of the datasets with [177]. **(B)** Integrative analysis of the indicated timepoints and samples. **(C)** UMAPs for the individual timepoints highlighting AMFs, AMF-like cells, and FAMs in addition to the corresponding cluster frequencies. Note that AMFs and AMF-like cells cluster together with Cthrc1+ myofibroblasts (FAMs) identified in Tsukui et. Al 2020. **(D)** UMAPs for *Cthrc1* across the different timepoints and samples. **(E-L)** UMAPs from the integrative analysis showing single- and double-positive cells for the indicated genes. **(M)** GO analysis of the top DEGs in the AMF/AMF-like/FAM cluster. **(N)** Gene ontology analysis of top DEGs in the AMF/AMF-like/FAM cluster. AF1: Alveolar fibroblasts 1; AF2: Alveolar fibroblasts 2/Matrix fibroblasts 2/Adventitial fibroblasts; AMFs: Alveolar myofibroblasts; Bleo: Bleomycin; FAMs: Fibrosis-associated myofibroblasts; i.p.: Intraperitoneal injection; PeriFBs: Peribronchial fibroblasts; PR8: A/Puerto Rico/8/34 H1N1; s.c.: Subcutaneous injection; SMCs: Smooth muscle cells; Tam: Tamoxifen.

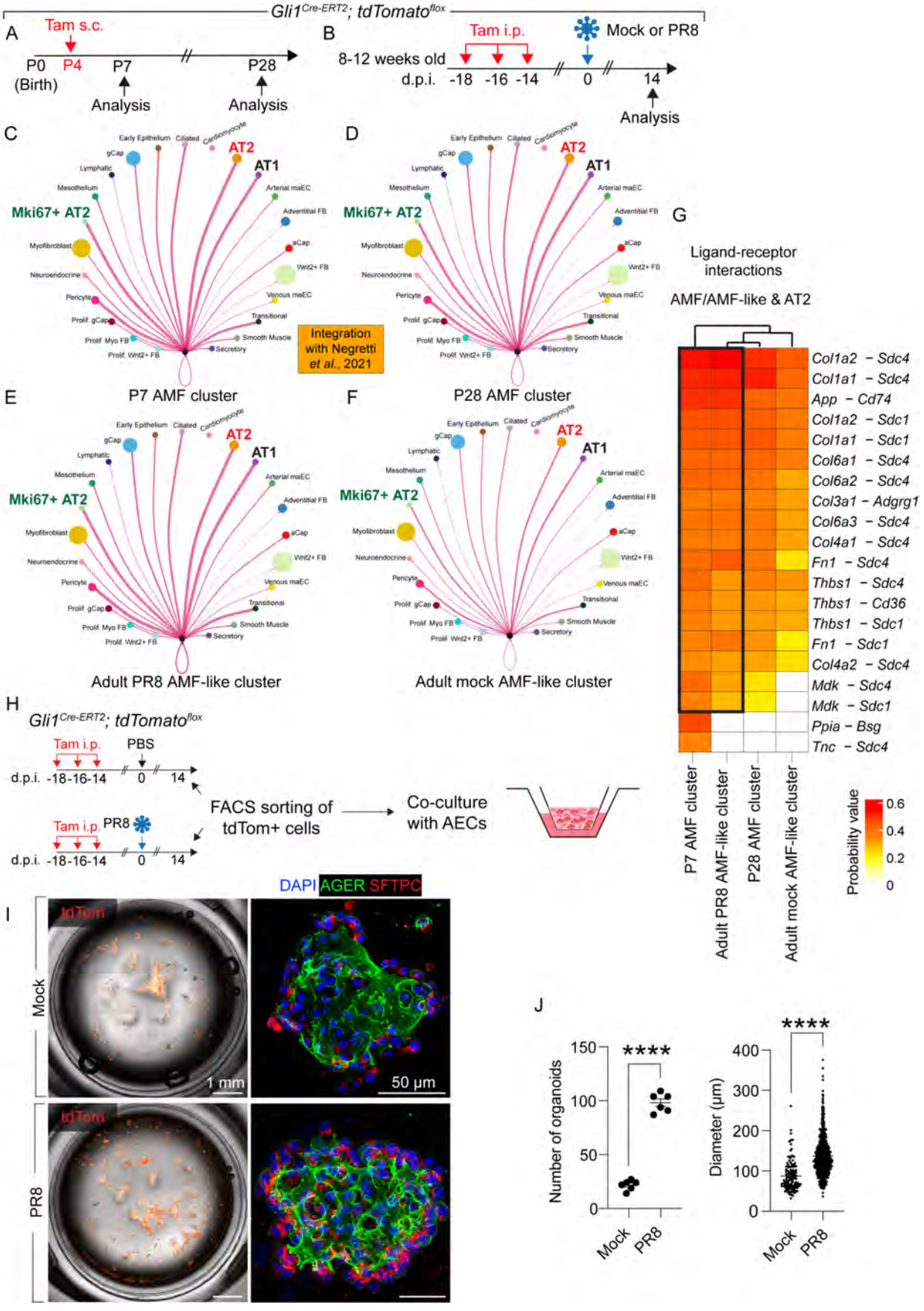
Gli1Cre-ERT2; tdTomatoflox
A
Tam s.c.
P0 (Birth)
P4
P7
Analysis
P28
Analysis
B
Tam i.p.
Mock or PR8
8-12 weeks old
d.p.i. -18 -16 -14 0 14
Analysis
C
D
AT2
AT1
Mki67+ AT2
Integration with Negretti et al., 2021
E
P7 AMF cluster
F
P28 AMF cluster
Adult PR8 AMF-like cluster
Adult mock AMF-like cluster
G
Ligand-receptor interactions
AMF/AMF-like & AT2
Col1a2 – Sdc4
Col1a1 – Sdc4
App – Cd74
Col1a2 – Sdc1
Col1a1 – Sdc1
Col6a1 – Sdc4
Col6a2 – Sdc4
Col3a1 – Adgrg1
Col6a3 – Sdc4
Col4a1 – Sdc4
Fn1 – Sdc4
Thbs1 – Sdc4
Thbs1 – Cd36
Thbs1 – Sdc1
Fn1 – Sdc1
Col4a2 – Sdc4
Mdk – Sdc4
Mdk – Sdc1
Ppia – Bsg
Tnc – Sdc4
P7 AMF cluster
Adult PR8 AMF-like cluster
P28 AMF cluster
Adult mock AMF-like cluster
Probability value
0.6
0.4
0.2
0
H
Gli1Cre-ERT2; tdTomatoflox
Tam i.p.
PBS
d.p.i. -18-16-14 0 14
Tam i.p. PR8
d.p.i. -18-16-14 0 14
FACS sorting of tdTom+ cells
Co-culture with AECs
I
DAPI AGER SFTPC
tdTom
Mock
PR8
1 mm
50 µm
J
Number of organoids
Diameter (µm)
****
****
Mock
PR8

Fig. 10 AMF-like cells support AT2 growth ex vivo.

(**A, B)** Timeline and experimental design. The datasets shown in Fig. S5 were integrated with the mouse lung development atlas**. (C-F)** Cell-cell communication networks highlighting interactions between AMFs & AMF-like cells with other cell types. **(G)** Heatmap showing the top ligand-receptor interaction candidates. **(H)** Timeline and experimental design for the generation of organoids. **(I)** Overview of wells with organoids at day 21 and immunofluorescence using indicated antibodies. **(J)** Quantification of organoid number and size. (H-J) n = 6 per group. Data are represented as mean +/- SEM. **** $P < 0.0001$. Scale bars: (I) 1 mm for well overviews and 50 µm for immunofluorescence. aCap: aerocytes; Adventitial FB: Adventitial fibroblasts; AMF: Alveolar myofibroblasts; Arterial maEC: macrovascular arterial endothelium; AT1: Alveolar type 1 cells; AT2: Alveolar type 2 cells; gCap: general capillary cells; i.p.: Intraperitoneal injection; PR8: A/Puerto Rico/8/34 H1N1; s.c.: Subcutaneous injection; Prolif. MyoFB: Proliferative myofibroblasts; Tam: Tamoxifen; Venous maEC: macrovascular venous endothelium; Wnt2+ FB: Wnt2+ fibroblasts. (C-F) Thickness of line indicates interaction strength.

4.2.6. Pre-existing FGF10+ alveolar fibroblasts do not give rise to AMF-like cells

To investigate whether AMF-like cells appearing after influenza infection share the same cellular origin as those seen in lung fibrosis. FAMs have been shown to be of mesenchymal origin and featuring an important role for the transcription factor TBX4 [178]. It has also been previously reported that FAMs derive from FGF10+ lipofibroblasts, a cell type that belongs to AFs [179–181]. In previous work, FGF10+ cells, a population that predominantly includes AFs has been shown to contribute to myofibroblast formation in the fibrotic lung . To further explore this, the recently developed *Fgf10*$^{Cre\text{-}ERT2}$ mouse line was used for lineage tracing of AFs in the adult lung [5,182–184]. This approach contrasts with previous methods where Cre activity was primarily active during embryonic development. Mice were treated with tamoxifen to label pre-existing FGF10+ cells, and two weeks after the final tamoxifen injection, they were infected with the PR8 influenza virus (**Fig. 11A, B**). Histological analysis showed that lineage-labeled cells representing AFs were dramatically lost and were very few during regeneration (**Fig. 11C-G**). *Cthrc1* expression was, as expected, upregulated in response to PR8 infection (**Fig. 11C-F, H**). While some tdTom+ cells expressed *Cthrc1* at baseline (mock), this expression was dramatically lost after infection (**Fig. 11C-F, I, J**).

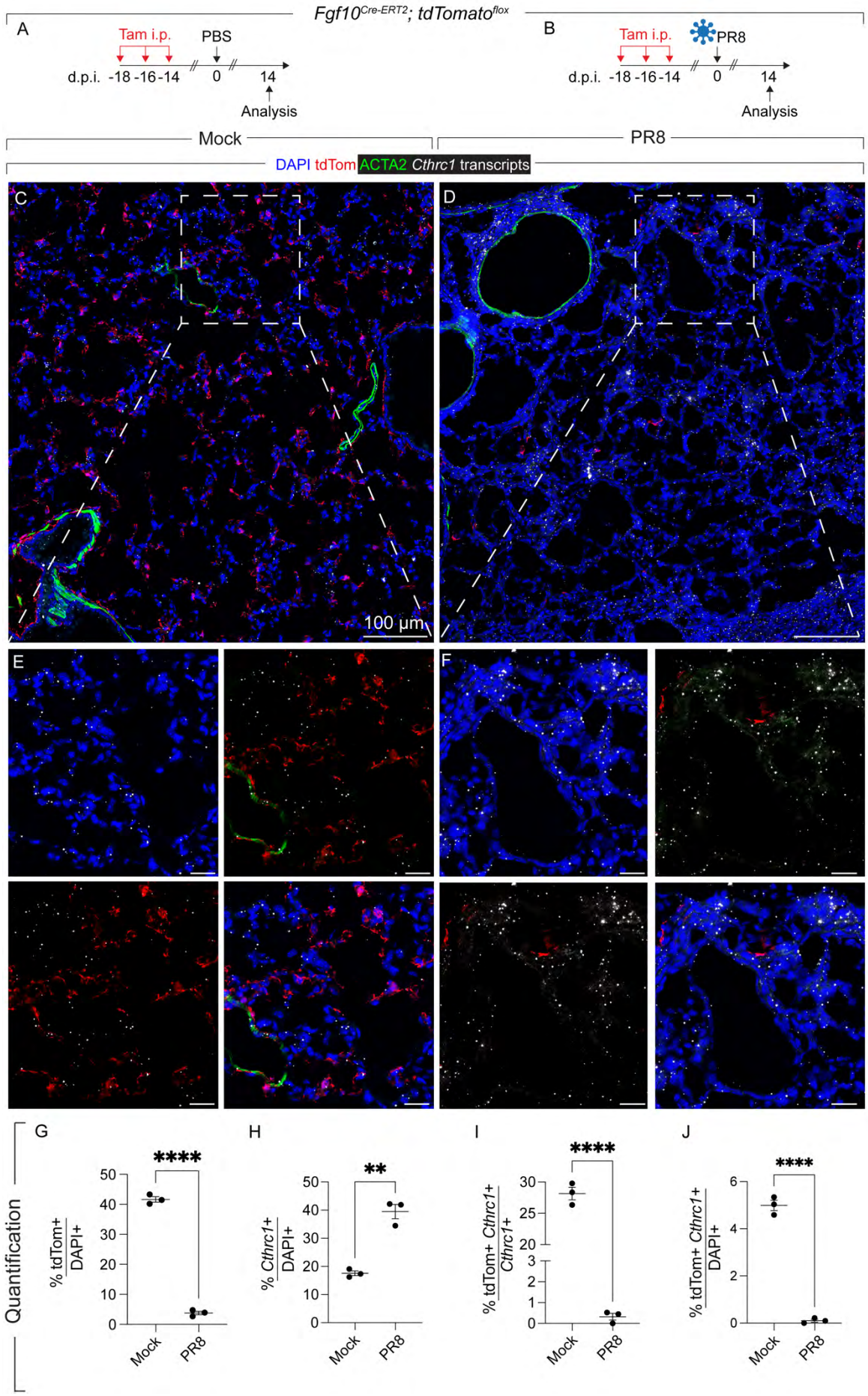
Fgf10Cre-ERT2; tdTomatoflox
A
Tam i.p.
PBS
d.p.i. -18 -16 -14 0 14
Analysis
B
Tam i.p.
PR8
d.p.i. -18 -16 -14 0 14
Analysis
Mock
PR8
DAPI tdTom ACTA2 Cthrc1 transcripts
C
D
100 µm
E
F
Quantification
G
% tdTom+ DAPI+
****
Mock
PR8
H
% Cthrc1+ DAPI+
**
I
% tdTom+ Cthrc1+ Cthrc1+
****
J
% tdTom+ Cthrc1+ DAPI+
****

Fig. 11 Pre-existing FGF10+ alveolar fibroblasts do not contribute to *Cthrc1*+ AMF-like cells after influenza virus infection.

(A, B) Timeline and experimental design. **(C-F)** RNAScope for *Cthrc1* and immunofluorescence for ACTA2 counterstained with DAPI in mock and PR8 samples. **(G-J)** Quantification of cell populations. i.p.: Intraperitoneal injection; PR8: A/Puerto Rico/8/34 H1N1; Tam: Tamoxifen. n = 3 per group. Data are represented as mean +/- SEM. ** $P < 0.01$; **** $P < 0.0001$. Scale bars: 100 µm.

4.3. Test the functional requirement of AMF-like cells for lung regeneration

4.3.1. Selective ablation of P4-labeled GLI1+ cells impairs alveolar regeneration following influenza virus-induced lung injury

Our longitudinal lineage-tracing data suggest that a portion of cells labeled at P4 survive into adulthood and might be important to promote regeneration following PR8 infection. Thus, taking advantage of the sequential control of recombination and ablation offered by the *Gli1*$^{Cre\text{-}ERT2}$*; tdTomato*^{flox} mice were crossed with *iDTR*^{flox} mice to generate *Gli1*$^{Cre\text{-}ERT2}$*; tdTomato*^{flox}*; iDTR*^{flox} mice to label developmental AMFs at P4, let the animals reach adulthood, infect them with PR8, and ablate surviving lineage-labeled cells during the regeneration phase **(Fig. 12)**. Littermate (*Gli1*$^{Cre\text{-}ERT2}$*; tdTomato*^{flox}*; iDTR*^{flox}) controls were also infected with PR8 but received PBS instead of DTX **(Fig. 12B)**. To better contextualize the data, lungs from P7 and P56 time points (both labeled at P4) were included in the histological analysis **(Fig. 12A)**. The IF data demonstrated that while the number of AMFs and their descendants dramatically decreases from P7 to P56 **(Fig. 12C, D, K)**, but these P4-labeled GLI1+ cells expand upon infection **(Fig. 12E, K)**, and they are significantly ablated in the PR8+DTX group **(Fig. 12F, K)**. Around 62.3% of tdTom+ cell express *Cthrc1* in PR8-infected lungs, but this phenomenon dramatically decreases in ablated lungs **(Fig. 12L)**. In PR8-infected lungs, around 48-53% of CTHRC1+ cells derive from lineage-labeled cells **(Fig. 12M)**. Confirming that ablation dramatically targeted *Cthrc1*+ tdTom+ cells, in the lung parenchyma **(Fig. 12N)**. Importantly, histological analysis revealed that ablated lungs showed impaired regeneration with persistent damage **(Fig. 12O-R)**, as well as dysplastic repair as evident by KRT5+ cell accumulation **(Fig. 14)**. On the contrary, PBS-treated control mice showed significant regeneration, with tdTom+ cells occupying alveolar walls of the regenerating areas that are adjacent to still non-resolved regions **(Fig. 12E)**. Of note, tdTom+ cells were observed near AT2s, suggesting crosstalk between the AMF as a mesenchymal niche cell and AT2 as an epithelial stem and progenitor cells. The alveolosphere assays shown in **Fig. 10I-J** support the notion that the GLI1+ cell lineage serves as a niche for AT2 as 1) GLI1+ cells are permissive for alveolosphere formation and 2) GLI1+ cells

derived from PR8-infected lungs display higher potential to support AT2 growth compared to those isolated from mock-infected lungs.

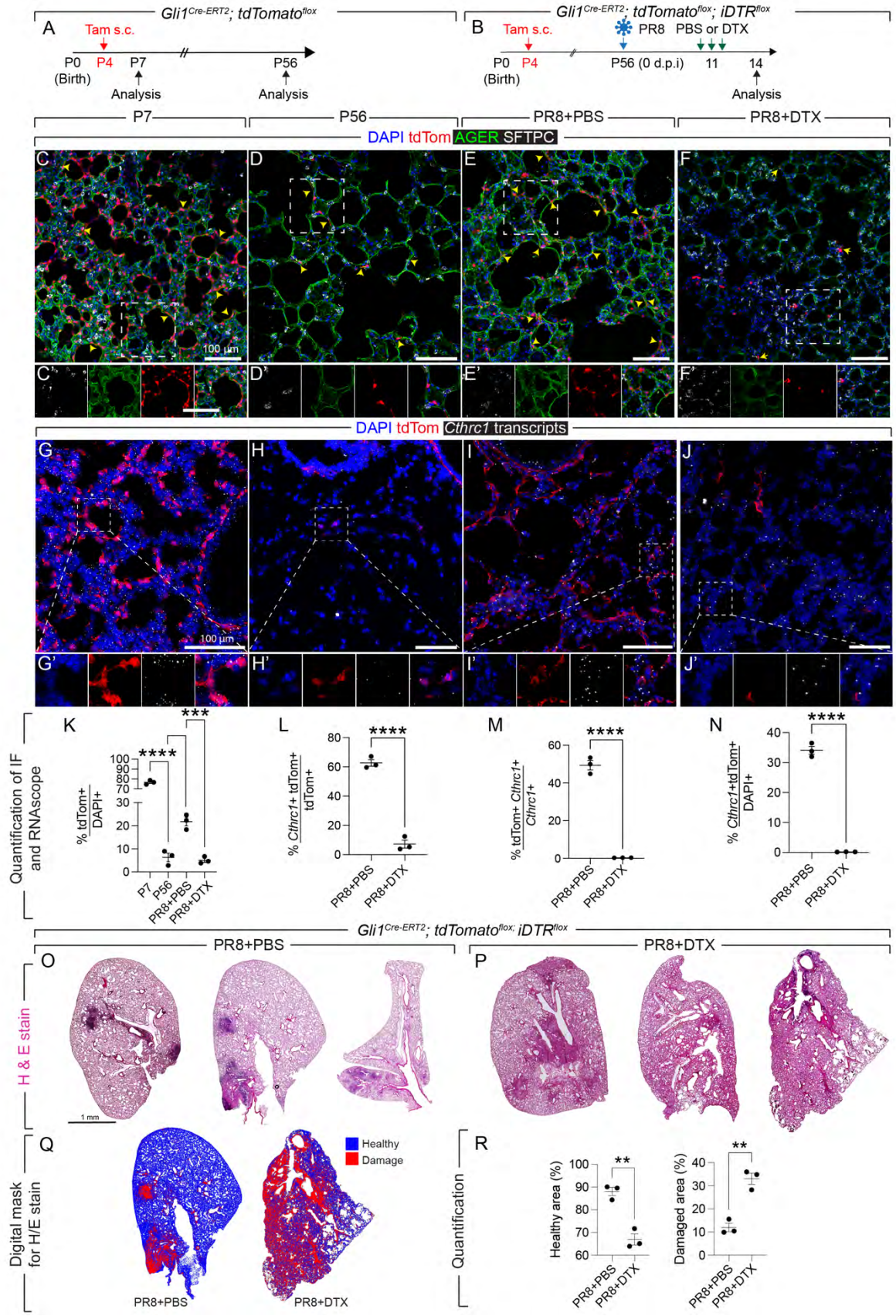
Gli1Cre-ERT2; tdTomatoflox
A
Tam s.c.
P0 (Birth)
P4
P7
Analysis
P56
Analysis
Gli1Cre-ERT2; tdTomatoflox; iDTRflox
B
Tam s.c.
PR8
PBS or DTX
P0 (Birth)
P4
P56 (0 d.p.i)
11
14
Analysis
P7
P56
PR8+PBS
PR8+DTX
DAPI tdTom AGER SFTPC
C
D
E
F
100 µm
C'
D'
E'
F'
DAPI tdTom Cthrc1 transcripts
G
H
I
J
100 µm
G'
H'
I'
J'
Quantification of IF and RNAscope
K
% tdTom+ DAPI+
****
***
P7
P56
PR8+PBS
PR8+DTX
L
% Cthrc1+ tdTom+ tdTom+
****
PR8+PBS
PR8+DTX
M
% tdTom+ Cthrc1+ Cthrc1+
****
PR8+PBS
PR8+DTX
N
% Cthrc1+tdTom+ DAPI+
****
PR8+PBS
PR8+DTX
Gli1Cre-ERT2; tdTomatoflox; iDTRflox
PR8+PBS
PR8+DTX
H & E stain
O
P
1 mm
Digital mask for H/E stain
Q
Healthy
Damage
PR8+PBS
PR8+DTX
Quantification
R
Healthy area (%)
**
PR8+PBS
PR8+DTX
Damaged area (%)
**
PR8+PBS
PR8+DTX

Fig. 12 Ablation of P4-labeled GLI1+ cells during the regeneration phase leads to persistent damage following influenza A virus-induced lung injury.

(A, B) Timeline and experimental design. **(C-F)** Immunofluorescence for AGER and SFTPC in the different experimental groups. The endogenous tdTomato signal is shown in red. The dashed boxes are magnified in **(C'-F').** **(G-J)** Immunofluorescence for CTHRC1 in the different experimental groups. The endogenous tdTomato signal is shown in red. The dashed boxes are magnified in **(G'-J').** **(K-N)** Quantification of the different cell populations shown by immunofluorescence. **(O, P)** Hematoxylin and eosin staining of control and ablated lungs. **(Q, R)** Quantification of lung damage. DTX: Diphtheria toxin; i.p.: Intraperitoneal injection; IF: Immunofluorescence; s.c.: Subcutaneous injection; Tam: Tamoxifen. n = 3 per group. Data are represented as mean +/- SEM. ** $P < 0.01$; *** $P < 0.001$; **** $P < 0.0001$. Scale bars: 100 µm.

4.3.2. Ablation of P4-labeled GLI1+ cells following influenza A virus-induced lung injury leads to aberrant repair and dysplastic repair

Ablation of P4-labeled GLI1+ cells following IAV-infection significantly impacts lung repair processes, revealing pronounced structural alterations leading to dysplastic and aberrant tissue remodeling (**Fig. 13A, B**). Quantitative analysis using obtained digital masks highlighted this interstitial deposition of collagen fiber stained with aniline blue in the PR8-DTX group compared to the PR8-PBS control group (**Fig. 13C, D**).

Immunofluorescence staining with specific antibodies for ACTA2 and KRT5 demonstrated disrupted cellular and extracellular matrix patterns, further underscoring the role of these cells in maintaining proper lung repair mechanisms (**Fig. 14 A-D'**).

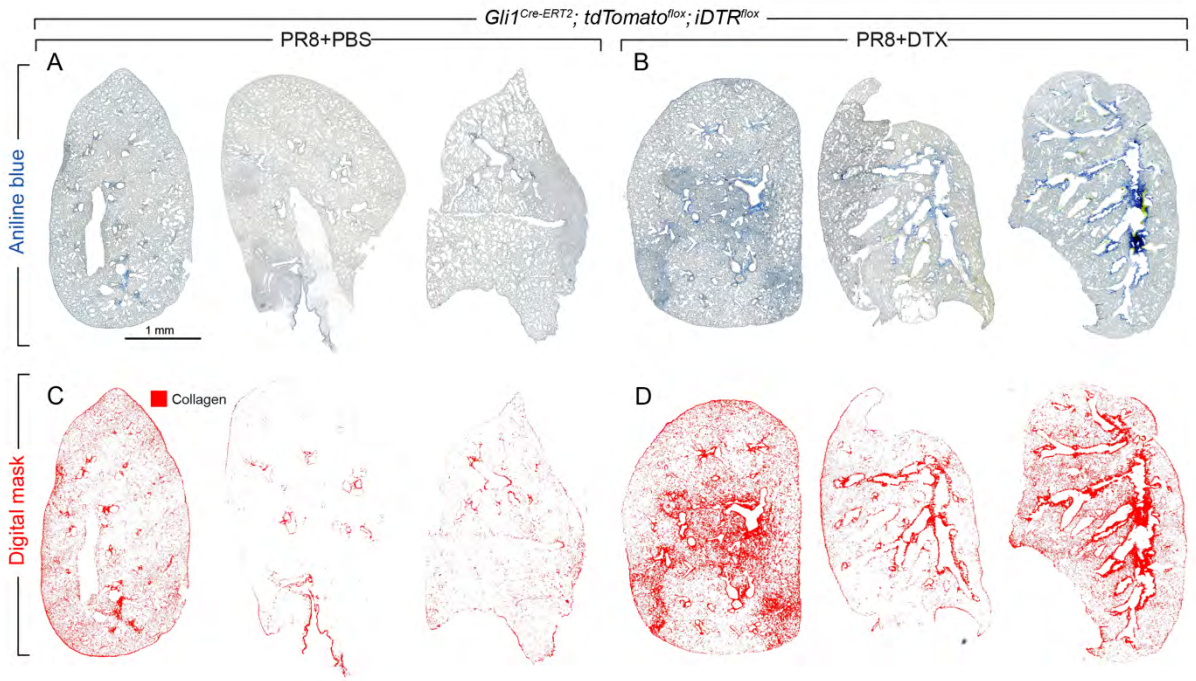

Fig. 13. Ablation of P4-labeled GLI1+ cells following influenza A virus-induced lung injury leads to aberrant repair and accumulation of collagen

(A, B) Aniline blue staining in PR8-PBS and PR8-DTX experimental group. **(C, D)** Digital mask acquired following Orbit quantification shown in red. DTX: Diphtheria toxin; PR8: A/Puerto Rico/8/34 H1N1. n= 3 per group. Scale bars: 1 mm.

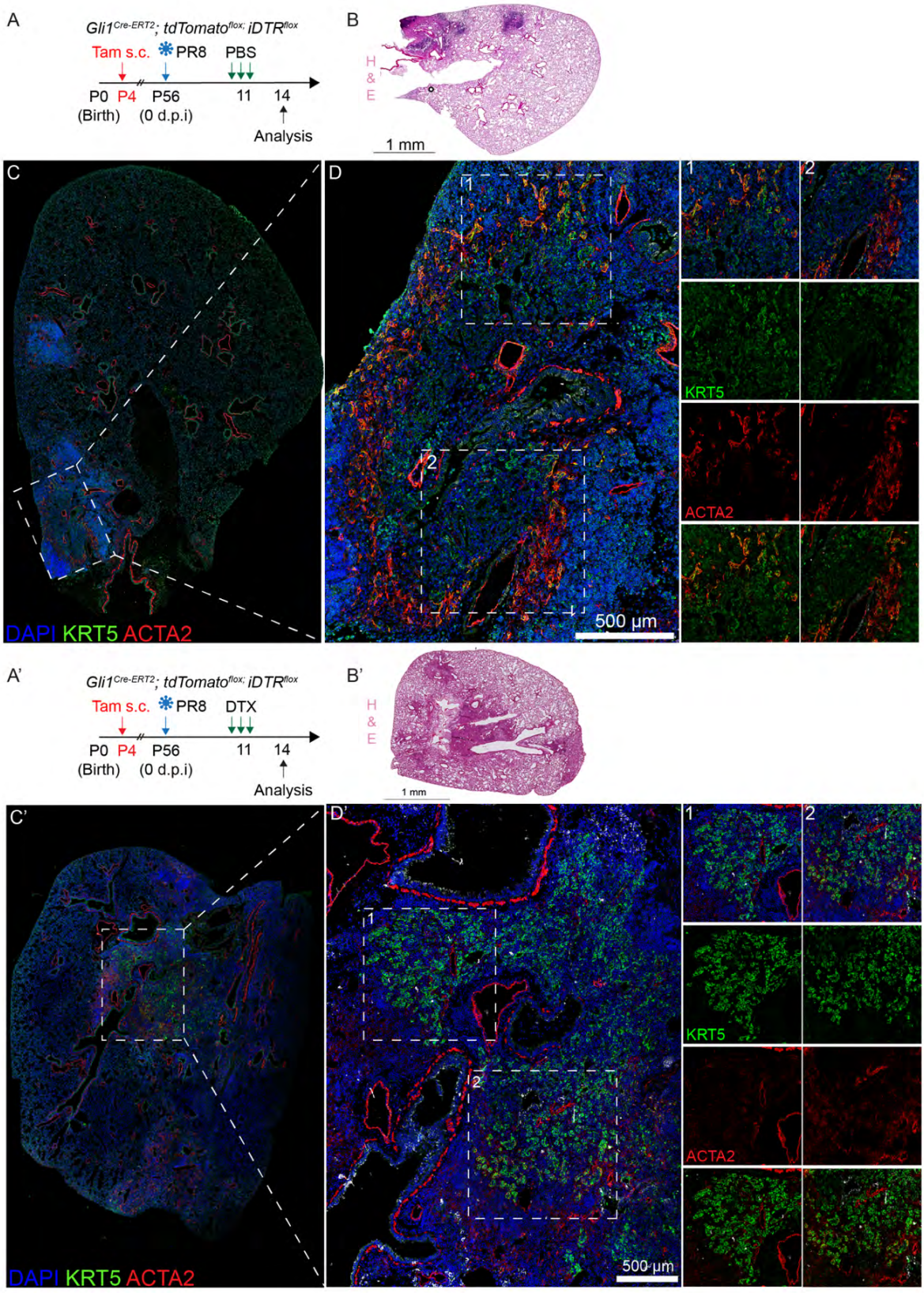
A
Gli1Cre-ERT2; tdTomatoflox; iDTRflox
Tam s.c.
PR8
PBS
P0 P4 P56
11 14
(Birth) (0 d.p.i)
Analysis
B
H & E
1 mm
C
DAPI KRT5 ACTA2
D
1
2
500 µm
KRT5
ACTA2
A'
Gli1Cre-ERT2; tdTomatoflox; iDTRflox
Tam s.c.
PR8
DTX
P0 P4 P56
11 14
(Birth) (0 d.p.i)
Analysis
B'
H & E
1 mm
C'
DAPI KRT5 ACTA2
D'
1
2
500 µm
KRT5
ACTA2

Fig. 14 Ablation of the P4-labeled GLI1+ cells enhance dysplastic repair following influenza-A virus infection.

(A, A') Timeline and experimental design. **(B, B')** Representative hematoxylin and eosin stains. Scale bars: 1mm. **(C, C')** Immunofluorescence using the indicated antibodies. **(D, D')** High-magnification images of the regions shown in dashed boxes in (C, C'). Single-channel images of the regions marked in (D, D') are shown in the right panel. DTX: Diphtheria toxin; i.p.: Intraperitoneal injection; PR8: A/Puerto Rico/8/34 H1N; s.c.: Subcutaneous injection; Tam: Tamoxifen. Scale bars: 500 μm.

4.3.3. Ablation of GLI1+ cells preferentially depletes AMF-like cells and impairs alveolar regeneration following influenza virus-induced lung injury

The data described above suggest that GLI+ cells emerge and expand in response to influenza virus-induced lung injury. To test the requirement of adult GLI1+ cells, *Gli1*$^{Cre\text{-}ERT2}$*; tdTomato*^{flox}*; iDTR*^{flox} mice were infected with PR8, cells were labeled, and DTX or PBS was administered at days 10, 11, and 12 **(Fig. 15A, B)**. Since the GLI1+ population is heterogeneous, it was pertinent to determine which clusters are depleted upon ablation and whether the failed regeneration phenotype is associated with loss of MyoFBs. Therefore, the remaining tdTom+ cells from DTX-treated animals and total tdTom+ cells from PBS-treated animals were FACS-sorted and subjected to scRNA-seq (**Fig. 15E, F**). The analysis revealed that the MyoFB cluster was preferentially depleted while the proportion of the AF1/2 clusters was not significantly altered (**Fig. 15E-K**). GSEA was performed for the AMF signature in the MyoFB cluster and a highly significant downregulation of this signature was observed in the ablated group (**Fig. 15L**). A heatmap showing downregulation of selected genes is shown in (**Fig. 16D**).

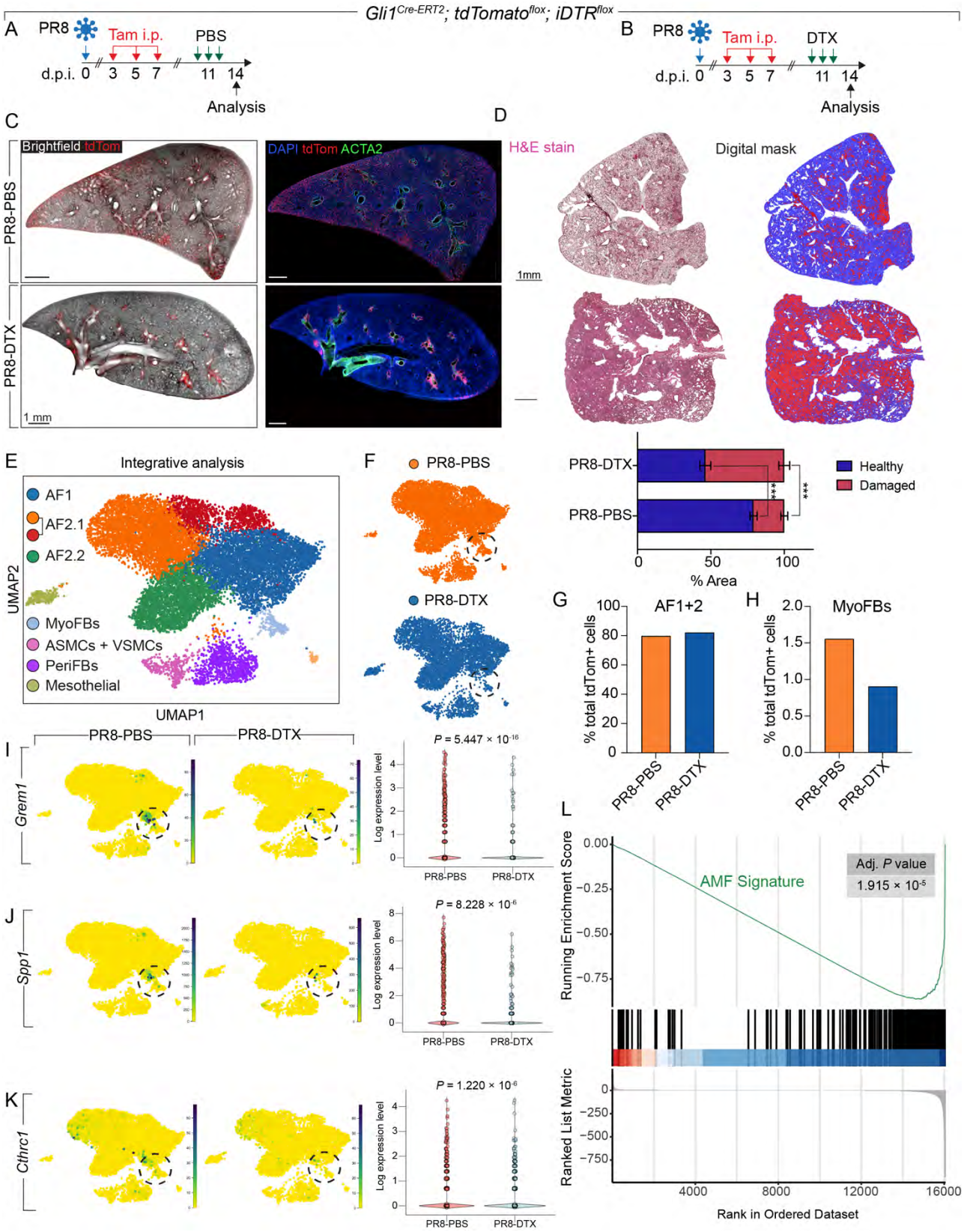
Gli1Cre-ERT2; tdTomatoflox; iDTRflox
A
PR8
Tam i.p.
PBS
d.p.i. 0 3 5 7 11 14
Analysis
B
PR8
Tam i.p.
DTX
d.p.i. 0 3 5 7 11 14
Analysis
C
PR8-PBS
PR8-DTX
Brightfield tdTom
DAPI tdTom ACTA2
1 mm
D
H&E stain
Digital mask
1mm
PR8-DTX
PR8-PBS
Healthy
Damaged
***
0 50 100
% Area
E
Integrative analysis
AF1
AF2.1
AF2.2
MyoFBs
ASMCs + VSMCs
PeriFBs
Mesothelial
UMAP2
UMAP1
F
PR8-PBS
PR8-DTX
G
AF1+2
% total tdTom+ cells
100 80 60 40 20 0
PR8-PBS
PR8-DTX
H
MyoFBs
% total tdTom+ cells
2.0 1.5 1.0 0.5 0.0
PR8-PBS
PR8-DTX
I
Grem1
PR8-PBS
PR8-DTX
P = 5.447 × 10-16
Log expression level
PR8-PBS
PR8-DTX
J
Spp1
P = 8.228 × 10-6
Log expression level
PR8-PBS
PR8-DTX
K
Cthrc1
P = 1.220 × 10-6
Log expression level
PR8-PBS
PR8-DTX
L
AMF Signature
Adj. P value
1.915 × 10-5
Running Enrichment Score
0.00 −0.25 −0.50 −0.75
Ranked List Metric
0 −250 −500 −750
4000 8000 12000 16000
Rank in Ordered Dataset

Fig. 15 GLI1+ cell ablation during regeneration preferentially depletes AMF-like cells and significantly downregulates the AMF signature.

(A, B) Timeline and experimental design. **(C)** Brightfield and fluorescent images validating tdTom+ cell ablation. **(D)** Hematoxylin and eosin stains and digital masks showing impaired regeneration upon cell ablation. **(E)** Integrative analysis of control and ablated samples. **(F)** UMAPs for the individual samples highlighting the MyoFB cluster. **(G, H)** Quantifications of AF1/2 and MyoFB clusters in both experimental conditions. **(I-K)** UMAPs showing selected MyoFB marker genes in both experimental conditions. **(L)** Gene set enrichment analysis (GSEA) showing significant downregulation of the P7 AMF signature (top 200 DEGs extracted from P7 scRNA-seq dataset in Fig. 3 in the PR8-DTX sample. (C, D) n = 3 per group. Data are represented as mean +/- SEM. *** $P < 0.001$. AF1: Alveolar fibroblasts 1; AF2: Alveolar fibroblasts 2/Matrix fibroblasts 2/Adventitial fibroblasts; DTX: Diphtheria toxin; Hi. Prolif. FBs: Highly proliferative fibroblasts; i.p.: Intraperitoneal injection; MyoFBs: Myofibroblasts; PeriFBs: Peribronchial fibroblasts; PR8: A/Puerto Rico/8/34 H1N1; SMCs: Smooth muscle cells; Tam: Tamoxifen. n =3 animals per group. The initial number of cells sequenced for PR8-PBS and PR8-DTX was 8,230 and 6,075, respectively. Cluster 10 (leiden 0.4) was identified as a contaminant and therefore removed. The final number of cells analyzed for PR8-PBS and PR8-DTX are 8,199 and 6,049 respectively.

4.3.4. The failed regeneration phenotype after ablation of GLI1+ is associated with loss of MyoFBs and not AFs

As another layer of validation to confirm that AMF-like MyoFBs are preferentially ablated (**Fig. 16A**), GSEA for AF1 and AF2 signatures were also carried out in the respective clusters and, unlike the AMF signature, we could not detect strong differences in the ablated samples compared to controls (**Fig. 16B, C, E, F**). Finally, GO analysis of the MyoFB AMF-like cluster showed that while typical developmental and ECM pathways were highly enriched in the control group, these pathways were not enriched in the ablated sample (**Fig. 16G**); rather, the top pathways in the ablated sample include apoptotic and cell death pathways in addition to metabolic processes (**Fig. 16G**).

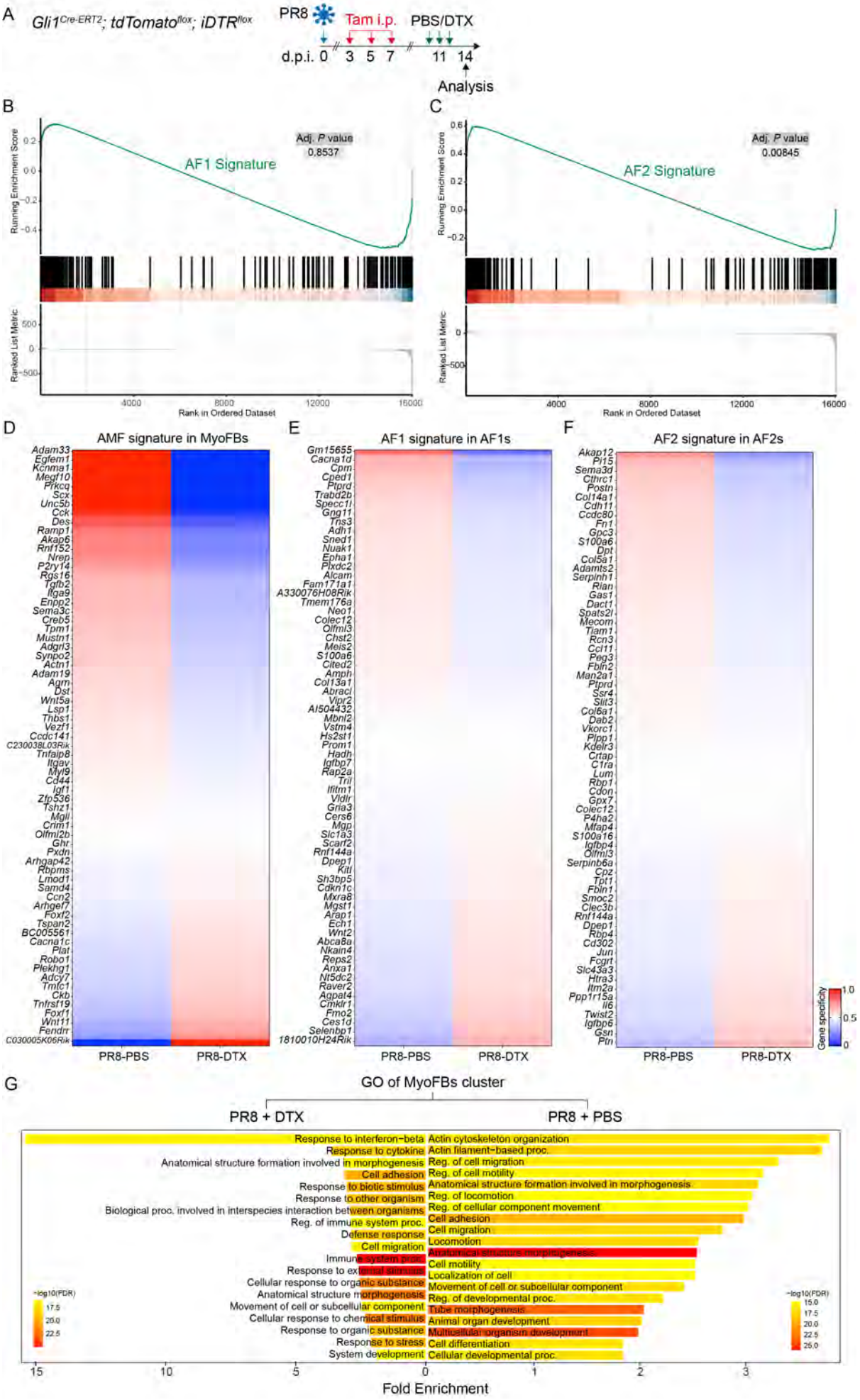
A
Gli1Cre-ERT2; tdTomatoflox; iDTRflox
PR8
Tam i.p.
PBS/DTX
d.p.i. 0 3 5 7 11 14
Analysis
B
AF1 Signature
Adj. P value
0.8537
Running Enrichment Score
Ranked List Metric
Rank in Ordered Dataset
C
AF2 Signature
Adj. P value
0.00845
D
AMF signature in MyoFBs
E
AF1 signature in AF1s
F
AF2 signature in AF2s
PR8-PBS
PR8-DTX
Gene specificity
G
GO of MyoFBs cluster
PR8 + DTX
PR8 + PBS
Response to interferon-beta
Response to cytokine
Anatomical structure formation involved in morphogenesis
Cell adhesion
Response to biotic stimulus
Response to other organism
Biological proc. involved in interspecies interaction between organisms
Reg. of immune system proc.
Defense response
Cell migration
Immune system proc.
Response to external stimulus
Cellular response to organic substance
Anatomical structure morphogenesis
Movement of cell or subcellular component
Cellular response to chemical stimulus
Response to organic substance
Response to stress
System development
Actin cytoskeleton organization
Actin filament-based proc.
Reg. of cell migration
Reg. of cell motility
Anatomical structure formation involved in morphogenesis
Reg. of locomotion
Reg. of cellular component movement
Cell adhesion
Cell migration
Locomotion
Anatomical structure morphogenesis
Cell motility
Localization of cell
Movement of cell or subcellular component
Reg. of developmental proc.
Tube morphogenesis
Animal organ development
Multicellular organism development
Cell differentiation
Cellular developmental proc.
-log10(FDR)
Fold Enrichment

Fig. 16 Ablation of GLI1+ cells preferentially downregulate the AMF but not the alveolar fibroblast gene signature.

(A) Timeline and experimental design. **(B)** Gene set enrichment analysis for the P7 AF1 signature (top 200 DEGs) in the AF1 cluster in PBS and DTX groups. **(C)** Gene set enrichment analysis for the P7 AF2 signature (top 200 DEGs) in the AF2 clusters in PBS and DTX groups. **(D)** Heatmap showing the top 200 DEGs of the P7 AMF signature in the MyoFB (AMF-like) cluster in PBS and DTX groups. Every third gene is shown. **(E)** Heatmap showing the P7 AF1 signature (the top 200 DEGs) in the AF1 cluster in PBS and DTX groups. Every third gene is shown. **(F)** Heatmap showing the P7 AF2 signature in the AF2 clusters in PBS and DTX groups. Every third gene is shown. **(G)** Gene ontology analysis for the top 500 DEGs in control and ablated samples. AF1: Alveolar fibroblasts 1; AF2: Alveolar fibroblasts 2/Matrix fibroblasts 2/Adventitial fibroblasts; AMF: Alveolar myofibroblast; DTX: Diphtheria toxin; i.p.: Intraperitoneal injection; PR8: A/Puerto Rico/8/34 H1N1; Tam: Tamoxifen.

4.3.5. AMF-like cells are severely reduced in human COPD lungs and their persistent activation is associated with lethal non-resolving fibrotic ARDS

To investigate the significance of our findings in the human context, IF was carried out on sections from human donor and COPD lung explants. While donor lungs showed baseline levels of CTHRC1 and KI-67 expression in the alveolar regions **(Fig. 17A, C, E)**, the expression of these markers was almost completely diminished in the enlarged alveoli of emphysematous COPD lungs **(Fig. 17B, D, F)**. Gene expression analysis using lung homogenates from these explanted lungs confirmed the strong downregulation of *GLI1* **(Fig. 17G)** and *CTHRC1* **(Fig. 17H)**. Finally, IF on lung sections from autopsies from IAV ARDS patients revealed strong expression of ACTA2 and CTHRC1 in heavily remodeled regions of the lung, a pattern that is reminiscent of interstitial lung disease such as idiopathic pulmonary fibrosis (IPF) **(Fig. 17I-K)**. These findings indicate that persistent activation of AMF-like cells in response to IAV-induced pneumonia is likely linked to non-resolving fibrosis in lethal ARDS.

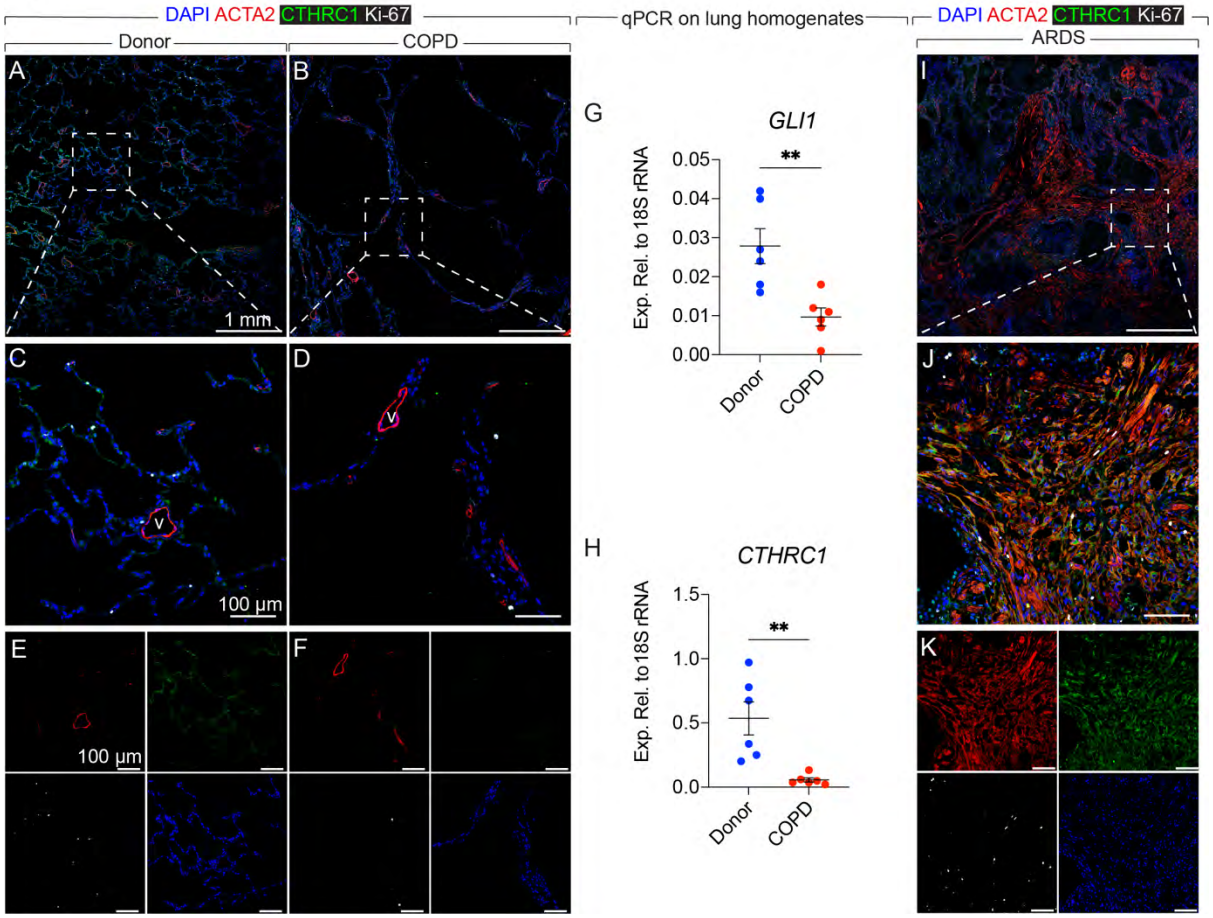

Fig. 17 Perturbation of AMF-like cells is associated with failed regeneration in the human lung.

(A, B) Immunofluorescence using the indicated antibodies on donor and COPD lung explants. **(C, D)** High-magnification images of the regions shown in the dashed boxes in (A, B). The letter “v” in (C, D) indicates blood vessels. **(E-F)** Single-channel images of the regions shown in (C, D). **(G, H)** Quantitative PCR on lung homogenates from donor and COPD lung samples. **(I)** Immunofluorescence using the indicated antibodies on an ARDS lung autopsy. **(J)** High-magnification image of the region shown in the dashed box in (I). **(K)** Single-channel images of the region shown in (J). (G, H) n = 6 per group. Data are represented as mean +/- SEM. ** $P < 0.01$. Scale bars: (A, B, I) 1 mm; (C, D, E, F, J, K) 100 µm. ARDS: Acute respiratory distress syndrome; COPD: Chronic obstructive pulmonary disease.

4.4. Model

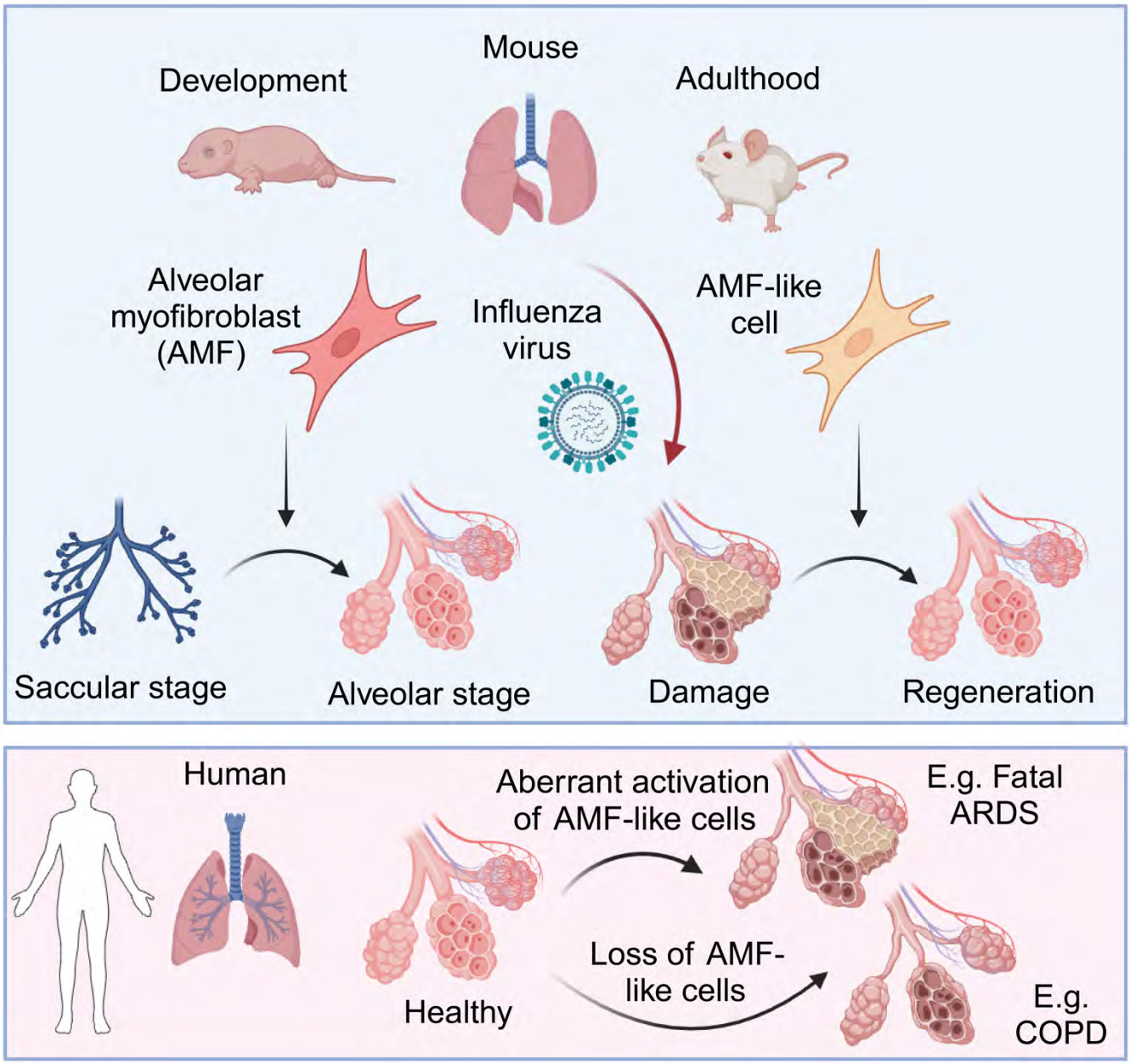

Fig. 18 Model for the role of the AMFs and AMF-like cells in development and regeneration [175]**.**

5. Discussion

5.1. AMFs in lung development, lung homeostasis and aging

Mouse lung development is a meticulously coordinated process involving multiple stages and diverse cell types, each regulated by specific signalling pathways. This development is significantly influenced by mesenchymal-epithelial interactions, which depend on paracrine signalling mediated by secreted ligands and direct cell-cell contacts [185,186]. Previous literature has alluded to the fact that alveolar myofibroblasts (AMFs) play a crucial role in lung development, particularly during the alveolarization phase, which is essential for forming the intricate alveolar network necessary for efficient gas exchange [79]. Despite the importance of the AMF lineage in orchestrating this critical part of lung development, this cell type remains vastly understudied [35,44]. With this study we aim to better our understanding by providing temporal characterization of AMFs during lung development, homoeostatic as well as the aging lung. Using genetic lineage tracing, scRNA-seq, and histological analysis, we uncover the dynamic behaviour of AMFs, our data confirmed that ACTA2+ PDGFRα+ cells are hallmarks of AMFs during the early postnatal period, specifically at postnatal day 7. These cells exhibit high proliferative activity during this period, consistent with their role in promoting alveolar formation through the deposition of ECM components that scaffold the developing alveoli. Unlike previous reports [48,50], we could also observe the persistence of these cells beyond the completion of alveologenesis and into adulthood, albeit in a reduced and less proliferative state. The gradual decline of AMFs during postnatal lung maturation aligns with existing literature which describes the resolution of alveolar myofibroblasts [187 41,48]. Our data also indicate that a subset of these cells persists into adulthood, particularly those traced using the *Gli1*$^{Cre\text{-}ERT2}$ model, which marks cells responding to hedgehog signalling during neonatal development. This persistence may reflect the existence of a reserve population of *Ptch1* responsive fibroblasts that can be reactivated under specific conditions, such as lung injury, to contribute to the tissue repair. These results also suggest a potential transition into other fibroblast lineages or maintenance of a quiescent state until reactivation is necessary. As the lung matures, the remaining AMFs appear to transition into a

homeostatic role, potentially involved in maintaining alveolar structure and function. The observation that these cells continue to express PDGFRα and maintain a more AF-like phenotype suggests that they may contribute to the ongoing turnover and maintenance of the lung's ECM, which is crucial for the integrity and functionality of the alveoli. This finding is further corroborated by recent literature showing that lung fibroblasts, although less active post-development, can be reprogrammed into a more proliferative and ECM-producing state in response to injury or disease[188]. Such reprogramming underscores the plasticity of fibroblasts and their ability to adapt to the changing needs of the lung [179,189].

Our lineage-tracing data demonstrating the persistence of AMFs into adulthood and even into aging, albeit in a less active form, also raises important questions about their potential involvement in age-related lung diseases, such as IPF and COPD. The presence of these cells in aged lungs might also predispose the tissue to fibrotic responses under pathological conditions. This hypothesis is supported by literature suggesting that aging is associated with increased fibroblast activity and ECM deposition, leading to fibrosis [190,191]. The findings that *Gli1*+ AMFs are more persistent than *Acta2*+ AMFs indicate that different subpopulations of myofibroblasts may have distinct roles in lung maintenance and response to injury, potentially providing targets for age-related chronic lung diseases. There are currently no transgenic or knockin mouse lines that allow exclusive labeling of AMFs without collateral labeling of other populations, such as SMCs or AFs. Moreover, while our scRNA-seq analyis deconvolutes the cellular heterogeneity of labeled populations and can also predict differentiation trajectories, it cannot trace the cell origin at later time points or during aging. This limitation hinders our ability to fully understand the dynamic changes and lineage relationships of AMFs over time. Future research using intersectional genetics will allow the neonatal labeling of a pure AMF population and following the fate of these cells during adulthood.

5.2. AMF-like cells in lung Injury and regeneration

The data involving lineage-tracing raised important question about implication of AMFs and their descendant quiescent progeny whether they mimic an AMF-like program playing a crucial role in the lung regeneration. There is also a growing consensus that developmental mechanisms are recapitulated during repair and

regeneration in the adult lung following injury. This concept is particularly relevant in conditions such as IPF and ARDS, where repetitive microinjuries trigger a cycle of injury and repair, ultimately hijacking morphogenic pathways and leading to aberrant remodelling, fibrosis, and respiratory failure. Using animal models for compensatory lung growth following pneumonectomy, balanced regeneration after cigarette smoke exposure, and alveolar repair following influenza-virus-induced ARDS, our findings reveal that mesenchymal cells with an AMF-like program emerge in models of compensatory lung growth after unilateral pneumonectomy and GLI1+ mesenchymal cells emerge to promote balanced alveolar regeneration following cigarette-smoke-induced emphysema. These cells contribute significantly to alveolar regeneration by driving *de novo* alveolarization, thereby playing a crucial role in repair and remodelling lung tissue. Previously, it has been shown that *Gli1*+ mesenchymal cells promote metaplastic differentiation of airway progenitors into KRT5+ basal cells and nancanonical GLI1 signaling has been shown to promote stemness in lung adenocarcinoma [192,193]. We provide evidence that these mesenchymal cells exhibit a gene expression profile with a substantial overlap with the developmental AMFs. This includes upregulation of genes related to ECM organization, proliferation and cell motility, such as *Cthrc1*, *Piezo2, Mki67* and *Nrep*. Our integration approach confirmed that AMFs and the myofibroblasts emerging after influenza infection indeed share a conserved transcriptomic signature with developmental AMFs, gene ontology analysis revealed enrichment with terms like cell division, cell cycle, cellular differentiation and cell proliferation beside tissue development and tube morphogenesis. These data further suggests that the mechanisms driving lung structure and formation during development are redeployed to repair and restore lung function after injury, demonstrating that a subset of mesenchymal cells that mimic developmental AMFs plays a crucial role in lung repair. Our data also indicate a strong interaction between AMF-like cells and AT2 cells which is of particular interest, as AMF-like cells may provide a mesenchymal niche essential for AT2 cell maintenance and proliferation. Recent literature has shown that during lung development, AMFs interact closely with AT1 cells through signalling pathways involving PDGF, WNT, SHH, and IGF [35,42,194]. Disruption of these pathways impairs alveolarization, suggesting that similar interactions are critical during adult lung regeneration. Our data showing AMF-like cells supporting AT2 cell function during Influenza-induced ARDS further

underscores their importance in facilitating epithelial regeneration and highlights the intricate crosstalk between mesenchymal and epithelial compartments crucial for effective tissue repair.

Another intriguing aspect of this study is the strong similarity between AMF-like cells and profibrotic FAMs. Our previous work along with other studies has shown that FGF10+ or PDGFRA+ AFs as source of FAM [179,195] . Our data further suggestes that FGF10+ AFs do not give rise to AMF-like cells during lung regeneration in contrast to aberrant repair and fibrosis where we and others have shown that they are an important source of FAMs [178,193,194]. While the latter cells are detrimental to AT2s, AMF-like cells may represent niche cells that promote the growth of AT2s. Whether the cellular origin per se determines if the arising MyoFBs are regenerative (AMF-like) or profibrotic (FAM) requires further investigations. Some recent reports have also identified *Cthrc1* and *Postn+ as* a marker of transitional fibroblasts that give rise to FAMs [196]. In contrast to AMF-like cells, other mesenchymal populations such as peribronchial fibroblasts (PeriFBs) might also play distinct roles in lung repair. PeriFBs and PeriFB-like cells are thought to be more involved in airway repair rather than alveolar regeneration [174,197]. Ex vivo alveolosphere assays also confirms that enrichment of AMF-like cells, but not PeriFBs (Data not shown), enhances colony forming efficiency in alveolosphere formation, indicating that AMF-like cells possess the specific morphogenic potential required for regenerating alveolar compartments. To date, there is a gap in the knowledge regarding fibroblasts heterogeneity, a recent study and initiative “CellCards” [168] has helped bridge this divide but further work in this direction is needed to develop a comprehensive lung mesenchymal cell atlas to demystify both the lung fibroblast biology and their pathology [78].

Advances in the sequential labelling and timely controlled deletion of cells in transgenic mice using cre-inducible expression of the diphtheria toxin receptor (DTR) have significantly expanded our ability to investigate the functional requirements of specific genes in lung injuries [198–201]. This approach allows to precisely target and delete specific cell populations at desired time points, providing a powerful tool to study the roles of these cells and their underlying mechanisms under pathological conditions. In this lieu, previous studies have shown that ablation of *Gli1+* cells ameliorates multi-organ fibrosis [202], we have recently shown that

partial ablation of GLI1+ cells greatly prevented vascular remodeling in response to hypoxia and attenuated the increase in right ventricular systolic pressure and right heart hypertrophy [96]. Our data in this study suggest that the selective ablation of both P4-labeled GLI1+ cells and GLI+ AMF-like cells in adult lungs significantly impaired the repair processes, leading to exaggerated dysplastic repair in areas of extensive damage. This finding is particularly notable given the relatively low abundance of AMF-like cells, yet their critical role in maintaining lung homeostasis and promoting effective regeneration. Taken together, our data with comprehensive transcriptomic profiling of AMF-like cells throughout lung development, adulthood, and regeneration reveals that adult AMF-like cells upregulate a developmental gene signature during alveolar regeneration. This ability of AMFs to reactivate developmental programs and deploy their specific morphogenic potential underscore their significance in both normal and pathological lung repair processes further supporting the idea that these cells recapitulate developmental processes to drive tissue repair. Importantly, the ablation of AMF-like cells disrupts these processes, leading to impaired regeneration and increased fibrosis, particularly in pathological conditions such as severe ARDS.

5.3. Implications for regeneration and therapeutic strategies

Previous studies have associated lung mesenchymal cells with various human diseases. These cells play a critical role in the development, maintenance, and repair of lung tissue by participating in several signalling pathways that regulate homeostasis, maintain pulmonary homeostasis and modulate immune response by releasing trophic factors and responds to injury [51,203–205]. However, in chronic lung diseases, their ability to facilitate repair is diminished, contributing to disease pathogenesis through altered secretory and immunomodulatory properties [206,207]. In chronic obstructive pulmonary disease (COPD), mesenchymal cells contribute to pathological remodelling of the lung tissue. COPD is often complicated by pulmonary hypertension (PH), where the increased pressure in the pulmonary arteries exacerbates the disease. In this context, we have recently shown that *GLI1* is upregulated in COPD lungs with pulmonary hypertension. Additionally, in COPD with emphysema, the destruction of alveolar structures is partly driven by the dysregulated activity of mesenchymal cells, which fail to repair the damaged tissue

effectively [95]. Idiopathic pulmonary fibrosis (IPF) is another condition where lung mesenchymal cells are significantly involved. In IPF, these cells become activated and proliferate abnormally, leading to excessive deposition of extracellular matrix and fibrosis, this pathological process results in the stiffening of lung tissue and severe impairment of gas exchange [208–211]. Notably, our previous work has identified metformin and rosiglitazone in the management of TGFβ1-mediated fibrogenesis [179,212]. Acute respiratory distress syndrome (ARDS) is a severe condition characterized by rapid onset of widespread inflammation in the lungs [98,213]. Lung mesenchymal cells are also implicated in the inflammatory response and tissue repair processes in the ARDS [214]. However, their role just like other chronic lung disease can be a double-edged sword. While these cells contribute to the repair of damaged alveolar structures, their excessive activation can lead to fibrosis and long-term impairment of lung function. The interplay between mesenchymal cells with other niches such as immune, epithelial and endothelial cells is a complex process and remains an area of active research. To further understand our findings from murine models in human disease, we analysed human tissue material from patients with COPD and influenza-induced ARDS. Our findings revealed that AMF-like cells are severely reduced in human COPD lungs, where this dysregulation and lack of mechanical force exerted by these cells might contribute to ineffective repair of alveolar structures and the progression of emphysema. Our data also indicate that their persistent activation is associated with lethal non-resolving fibrotic ARDS, further complicating the disease and reducing recovery chances. Future research should focus on identifying specific markers and response pathways involved in AMF activation during regeneration, which could reveal potential therapeutic targets for modulating AMF-like activity. Targeting these pathways could help mitigate damage by ensuring timely activation of AMFs while preventing their divergence into a fibrotic, FAM-like phenotype, thereby allowing necessary repair processes to proceed. The persistence of AMFs into adulthood and the emergence of AMF-like cells during injury repair suggest that these cells could be harnessed to enhance repair in conditions where lung function is compromised. Conversely, controlled upregulation of the AMF-like program might benefit conditions where lung regeneration is impaired, such as aging or chronic lung diseases. However, precise modulation of the AMF program might prevent the activation of fibrotic pathways that could worsen lung pathology.

Collectively, these findings suggest that AMF-like cells are key players in lung regeneration, with their activity finely balanced between promoting scarless regeneration and potentially leading to non-resolving fibrosis. This balance is influenced by the microenvironmental and molecular cues they receive, which can either support their regenerative potential or drive them towards a fibrotic phenotype. Manipulating these cues offers a promising avenue for developing innovative therapeutic strategies aimed at promoting alveolar regeneration in chronic lung diseases. Future research should focus on elucidating the signalling mechanisms that balance repair and fibrosis in AMF-like cells, with the aim of developing targeted therapies that promote lung regeneration without inducing fibrosis.

6. Conclusion

This study provides a comprehensive characterization of alveolar myofibroblasts (AMFs) and their critical roles in lung development, homeostasis, and regeneration. Our findings underscore the pivotal role of AMFs in forming and maintaining alveolar structures during lung maturation and their reactivation in response to lung injury. The persistence of AMFs into adulthood and their reactivation as AMF-like cells during lung regeneration highlight their significance in both normal and pathological lung repair processes.

AMFs are characterized by expression of ACTA2+ PDGFRα+, are highly proliferative during the early postnatal period, contributing to alveolar formation through ECM deposition. Contrary to previous reports, a subset of these cells persists beyond developmental alveologenesis into adulthood, maintaining a homeostatic role in the lung. AMF-like cells re-emerge during lung regeneration following pneumonectomy, cigarette smoke exposure, and influenza-virus-induced ARDS. These cells recapitulate developmental programs to drive de novo alveolarization, playing a crucial role in tissue repair. AMF-like cells interact closely with alveolar type II (AT2) cells, providing a supportive niche essential for effective tissue repair. This interaction is critical for maintaining lung homeostasis and facilitating recovery from injury. While AMF-like cells are essential for promoting regeneration, their prolonged activation under pathological conditions can lead to non-resolving fibrosis. This dual role highlights the need for precise modulation of AMF activity to balance repair and fibrosis.

The findings suggest potential therapeutic strategies targeting AMF-like cells to enhance lung repair while minimizing the risk of fibrosis. Understanding the molecular cues that govern AMF activation and differentiation could lead to innovative treatments for chronic lung diseases.

7. Limitations

Despite the advances laid forward by this work, several limitations should be acknowledged. The conclusions drawn from this study are primarily based on mouse models, including those involving pneumonectomy, cigarette smoke exposure, and influenza virus-induced lung injury. While these models are highly informative, there may be differences in AMF-like cell behaviour and lung regeneration mechanisms between mice and humans. Therefore, the direct translation of these findings to human lung disease requires further validation in human tissue samples to ensure conserved phenotype between the two or utilize advanced humanized models. The study provides a critical snapshot of AMFs and AMF-like cell behaviour at various stages of development, homeostasis, aging, and regeneration. However, the inherently dynamic nature of lung regeneration challenges the temporal resolution of scRNA-seq and related analyses, potentially obscuring the full continuum of cellular transitions and interactions over time. Future studies could greatly benefit from longitudinal approaches that enable real-time tracking of these cells across different stages of injury and repair. Advanced single-cell lineage tracing technologies, such as heritable DNA barcoding, could be employed to integrate lineage history with single-cell transcriptomic profiles [215]. This approach would offer a more comprehensive and precise understanding of cellular dynamics during lung regeneration, capturing the intricate temporal patterns that current methods may miss. The heterogeneity within lung fibroblasts population remains another area of uncertainty. The findings suggest that different subpopulations of AMF-like cells may have distinct roles in balanced regeneration versus fibrosis. However, the exact molecular markers, transcription factors and signalling pathways that define and influence these subpopulations are not fully elucidated, leaving gaps in the understanding of how to selectively target regenerative versus AMF-like cell driven-fibrotic phenotype switching. We also incorporated ex vivo assays, including alveolosphere formation, to evaluate the regenerative potential of AMF-like cells. While these assays are instrumental in providing insights, they may not fully replicate the intricate in vivo lung environment, where diverse cell types and biophysical forces converge. Consequently, the findings from ex vivo

models should be interpreted with caution and rigorously validated in vivo to confirm their applicability to bona fide lung regeneration processes. Additionally, in vivo validation could reveal context-dependent behaviours of AMF-like cells that are not evident in ex vivo conditions, further emphasizing the importance of complementary in vivo studies. A more comprehensive understanding of lung regeneration will likely require integrating ex vivo findings with advanced models such as PCLS that better mimic the complexity of the lung's microenvironment. Given these limitations, future research could greatly benefit by using dual recombinase-mediated intersectional genetic reporters [216–218], where using both Dre-rox and Cre-loxP recombinations will allow labelling of a pure AMF population neonatally and following the fate of these cells during adulthood, therefore improving the temporal resolution of such investigations. Another important area of focus should be the development of targeted therapeutic strategies that can modulate AMF-like cell activity without affecting other vital cellular functions. This could include the use of nanoparticle-based delivery systems or localized gene editing techniques [219]. Incorporating studies on the role of biophysical forces, such as mechanical stretch and lung biomechanics, in the activation of AMF-like cells during regeneration [220]. Understanding how these forces interact with molecular signals could lead to new approaches for targeted lung repair.

8. Summary

This work investigated the critical role of AMFs in lung development, homeostasis, and regeneration, with a particular focus on their behaviour during postnatal lung maturation and in response to various lung injuries. Utilizing advanced genetic lineage tracing, scRNA-seq, and detailed histological techniques, this research explores the dynamic nature of AMFs and their descendants, revealing their significance not only in early lung development but also in adult lung repair processes. The study begins with a thorough examination of lung development, highlighting the prominent presence of AMFs during the alveolarization phase. AMFs, characterized by their ACTA2+ PDGFRα+ markers, play a pivotal role in forming the alveolar network by depositing essential ECM components. While these cells were traditionally thought to resolve after developmental alveologenesis, the findings suggest that a subset of AMFs persists into adulthood, particularly those responsive to hedgehog signalling during neonatal stages. This persistence suggests the existence of a reserve population of fibroblasts that can be reactivated under specific conditions, such as lung injury, to contribute to tissue repair.

In the context of lung injury, the study explores the reactivation of AMF-like cells during lung regeneration following pneumonectomy, cigarette smoke exposure, and influenza virus-induced ARDS. The results demonstrate that these cells recapitulate developmental programs to drive lung repair, particularly through the process of de novo alveolarization. However, a dual role of AMF-like cells is uncovered, showing that while they are essential for promoting regeneration, their prolonged activation under pathological conditions can lead to non-resolving fibrosis.

This work emphasizes the complex nature of AMFs and AMF-like cell behaviour, particularly their involvement in both scarless regeneration and fibrotic processes. It suggests that the balance between these outcomes is influenced by microenvironmental cues and molecular signals, offering potential avenues for therapeutic intervention. The study concludes with a call for further research into the mechanisms governing AMF-like cell activity, with the goal of developing targeted therapies that harness their regenerative potential while minimizing the risk of chronic lung diseases.

9. Zusammenfassung

Diese Arbeit untersucht die kritische Rolle von AMFs bei der Entwicklung, Homöostase sowie der Regeneration der Lunge mit einem besonderen Fokus auf ihr Verhalten während der postnatalen Lungenreifung und als Reaktion auf verschiedene Lungenverletzungen. Unter Verwendung fortschrittlicher genetischer Abstammungsanalysen, scRNA-Sequenzierung sowie detaillierter histologischer Techniken, erforscht diese Studie die dynamische Natur der AMFs und ihrer Nachkommen und zeigt ihre Bedeutung nicht nur in der frühen Lungenentwicklung, sondern auch in den Reparaturprozessen der adulten Lunge auf. Die Studie beginnt mit einer umfassenden Untersuchung der Lungenentwicklung und hebt die starke Präsenz der AMFs während der Alveolarisierungsphase hervor. AMFs, welche durch ihre ACTA2+ PDGFRα+ Marker gekennzeichnet werden, spielen eine zentrale Rolle bei der Bildung des alveolären Netzwerkes durch Ablagerung wesentlicher ECM-Komponenten. Während man bisher davon ausging, dass sich diese Zellen nach der Alveologenese auflösen, deuten die Ergebnisse darauf hin, dass eine Untergruppe der AMFs bis ins Erwachsenenalter bestehen bleibt, insbesondere diejenigen, die während des neonatalen Stadiums auf Hedgehog-Signale reagieren. Diese Persistenz deutet auf eine Existenz einer Reservepopulation von Fibroblasten hin, welche unter bestimmten Bedingungen, wie beispielsweise nach einer Lungenverletzung, reaktiviert werden können, um zur Gewebereparatur beizutragen.

Im Zusammenhang mit Lungenverletzungen untersucht diese Studie die Reaktivierung von AMF-ähnlichen Zellen während der Regeneration der Lunge nach Pneumektomie, Zigarettenrauch-Exposition sowie Influenzavirus induziertem ARDS. Die Ergebnisse zeigen, dass diese Zellen Entwicklungsprogramme erneut durchlaufen, um die Lungenreparatur voranzutreiben, insbesondere durch den Prozess der de novo Alveolarisierung. Allerdings wird eine doppelte Rolle der AMF-ähnlichen Zellen aufgedeckt, welche zeigt, dass sie zwar für die Förderung der Regeneration wesentlich sind, ihre anhaltende Aktivierung unter pathologischen Bedingungen jedoch zu einer sich nicht auflösenden Fibrose führen kann.

Diese Arbeit unterstreicht die komplexe Natur der AMFs sowie das Verhalten AMF-ähnlicher Zellen, insbesondere ihre Beteiligung sowohl an narbenloser Regeneration als auch an fibrotischen Prozessen. Es deutet darauf hin, dass das

Gleichgewicht zwischen diesen Ergebnissen durch die Mikroumgebung und molekularen Signalen beeinflusst wird, was potenzielle Ansatzpunkte für therapeutische Eingriffe bietet. Die Studie schließt mit einem Aufruf zur weiteren Forschung der Mechanismen, welche die Aktivität der AMF-ähnlichen Zellen steuern, mit dem Ziel, gezielte Therapien zu entwickeln, die ihr regeneratives Potenzial nutzen, während das Risiko chronischer Lungenerkrankungen minimiert wird.

10. References

1. Kina, Y.P., Khadim, A., Seeger, W., and El Agha, E. (2021). The Lung Vasculature: A Driver or Passenger in Lung Branching Morphogenesis? Frontiers in Cell and Developmental Biology *8*.

2. Negretti, N.M., Plosa, E.J., Benjamin, J.T., Schuler, B.A., Habermann, A.C., Jetter, C.S., Gulleman, P., Bunn, C., Hackett, A.N., Ransom, M., et al. (2021). A single-cell atlas of mouse lung development. Development *148*, dev199512. https://doi.org/10.1242/dev.199512.

3. Duong, T.E., Wu, Y., Sos, B.C., Dong, W., Limaye, S., Rivier, L.H., Myers, G., Hagood, J.S., and Zhang, K. (2022). A single-cell regulatory map of postnatal lung alveologenesis in humans and mice. Cell Genomics *2*, 100108. https://doi.org/10.1016/j.xgen.2022.100108.

4. Domyan, E.T., and Sun, X. (2011). Patterning and Plasticity in Development of the Respiratory Lineage. Dev Dyn *240*, 477–485. https://doi.org/10.1002/dvdy.22504.

5. El Agha, E., Herold, S., Al Alam, D., Quantius, J., MacKenzie, B., Carraro, G., Moiseenko, A., Chao, C.-M., Minoo, P., Seeger, W., et al. (2014). Fgf10-positive cells represent a progenitor cell population during lung development and postnatally. Development (Cambridge, England) *141*, 296–306. https://doi.org/10.1242/dev.099747.

6. Bellusci, S., Grindley, J., Emoto, H., Itoh, N., and Hogan, B.L.M. (1997). Fibroblast Growth Factor 10 (FGF10) and branching morphogenesis in the embryonic mouse lung. Development *124*, 4867–4878. https://doi.org/10.1242/dev.124.23.4867.

7. Ramalho-Santos, M., Melton, D.A., and McMahon, A.P. (2000). Hedgehog signals regulate multiple aspects of gastrointestinal development. Development *127*, 2763–2772. https://doi.org/10.1242/dev.127.12.2763.

8. Morrisey, E.E., and Hogan, B.L.M. (2010). Preparing for the First Breath: Genetic and Cellular Mechanisms in Lung Development. Developmental Cell *18*, 8–23. https://doi.org/10.1016/j.devcel.2009.12.010.

9. Ishii, T., Itoh, K., Takahashi, S., Sato, H., Yanagawa, T., Katoh, Y., Bannai, S., and Yamamoto, M. (2000). Transcription factor Nrf2 coordinately regulates a group of oxidative stress-inducible genes in macrophages. J Biol Chem *275*, 16023–16029. https://doi.org/10.1074/jbc.275.21.16023.

10. Zorn, A.M., and Wells, J.M. (2009). Vertebrate Endoderm Development and Organ Formation. Annual Review of Cell and Developmental Biology *25*, 221–251. https://doi.org/10.1146/annurev.cellbio.042308.113344.

11. Caprioli, A., Villasenor, A., Wylie, L.A., Braitsch, C., Marty-Santos, L., Barry, D., Karner, C.M., Fu, S., Meadows, S.M., Carroll, T.J., et al. (2015). Wnt4 is essential to normal mammalian lung development. Developmental Biology *406*, 222–234. https://doi.org/10.1016/j.ydbio.2015.08.017.

12. Ornitz, D.M., and Yin, Y. (2012). Signaling networks regulating development of the lower respiratory tract. Cold Spring Harbor perspectives in biology *4*. https://doi.org/10.1101/cshperspect.a008318.

13. Weaver, M., Dunn, N.R., and Hogan, B.L.M. (2000). Bmp4 and Fgf10 play opposing roles during lung bud morphogenesis. Development *127*, 2695–2704.

14. Hines, E.A., Jones, M.-K.N., Verheyden, J.M., Harvey, J.F., and Sun, X. (2013). Establishment of smooth muscle and cartilage juxtaposition in the developing mouse upper airways. Proceedings of the National Academy of Sciences *110*, 19444–19449. https://doi.org/10.1073/pnas.1313223110.

15. Establishment of smooth muscle and cartilage juxtaposition in the developing mouse upper airways | PNAS https://www.pnas.org/doi/full/10.1073/pnas.1313223110.

16. Chacón-Martínez, C.A., Koester, J., and Wickström, S.A. (2018). Signaling in the stem cell niche: regulating cell fate, function and plasticity. Development *145*, dev165399. https://doi.org/10.1242/dev.165399.

17. Metzger, R.J., Klein, O.D., Martin, G.R., and Krasnow, M.A. (2008). The branching programme of mouse lung development. Nature *453*, 745–750. https://doi.org/nature07005 [pii] 10.1038/nature07005.

18. Whitsett, J.A., Kalin, T.V., Xu, Y., and Kalinichenko, V.V. (2019). Building and Regenerating the Lung Cell by Cell. Physiol Rev *99*, 513–554. https://doi.org/10.1152/physrev.00001.2018.

19. Kadzik, R.S., Cohen, E.D., Morley, M.P., Stewart, K.M., Lu, M.M., and Morrisey, E.E. (2014). Wnt ligand/Frizzled 2 receptor signaling regulates tube shape and branch-point formation in the lung through control of epithelial cell shape. Proceedings of the National Academy of Sciences of the United States of America *111*, 12444–12449. https://doi.org/10.1073/pnas.1406639111.

20. Lin, C., Yao, E., Zhang, K., Jiang, X., Croll, S., Thompson-Peer, K., and Chuang, P.-T. (2017). YAP is essential for mechanical force production and epithelial cell proliferation during lung branching morphogenesis. eLife *6*, e21130. https://doi.org/10.7554/eLife.21130.

21. Li, M., Li, C., Liu, Y., Xing, Y., Hu, L., Borok, Z., Kwong, K.Y.-C., and Minoo, P. (2008). Mesodermal Deletion of Transforming Growth Factor-β Receptor II Disrupts Lung Epithelial Morphogenesis: CROSS-TALK BETWEEN TGF-β AND SONIC HEDGEHOG PATHWAYS *. Journal of Biological Chemistry *283*, 36257–36264. https://doi.org/10.1074/jbc.M806786200.

22. FGF9 and FGF10 activate distinct signaling pathways to direct lung epithelial specification and branching | Science Signaling https://www.science.org/doi/10.1126/scisignal.aay4353?url_ver=Z39.88-2003&rfr_id=ori:rid:crossref.org&rfr_dat=cr_pub%20%200pubmed.

23. Kugler, M.C., Joyner, A.L., Loomis, C.A., and Munger, J.S. (2015). Sonic Hedgehog Signaling in the Lung. From Development to Disease. Am J Respir Cell Mol Biol *52*, 1–13. https://doi.org/10.1165/rcmb.2014-0132TR.

24. Rajagopal, J., Carroll, T.J., Guseh, J.S., Bores, S.A., Blank, L.J., Anderson, W.J., Yu, J., Zhou, Q., McMahon, A.P., and Melton, D.A. (2008). Wnt7b stimulates embryonic lung growth by coordinately increasing the replication of epithelium and mesenchyme. Development *135*, 1625–1634. https://doi.org/10.1242/dev.015495.

25. Goss, A.M., Tian, Y., Tsukiyama, T., Cohen, E.D., Zhou, D., Lu, M.M., Yamaguchi, T.P., and Morrisey, E.E. (2009). Wnt2/2b and β-Catenin Signaling Are Necessary and Sufficient to Specify Lung Progenitors in the Foregut. Developmental Cell *17*, 290–298. https://doi.org/10.1016/j.devcel.2009.06.005.

26. Alejandre-Alcázar, M.A., Shalamanov, P.D., Amarie, O.V., Sevilla-Pérez, J., Seeger, W., Eickelberg, O., and Morty, R.E. (2007). Temporal and spatial regulation of bone morphogenetic protein signaling in late lung development. Developmental Dynamics *236*, 2825–2835. https://doi.org/10.1002/dvdy.21293.

27. Liu, K., Meng, X., Liu, Z., Tang, M., Lv, Z., Huang, X., Jin, H., Han, X., Liu, X., Pu, W., et al. (2024). Tracing the origin of alveolar stem cells in lung repair and regeneration. Cell *187*, 2428-2445.e20. https://doi.org/10.1016/j.cell.2024.03.010.

28. Weibel, E.R. (2015). On the Tricks Alveolar Epithelial Cells Play to Make a Good Lung. Am J Respir Crit Care Med *191*, 504–513. https://doi.org/10.1164/rccm.201409-1663OE.

29. Del Moral, P.-M., Sala, F.G., Tefft, D., Shi, W., Keshet, E., Bellusci, S., and Warburton, D. (2006). VEGF-A signaling through Flk-1 is a critical facilitator of early embryonic lung epithelial to endothelial crosstalk and branching morphogenesis. Developmental Biology *290*, 177–188. https://doi.org/10.1016/j.ydbio.2005.11.022.

30. Healy, A.M., Morgenthau, L., Zhu, X., Farber, H.W., and Cardoso, W.V. (2000). VEGF is deposited in the subepithelial matrix at the leading edge of branching airways and stimulates neovascularization in the murine embryonic lung. Dev Dyn *219*, 341–352. https://doi.org/10.1002/1097-0177(2000)9999:9999<::AID-DVDY1061>3.0.CO;2-M [pii] 10.1002/1097-0177(2000)9999:9999<::AID-DVDY1061>3.0.CO;2-M.

31. Lau, M., Masood, A., Yi, M., Belcastro, R., Li, J., and Tanswell, A.K. (2011). Long-term failure of alveologenesis after an early short-term exposure to a PDGF-receptor antagonist. Am J Physiol Lung Cell Mol Physiol *300*, L534-547. https://doi.org/10.1152/ajplung.00262.2010.

32. Rodríguez-Castillo, J.A., Pérez, D.B., Ntokou, A., Seeger, W., Morty, R.E., and Ahlbrecht, K. (2018). Understanding alveolarization to induce lung regeneration. Respiratory Research *19*, 148. https://doi.org/10.1186/s12931-018-0837-5.

33. Mammoto, A., and Mammoto, T. (2019). Vascular Niche in Lung Alveolar Development, Homeostasis, and Regeneration. Front Bioeng Biotechnol *7*, 318. https://doi.org/10.3389/fbioe.2019.00318.

34. Biasin, V., Crnkovic, S., Sahu-Osen, A., Birnhuber, A., El Agha, E., Sinn, K., Klepetko, W., Olschewski, A., Bellusci, S., Marsh, L.M., et al. (2020). PDGFRα and αSMA mark two distinct mesenchymal cell populations involved in parenchymal and vascular remodeling in pulmonary fibrosis. American journal of physiology. Lung cellular and molecular physiology *318*, L684—-L697. https://doi.org/10.1152/ajplung.00128.2019.

35. Li, C., Li, M., Li, S., Xing, Y., Yang, C.-Y., Li, A., Borok, Z., Langhe, S., and Minoo, P. (2015). Progenitors of Secondary Crest Myofibroblasts Are Developmentally Committed in Early Lung Mesoderm. Stem Cells *33*, 999–1012. https://doi.org/10.1002/stem.1911.

36. He, H., Chen, J., Zhao, J., Zhang, P., Qiao, Y., Wan, H., Wang, J., Mei, M., Bao, S., and Li, Q. (2021). PRMT7 targets of Foxm1 controls alveolar myofibroblast proliferation and differentiation during alveologenesis. Cell Death Dis *12*, 1–11. https://doi.org/10.1038/s41419-021-04129-1.

37. Kugler, M.C., Loomis, C.A., Zhao, Z., Cushman, J.C., Liu, L., and Munger, J.S. (2017). Sonic Hedgehog Signaling Regulates Myofibroblast Function during Alveolar Septum Formation in Murine Postnatal Lung. Am J Respir Cell Mol Biol *57*, 280–293. https://doi.org/10.1165/rcmb.2016-0268OC.

38. Branchfield, K., Li, R., Lungova, V., Verheyden, J.M., McCulley, D., and Sun, X. (2016). A three-dimensional study of alveologenesis in mouse lung. Developmental Biology *409*, 429–441. https://doi.org/10.1016/j.ydbio.2015.11.017.

39. Endale, M., Ahlfeld, S., Bao, E., Chen, X., Green, J., Bess, Z., Weirauch, M.T., Xu, Y., and Perl, A.K. (2017). Temporal, spatial, and phenotypical changes of PDGFRα expressing fibroblasts during late lung development. Dev Biol *425*, 161–175. https://doi.org/10.1016/j.ydbio.2017.03.020.

40. McGowan, S.E., Grossmann, R.E., Kimani, P.W., and Holmes, A.J. (2008). Platelet-derived growth factor receptor-alpha-expressing cells localize to the alveolar entry ring and have characteristics of myofibroblasts during pulmonary alveolar septal formation. Anat Rec (Hoboken) *291*, 1649–1661. https://doi.org/10.1002/ar.20764.

41. Zepp, J.A., Morley, M.P., Loebel, C., Kremp, M.M., Chaudhry, F.N., Basil, M.C., Leach, J.P., Liberti, D.C., Niethamer, T.K., Ying, Y., et al. (2021). Genomic, epigenomic, and biophysical cues controlling the emergence of the lung alveolus. Science *371*, eabc3172. https://doi.org/10.1126/science.abc3172.

42. Gao, F., Li, C., Smith, S.M., Peinado, N., Kohbodi, G., Tran, E., Loh, Y.-H.E., Li, W., Borok, Z., and Minoo, P. (2022). Decoding the IGF1 signaling gene regulatory network behind alveologenesis from a mouse model of

bronchopulmonary dysplasia. eLife *11*, e77522. https://doi.org/10.7554/eLife.77522.

43. Riccetti, M.R., Green, J., Taylor, T.J., and Perl, A.-K.T. (2024). Prenatal FGFR2 Signaling via PI3K/AKT Specifies the PDGFRA+ Myofibroblast. Am J Respir Cell Mol Biol *70*, 63–77. https://doi.org/10.1165/rcmb.2023-0245OC.

44. Li, R., Bernau, K., Sandbo, N., Gu, J., Preissl, S., and Sun, X. (2018). Pdgfra marks a cellular lineage with distinct contributions to myofibroblasts in lung maturation and injury response. eLife *7*, e36865. https://doi.org/10.7554/eLife.36865.

45. Li, C., Smith, S.M., Peinado, N., Gao, F., Li, W., Lee, M.K., Zhou, B., Bellusci, S., Pryhuber, G.S., Ho, H.-Y.H., et al. (2020). WNT5a-ROR Signaling Is Essential for Alveologenesis. Cells *9*, 384. https://doi.org/10.3390/cells9020384.

46. Khan, I.S., Molina, C., Ren, X., Auyeung, V.C., Cohen, M., Tsukui, T., Atakilit, A., and Sheppard, D. (2023). Impaired Myofibroblast Proliferation is a Central Feature of Pathologic Post-Natal Alveolar Simplification. Preprint at bioRxiv, https://doi.org/10.1101/2023.12.21.572766 https://doi.org/10.1101/2023.12.21.572766.

47. Gao, F., Li, C., Danopoulos, S., Al Alam, D., Peinado, N., Webster, S., Borok, Z., Kohbodi, G.A., Bellusci, S., and Minoo, P. (2022). Hedgehog-responsive PDGFRa(+) fibroblasts maintain a unique pool of alveolar epithelial progenitor cells during alveologenesis. Cell Rep *39*, 110608. https://doi.org/10.1016/j.celrep.2022.110608.

48. Hagan, A.S., Zhang, B., and Ornitz, D.M. (2020). Identification of a FGF18-expressing alveolar myofibroblast that is developmentally cleared during alveologenesis. Development *147*, dev181032. https://doi.org/10.1242/dev.181032.

49. Narvaez Del Pilar, O., Gacha Garay, M.J., and Chen, J. (2022). Three-axis classification of mouse lung mesenchymal cells reveals two populations of myofibroblasts. Development *149*, dev200081. https://doi.org/10.1242/dev.200081.

50. Yin, Y., Koenitzer, J.R., Patra, D., Dietmann, S., Bayguinov, P., Hagan, A.S., and Ornitz, D.M. (2024). Identification of a myofibroblast differentiation program during neonatal lung development. Development *151*, dev202659. https://doi.org/10.1242/dev.202659.

51. Nikolić, M.Z., Sun, D., and Rawlins, E.L. (2018). Human lung development: recent progress and new challenges. Development *145*, dev163485. https://doi.org/10.1242/dev.163485.

52. Rackley, C.R., and Stripp, B.R. (2012). Building and maintaining the epithelium of the lung. J Clin Invest *122*, 2724–2730. https://doi.org/10.1172/JCI60519.

53. Kajekar, R. (2007). Environmental factors and developmental outcomes in the lung. Pharmacology & Therapeutics *114*, 129–145. https://doi.org/10.1016/j.pharmthera.2007.01.011.

54. Hallberg, J., Iliadou, A., Anderson, M., de Verdier, M.G., Nihlén, U., Dahlbäck, M., Pedersen, N.L., Higenbottam, T., and Svartengren, M. (2010). Genetic and environmental influence on lung function impairment in Swedish twins. Respiratory Research *11*, 92. https://doi.org/10.1186/1465-9921-11-92.

55. Mullassery, D., and Smith, N.P. (2015). Lung development. Seminars in Pediatric Surgery *24*, 152–155. https://doi.org/10.1053/j.sempedsurg.2015.01.011.

56. Quach, H., Farrell, S., Wu, M.J.M., Kanagarajah, K., Leung, J.W.-H., Xu, X., Kallurkar, P., Turinsky, A.L., Bear, C.E., Ratjen, F., et al. (2024). Early human fetal lung atlas reveals the temporal dynamics of epithelial cell plasticity. Nat Commun *15*, 5898. https://doi.org/10.1038/s41467-024-50281-5.

57. Burri, P.H. (2006). Structural aspects of postnatal lung development - alveolar formation and growth. Biol Neonate *89*, 313–322. https://doi.org/92868 [pii] 10.1159/000092868.

58. Zeltner, T.B., Caduff, J.H., Gehr, P., Pfenninger, J., and Burri, P.H. (1987). The postnatal development and growth of the human lung. I. Morphometry. Respiration Physiology *67*, 247–267. https://doi.org/10.1016/0034-5687(87)90057-0.

59. Acute Respiratory Distress Syndrome | New England Journal of Medicine https://www.nejm.org/doi/10.1056/NEJMra1608077.

60. Popper, H., Stacher-Priehse, E., Brcic, L., and Nerlich, A. (2022). Lung fibrosis in autoimmune diseases and hypersensitivity: how to separate these from idiopathic pulmonary fibrosis. Rheumatol Int *42*, 1321–1330. https://doi.org/10.1007/s00296-021-05002-2.

61. Dogrul, B.N., Kiliccalan, I., Asci, E.S., and Peker, S.C. (2020). Blunt trauma related chest wall and pulmonary injuries: An overview. Chinese Journal of Traumatology *23*, 125–138. https://doi.org/10.1016/j.cjtee.2020.04.003.

62. Dries, D.J., and Endorf, F.W. (2013). Inhalation injury: epidemiology, pathology, treatment strategies. Scandinavian Journal of Trauma, Resuscitation and Emergency Medicine *21*, 31. https://doi.org/10.1186/1757-7241-21-31.

63. Vogelmeier, C.F., Criner, G.J., Martinez, F.J., Anzueto, A., Barnes, P.J., Bourbeau, J., Celli, B.R., Chen, R., Decramer, M., Fabbri, L.M., et al. (2017). Global Strategy for the Diagnosis, Management, and Prevention of Chronic Obstructive Lung Disease 2017 Report. GOLD Executive Summary. Am J Respir Crit Care Med *195*, 557–582. https://doi.org/10.1164/rccm.201701-0218PP.

64. Wolters, P.J., Collard, H.R., and Jones, K.D. (2014). Pathogenesis of Idiopathic Pulmonary Fibrosis. Annual Review of Pathology: Mechanisms of Disease *9*, 157–179. https://doi.org/10.1146/annurev-pathol-012513-104706.

65. Kheirollahi, V., Khadim, A., Kiliaris, G., Korfei, M., Barroso, M.M., Alexopoulos, I., Vazquez-Armendariz, A.I., Wygrecka, M., Ruppert, C., Guenther, A., et al. (2022). Transcriptional Profiling of Insulin-like Growth Factor Signaling Components in Embryonic Lung Development and Idiopathic Pulmonary Fibrosis. Cells *11*, 1973. https://doi.org/10.3390/cells11121973.

66. Lingampally, A., Truchi, M., Mauduit, O., Delcroix, V., Vasquez-Pacheco, E., Gautier-Isola, M., Chu, X., Khadim, A., Chao, C.-M., Zabihi, M., et al. (2024). Evidence for a lipofibroblast-to-Cthrc1+ myofibroblast reversible switch during the development and resolution of lung fibrosis in young mice. European Respiratory Journal. https://doi.org/10.1183/13993003.00482-2023.

67. Perlman, R.L. (2016). Mouse models of human disease: An evolutionary perspective. Evolution, Medicine, and Public Health *2016*, 170–176. https://doi.org/10.1093/emph/eow014.

68. Rydell-Törmänen, K., and Johnson, J.R. (2019). The Applicability of Mouse Models to the Study of Human Disease. In Mouse Cell Culture: Methods and Protocols, I. Bertoncello, ed. (Springer), pp. 3–22. https://doi.org/10.1007/978-1-4939-9086-3_1.

69. D'Alessio, F.R. (2018). Mouse Models of Acute Lung Injury and ARDS. In Lung Innate Immunity and Inflammation: Methods and Protocols, S. Alper and W. J. Janssen, eds. (Springer), pp. 341–350. https://doi.org/10.1007/978-1-4939-8570-8_22.

70. Wright, J.L., Cosio, M., and Churg, A. (2008). Animal models of chronic obstructive pulmonary disease. American Journal of Physiology-Lung Cellular and Molecular Physiology *295*, L1–L15. https://doi.org/10.1152/ajplung.90200.2008.

71. B. Moore, B., Lawson, W.E., Oury, T.D., Sisson, T.H., Raghavendran, K., and Hogaboam, C.M. (2013). Animal Models of Fibrotic Lung Disease. Am J Respir Cell Mol Biol *49*, 167–179. https://doi.org/10.1165/rcmb.2013-0094TR.

72. Brown, L.M., Rannels, S.R., and Rannels, D.E. (2001). Implications of post-pneumonectomy compensatory lung growth in pulmonary physiology and disease. Respiratory Research *2*, 340. https://doi.org/10.1186/rr84.

73. Mouse Pneumonectomy Model of Compensatory Lung Growth https://app.jove.com/t/52294.

74. Voswinckel, R., Motejl, V., Fehrenbach, A., Wegmann, M., Mehling, T., Fehrenbach, H., and Seeger, W. (2004). Characterisation of post-pneumonectomy lung growth in adult mice. European Respiratory Journal *24*, 524–532. https://doi.org/10.1183/09031936.04.10004904.

75. Lechner, A.J., Driver, I.H., Lee, J., Conroy, C.M., Nagle, A., Locksley, R.M., and Rock, J.R. (2017). Recruited Monocytes and Type 2 Immunity Promote Lung Regeneration following Pneumonectomy. Cell Stem Cell *21*, 120—-134.e7. https://doi.org/10.1016/j.stem.2017.03.024.

76. Ding, B.-S., Nolan, D.J., Guo, P., Babazadeh, A.O., Cao, Z., Rosenwaks, Z., Crystal, R.G., Simons, M., Sato, T.N., Worgall, S., et al. (2011). Endothelial-derived angiocrine signals induce and sustain regenerative lung alveolarization. Cell *147*, 539–553. https://doi.org/10.1016/j.cell.2011.10.003.

77. Rafii, S., Cao, Z., Lis, R., Siempos, I.I., Chavez, D., Shido, K., Rabbany, S.Y., and Ding, B.-S. (2015). Platelet-derived SDF-1 primes the pulmonary capillary vascular niche to drive lung alveolar regeneration. Nat Cell Biol *17*, 123–136. https://doi.org/10.1038/ncb3096.

78. Agha, E.E., and Thannickal, V.J. (2023). The lung mesenchyme in development, regeneration, and fibrosis. J Clin Invest *133*. https://doi.org/10.1172/JCI170498.

79. Li, R., Li, X., Hagood, J., Zhu, M.-S., and Sun, X. (2021). Myofibroblast contraction is essential for generating and regenerating the gas-exchange surface. J Clin Invest *130*. https://doi.org/10.1172/JCI132189.

80. Kaza, A.K., Kron, I.L., Leuwerke, S.M., Tribble, C.G., and Laubach, V.E. (2002). Keratinocyte Growth Factor Enhances Post-Pneumonectomy Lung Growth by Alveolar Proliferation. Circulation *106*, I–120. https://doi.org/10.1161/01.cir.0000032918.33237.04.

81. Paxson, J.A., Parkin, C.D., Iyer, L.K., Mazan, M.R., Ingenito, E.P., and Hoffman, A.M. (2009). Global gene expression patterns in the post-pneumonectomy lung of adult mice. Respir Res *10*, 92. https://doi.org/10.1186/1465-9921-10-92.

82. Liu, Z., Wu, H., Jiang, K., Wang, Y., Zhang, W., Chu, Q., Li, J., Huang, H., Cai, T., Ji, H., et al. (2016). MAPK-Mediated YAP Activation Controls Mechanical-Tension-Induced Pulmonary Alveolar Regeneration. Cell Reports *16*, 1810–1819. https://doi.org/10.1016/j.celrep.2016.07.020.

83. Tsikis, S.T., Klouda, T., Hirsch, T.I., Fligor, S.C., Liu, T., Kim, Y., Pan, A., Quigley, M., Mitchell, P.D., Puder, M., et al. (2023). A pneumonectomy model to study flow-induced pulmonary hypertension and compensatory lung growth. Cell Reports Methods *3*. https://doi.org/10.1016/j.crmeth.2023.100613.

84. Sentenac, P., Samarani, G., Bideaux, P., Sicard, P., Bourdois, B., Richard, S., Colson, P.H., and Eddahibi, S. (2021). Pulmonary hypertension after pneumonectomy: a preclinical model in rats and human pulmonary endothelial cells. European Journal of Cardio-Thoracic Surgery *59*, 147–154. https://doi.org/10.1093/ejcts/ezaa277.

85. Kobayashi, Y., Tata, A., Konkimalla, A., Katsura, H., Lee, R.F., Ou, J., Banovich, N.E., Kropski, J.A., and Tata, P.R. (2020). Persistence of a regeneration-associated, transitional alveolar epithelial cell state in pulmonary fibrosis. Nat Cell Biol *22*, 934–946. https://doi.org/10.1038/s41556-020-0542-8.

86. Identification of a novel subset of alveolar type 2 cells enriched in PD-L1 and expanded following pneumonectomy - PubMed https://pubmed.ncbi.nlm.nih.gov/33863742/.

87. Brown, L.M., Malkinson, A.M., Rannels, D.E., and Rannels, S.R. (1999). Compensatory Lung Growth after Partial Pneumonectomy Enhances Lung Tumorigenesis Induced by 3-Methylcholanthrene1. Cancer Research *59*, 5089–5092.

88. White, A., Kucukak, S., Bueno, R., Servais, E., Lee, D.N., Colson, Y., Jaklitsch, M., McNamee, C., Mentzer, S., Wee, J., et al. (2017). Pneumonectomy is safe and effective for non-small cell lung cancer following induction therapy. Journal of Thoracic Disease *9*. https://doi.org/10.21037/jtd.2017.10.92.

89. Thane, K., Ingenito, E.P., and Hoffman, A.M. (2014). Lung regeneration and translational implications of the postpneumonectomy model. Translational Research *163*, 363–376. https://doi.org/10.1016/j.trsl.2013.11.010.

90. Barnes, P.J. (2000). Chronic Obstructive Pulmonary Disease. New England Journal of Medicine *343*, 269–280. https://doi.org/10.1056/NEJM200007273430407.

91. Barnes, P.J., Burney, P.G.J., Silverman, E.K., Celli, B.R., Vestbo, J., Wedzicha, J.A., and Wouters, E.F.M. (2015). Chronic obstructive pulmonary disease. Nature Reviews Disease Primers *1*, 15076. https://doi.org/10.1038/nrdp.2015.76.

92. Cerveri, I., Dore, R., Corsico, A., Zoia, M.C., Pellegrino, R., Brusasco, V., and Pozzi, E. (2004). Assessment of emphysema in COPD: a functional and radiologic study. Chest *125*, 1714–1718. https://doi.org/10.1378/chest.125.5.1714.

93. Goldklang, M., and Stockley, R. (2016). Pathophysiology of Emphysema and Implications. Chronic Obstr Pulm Dis *3*, 454–458. https://doi.org/10.15326/jcopdf.3.1.2015.0175.

94. Li, T., Fanning, K.V., Nyunoya, T., Chen, Y., and Zou, C. (2020). Cigarette smoke extract induces airway epithelial cell death via repressing PRMT6/AKT signaling. Aging (Albany NY) *12*, 24301–24317. https://doi.org/10.18632/aging.202210.

95. Hadzic, S., Wu, C.-Y., Gredic, M., Pak, O., Loku, E., Kraut, S., Kojonazarov, B., Wilhelm, J., Brosien, M., Bednorz, M., et al. (2023). Fibroblast growth factor 10 reverses cigarette smoke- and elastase-induced emphysema and pulmonary hypertension in mice. European Respiratory Journal *62*. https://doi.org/10.1183/13993003.01606-2022.

96. Chu, X., Kheirollahi, V., Lingampally, A., Chelladurai, P., Valasarajan, C., Vazquez-Armendariz, A.I., Hadzic, S., Khadim, A., Pak, O., Rivetti, S., et al. (2024). GLI1+ Cells Contribute to Vascular Remodeling in Pulmonary

Hypertension. Circulation Research *134*, e133–e149. https://doi.org/10.1161/CIRCRESAHA.123.323736.

97. Sethi, J.M., and Rochester, C.L. (2000). SMOKING AND CHRONIC OBSTRUCTIVE PULMONARY DISEASE. Clinics in Chest Medicine *21*, 67–86. https://doi.org/10.1016/S0272-5231(05)70008-3.

98. Short, K.R., Kroeze, E.J.B.V., Fouchier, R.A.M., and Kuiken, T. (2014). Pathogenesis of influenza-induced acute respiratory distress syndrome. The Lancet Infectious Diseases *14*, 57–69. https://doi.org/10.1016/S1473-3099(13)70286-X.

99. Jha, A., Jarvis, H., Fraser, C., and Openshaw, P.J. (2016). Respiratory Syncytial Virus. In SARS, MERS and other Viral Lung Infections Wellcome Trust–Funded Monographs and Book Chapters., D. S. Hui, G. A. Rossi, and S. L. Johnston, eds. (European Respiratory Society).

100. Bridges, J.P., Vladar, E.K., Huang, H., and Mason, R.J. (2022). Respiratory epithelial cell responses to SARS-CoV-2 in COVID-19. Thorax *77*, 203–209. https://doi.org/10.1136/thoraxjnl-2021-217561.

101. Fajgenbaum, D.C., and June, C.H. (2020). Cytokine Storm. New England Journal of Medicine *383*, 2255–2273. https://doi.org/10.1056/NEJMra2026131.

102. Chemani, C., Imberty, A., de Bentzmann, S., Pierre, M., Wimmerová, M., Guery, B.P., and Faure, K. (2009). Role of LecA and LecB Lectins in Pseudomonas aeruginosa-Induced Lung Injury and Effect of Carbohydrate Ligands. Infection and Immunity *77*, 2065–2075. https://doi.org/10.1128/iai.01204-08.

103. Sawa, T. (2014). The molecular mechanism of acute lung injury caused by Pseudomonas aeruginosa: from bacterial pathogenesis to host response. Journal of Intensive Care *2*, 10. https://doi.org/10.1186/2052-0492-2-10.

104. Rai, P., Parrish, M., Tay, I.J.J., Li, N., Ackerman, S., He, F., Kwang, J., Chow, V.T., and Engelward, B.P. (2015). Streptococcus pneumoniae secretes hydrogen peroxide leading to DNA damage and apoptosis in lung cells. Proceedings of the National Academy of Sciences *112*, E3421–E3430. https://doi.org/10.1073/pnas.1424144112.

105. Skerrett, S.J., Martin, T.R., Chi, E.Y., Peschon, J.J., Mohler, K.M., and Wilson, C.B. (1999). Role of the type 1 TNF receptor in lung inflammation after inhalation of endotoxin or Pseudomonas aeruginosa. American Journal of Physiology-Lung Cellular and Molecular Physiology *276*, L715–L727. https://doi.org/10.1152/ajplung.1999.276.5.L715.

106. Whitsett, J.A., and Alenghat, T. (2015). Respiratory epithelial cells orchestrate pulmonary innate immunity. Nat Immunol *16*, 27–35. https://doi.org/10.1038/ni.3045.

107. Li, D., and Wu, M. (2021). Pattern recognition receptors in health and diseases. Sig Transduct Target Ther *6*, 1–24. https://doi.org/10.1038/s41392-021-00687-0.

108. Sethi, S. (2000). Infectious Etiology of Acute Exacerbations of Chronic Bronchitis. CHEST *117*, 380S-385S. https://doi.org/10.1378/chest.117.5_suppl_2.380S.

109. Molyneaux, P.L., and Maher, T.M. (2013). The role of infection in the pathogenesis of idiopathic pulmonary fibrosis. European Respiratory Review *22*, 376–381. https://doi.org/10.1183/09059180.00000713.

110. Brown, E.G. (2000). Influenza virus genetics. Biomedicine & Pharmacotherapy *54*, 196–209. https://doi.org/10.1016/S0753-3322(00)89026-5.

111. Wu, S., Metcalf, J.P., and Wu, W. (2011). Innate immune response to influenza virus: Current Opinion in Infectious Diseases *24*, 235–240. https://doi.org/10.1097/QCO.0b013e328344c0e3.

112. Moreira, E.A., Yamauchi, Y., and Matthias, P. (2021). How Influenza Virus Uses Host Cell Pathways during Uncoating. Cells *10*, 1722. https://doi.org/10.3390/cells10071722.

113. Byrd-Leotis, L., Jia, N., Dutta, S., Trost, J.F., Gao, C., Cummings, S.F., Braulke, T., Müller-Loennies, S., Heimburg-Molinaro, J., Steinhauer, D.A., et al. (2019). Influenza binds phosphorylated glycans from human lung. Science Advances *5*, eaav2554. https://doi.org/10.1126/sciadv.aav2554.

114. Smed-Sörensen, A., Chalouni, C., Chatterjee, B., Cohn, L., Blattmann, P., Nakamura, N., Delamarre, L., and Mellman, I. (2012). Influenza A virus infection of human primary dendritic cells impairs their ability to cross-present antigen to CD8 T cells. PLoS Pathog *8*, e1002572. https://doi.org/10.1371/journal.ppat.1002572.

115. Liu, M., Huang, L.Z.X., Smits, A.A., Büll, C., Narimatsu, Y., van Kuppeveld, F.J.M., Clausen, H., de Haan, C.A.M., and de Vries, E. (2022). Human-type sialic acid receptors contribute to avian influenza A virus binding and entry by hetero-multivalent interactions. Nat Commun *13*, 4054. https://doi.org/10.1038/s41467-022-31840-0.

116. Herold, S., Becker, C., Ridge, K.M., and Budinger, G.R.S. (2015). Influenza virus-induced lung injury: pathogenesis and implications for treatment. European Respiratory Journal *45*, 1463–1478. https://doi.org/10.1183/09031936.00186214.

117. Iuliano, A.D., Roguski, K.M., Chang, H.H., Muscatello, D.J., Palekar, R., Tempia, S., Cohen, C., Gran, J.M., Schanzer, D., Cowling, B.J., et al. (2018). Estimates of global seasonal influenza-associated respiratory mortality: a modelling study. The Lancet *391*, 1285–1300. https://doi.org/10.1016/S0140-6736(17)33293-2.

118. Taubenberger, J.K., and Morens, D.M. (2020). The 1918 Influenza Pandemic and Its Legacy. Cold Spring Harb Perspect Med *10*, a038695. https://doi.org/10.1101/cshperspect.a038695.

119. Tang, B.M., Cootes, T., and McLean, A.S. (2018). From Influenza-Induced Acute Lung Injury to Multiorgan Failure. Annual Update in Intensive Care and

Emergency Medicine 2019, 449–458. https://doi.org/10.1007/978-3-030-06067-1_35.

120. Wareing, M.D., Lyon, A.B., Lu, B., Gerard, C., and Sarawar, S.R. (2004). Chemokine expression during the development and resolution of a pulmonary leukocyte response to influenza A virus infection in mice. J Leukoc Biol *76*, 886–895. https://doi.org/10.1189/jlb.1203644.

121. Betakova, T., Kostrabova, A., Lachova, V., and Turianova, L. (2017). Cytokines Induced During Influenza Virus Infection. Curr Pharm Des *23*, 2616–2622. https://doi.org/10.2174/1381612823666170316123736.

122. Dou, D., Revol, R., Östbye, H., Wang, H., and Daniels, R. (2018). Influenza A Virus Cell Entry, Replication, Virion Assembly and Movement. Front Immunol *9*, 1581. https://doi.org/10.3389/fimmu.2018.01581.

123. Inhibiting influenza virus transmission using a broadly acting neuraminidase that targets host sialic acids in the upper respiratory tract (2024). mBio *15*. https://doi.org/10.1128/mbio.02203-23.

124. Yoshimura, A., Kuroda, K., Kawasaki, K., Yamashina, S., Maeda, T., and Ohnishi, S.-I. (1982). Infectious Cell Entry Mechanism of Influenza Virus. Journal of Virology *43*, 284–293. https://doi.org/10.1128/jvi.43.1.284-293.1982.

125. Pielak, R.M., and Chou, J.J. (2011). Influenza M2 proton channels. Biochim Biophys Acta *1808*, 522–529. https://doi.org/10.1016/j.bbamem.2010.04.015.

126. Luo, M. (2012). Influenza virus entry. Adv Exp Med Biol *726*, 201–221. https://doi.org/10.1007/978-1-4614-0980-9_9.

127. Hutchinson, E.C., and Fodor, E. (2012). Nuclear import of the influenza A virus transcriptional machinery. Vaccine *30*, 7353–7358. https://doi.org/10.1016/j.vaccine.2012.04.085.

128. Eisfeld, A.J., Neumann, G., and Kawaoka, Y. (2015). At the centre: influenza A virus ribonucleoproteins. Nat Rev Microbiol *13*, 28–41. https://doi.org/10.1038/nrmicro3367.

129. Li, J., Yu, M., Zheng, W., and Liu, W. (2015). Nucleocytoplasmic Shuttling of Influenza A Virus Proteins. Viruses *7*, 2668–2682. https://doi.org/10.3390/v7052668.

130. Brand, J.D., Lazrak, A., Trombley, J.E., Shei, R.-J., Adewale, A.T., Tipper, J.L., Yu, Z., Ashtekar, A.R., Rowe, S.M., Matalon, S., et al. (2018). Influenza-mediated reduction of lung epithelial ion channel activity leads to dysregulated pulmonary fluid homeostasis. JCI Insight *3*. https://doi.org/10.1172/jci.insight.123467.

131. Klomp, M., Ghosh, S., Mohammed, S., and Nadeem Khan, M. (2021). From virus to inflammation, how influenza promotes lung damage. Journal of Leukocyte Biology *110*, 115–122. https://doi.org/10.1002/JLB.4RU0820-232R.

132. Kosik, I., Angeletti, D., Gibbs, J.S., Angel, M., Takeda, K., Kosikova, M., Nair, V., Hickman, H.D., Xie, H., Brooke, C.B., et al. (2019). Neuraminidase inhibition contributes to influenza A virus neutralization by anti-hemagglutinin stem antibodies. J Exp Med *216*, 304–316. https://doi.org/10.1084/jem.20181624.

133. Betts, R.J., Prabhu, N., Ho, A.W.S., Lew, F.C., Hutchinson, P.E., Rotzschke, O., Macary, P.A., and Kemeny, D.M. (2012). Influenza A Virus Infection Results in a Robust, Antigen-Responsive, and Widely Disseminated Foxp3+ Regulatory T Cell Response. J Virol *86*, 2817–2825. https://doi.org/10.1128/JVI.05685-11.

134. Moser, E.K., Hufford, M.M., and Braciale, T.J. (2014). Late Engagement of CD86 after Influenza Virus Clearance Promotes Recovery in a FoxP3+ Regulatory T Cell Dependent Manner. PLoS Pathog *10*, e1004315. https://doi.org/10.1371/journal.ppat.1004315.

135. León, B., Bradley, J.E., Lund, F.E., Randall, T.D., and Ballesteros-Tato, A. (2014). FoxP3+ regulatory T cells promote influenza-specific Tfh responses by controlling IL-2 availability. Nat Commun *5*, 3495. https://doi.org/10.1038/ncomms4495.

136. Finn, C.M., Prokop, E., Dhume, K., and McKinstry, K. (2023). STAT1 expression controls CD4 T cell Th1 and Th17 effector functionality during influenza virus infection. The Journal of Immunology *210*, 75.48. https://doi.org/10.4049/jimmunol.210.Supp.75.48.

137. Li, Y., Yang, Y., Chen, D., Wang, Y., Zhang, X., Li, W., Chen, S., Wong, S.M., Shen, M., Akerley, B.J., et al. (2023). Memory Th17 cell-mediated protection against lethal secondary pneumococcal pneumonia following influenza infection. mBio *14*, e00519-23. https://doi.org/10.1128/mbio.00519-23.

138. Gaur, P., Ranjan, P., Sharma, S., Patel, J.R., Bowzard, J.B., Rahman, S.K., Kumari, R., Gangappa, S., Katz, J.M., Cox, N.J., et al. (2012). Influenza A Virus Neuraminidase Protein Enhances Cell Survival through Interaction with Carcinoembryonic Antigen-related Cell Adhesion Molecule 6 (CEACAM6) Protein *. Journal of Biological Chemistry *287*, 15109–15117. https://doi.org/10.1074/jbc.M111.328070.

139. Ivanov, S., Renneson, J., Fontaine, J., Barthelemy, A., Paget, C., Fernandez, E.M., Blanc, F., De Trez, C., Van Maele, L., Dumoutier, L., et al. (2013). Interleukin-22 Reduces Lung Inflammation during Influenza A Virus Infection and Protects against Secondary Bacterial Infection. J Virol *87*, 6911–6924. https://doi.org/10.1128/JVI.02943-12.

140. Laghlali, G., Lawlor, K.E., and Tate, M.D. (2020). Die Another Way: Interplay between Influenza A Virus, Inflammation and Cell Death. Viruses *12*, 401. https://doi.org/10.3390/v12040401.

141. Monticelli, L.A., Sonnenberg, G.F., Abt, M.C., Alenghat, T., Ziegler, C.G.K., Doering, T.A., Angelosanto, J.M., Laidlaw, B.J., Yang, C.Y., Sathaliyawala, T., et al. (2011). Innate lymphoid cells promote lung-tissue homeostasis after infection

with influenza virus. Nat Immunol *12*, 1045–1054. https://doi.org/10.1031/ni.2131.

142. Narasaraju, T., Ng, H.H., Phoon, M.C., and Chow, V.T.K. (2010). MCP-1 Antibody Treatment Enhances Damage and Impedes Repair of the Alveolar Epithelium in Influenza Pneumonitis. Am J Respir Cell Mol Biol *42*, 732–743. https://doi.org/10.1165/rcmb.2008-0423OC.

143. Ito, Y., Correll, K., Zemans, R.L., Leslie, C.C., Murphy, R.C., and Mason, R.J. (2015). Influenza induces IL-8 and GM-CSF secretion by human alveolar epithelial cells through HGF/c-Met and TGF-α/EGFR signaling. Am J Physiol Lung Cell Mol Physiol *308*, L1178-1188. https://doi.org/10.1152/ajplung.00290.2014.

144. Allard, B., Panariti, A., and Martin, J.G. (2018). Alveolar Macrophages in the Resolution of Inflammation, Tissue Repair, and Tolerance to Infection. Front. Immunol. *9*. https://doi.org/10.3389/fimmu.2018.01777.

145. Zuttion, M.S.S.R., Parimon, T., Yao, C., Stripp, B.R., Wang, Y., Soto, C.M., Ortega, Z., Li, X., Janssen, W.J., and Chen, P. (2024). Interstitial Macrophages Mediate Efferocytosis of Alveolar Epithelium during Influenza Infection. Am J Respir Cell Mol Biol *70*, 159–164. https://doi.org/10.1165/rcmb.2023-0217MA.

146. Zuo, W., Zhang, T., Wu, D.Z., Guan, S.P., Liew, A.-A., Yamamoto, Y., Wang, X., Lim, S.J., Vincent, M., Lessard, M., et al. (2015). p63+Krt5+ distal airway stem cells are essential for lung regeneration. Nature *517*, 616–620. https://doi.org/10.1038/nature13903.

147. Kumar, P.A., Hu, Y., Yamamoto, Y., Hoe, N.B., Wei, T.S., Mu, D., Sun, Y., Joo, L.S., Dagher, R., Zielonka, E., et al. (2011). Distal Airway Stem Cells Render Alveoli in Vitro and During Lung Regeneration Following H1N1 Influenza Infection. Cell *147*, 525–538. https://doi.org/10.1016/j.cell.2011.10.001.

148. Finn, J., Sottoriva, K., Pajcini, K.V., Kitajewski, J.K., Chen, C., Zhang, W., Malik, A.B., and Liu, Y. (2019). Dlk1-Mediated Temporal Regulation of Notch Signaling Is Required for Differentiation of Alveolar Type II to Type I Cells during Repair. Cell Reports *26*, 2942-2954.e5. https://doi.org/10.1016/j.celrep.2019.02.046.

149. Beppu, A.K., Zhao, J., Yao, C., Carraro, G., Israely, E., Coelho, A.L., Drake, K., Hogaboam, C.M., Parks, W.C., Kolls, J.K., et al. (2023). Epithelial plasticity and innate immune activation promote lung tissue remodeling following respiratory viral infection. Nat Commun *14*, 5814. https://doi.org/10.1038/s41467-023-41387-3.

150. Liberti, D.C., Kremp, M.M., Liberti, W.A., Penkala, I.J., Li, S., Zhou, S., and Morrisey, E.E. (2021). Alveolar epithelial cell fate is maintained in a spatially restricted manner to promote lung regeneration after acute injury. Cell Rep *35*, 109092. https://doi.org/10.1016/j.celrep.2021.109092.

151. Toulmin, S.A., Bhadiadra, C., Paris, A.J., Lin, J.H., Katzen, J., Basil, M.C., Morrisey, E.E., Worthen, G.S., and Eisenlohr, L.C. (2021). Type II alveolar cell

MHCII improves respiratory viral disease outcomes while exhibiting limited antigen presentation. Nat Commun *12*, 3993. https://doi.org/10.1038/s41467-021-23619-6.

152. Shenoy, A.T., Lyon De Ana, C., Arafa, E.I., Salwig, I., Barker, K.A., Korkmaz, F.T., Ramanujan, A., Etesami, N.S., Soucy, A.M., Martin, I.M.C., et al. (2021). Antigen presentation by lung epithelial cells directs CD4+ TRM cell function and regulates barrier immunity. Nat Commun *12*, 5834. https://doi.org/10.1038/s41467-021-26045-w.

153. Zheng, D., Limmon, G.V., Yin, L., Leung, N.H.N., Yu, H., Chow, V.T.K., and Chen, J. (2012). Regeneration of Alveolar Type I and II Cells from Scgb1a1-Expressing Cells following Severe Pulmonary Damage Induced by Bleomycin and Influenza. PLOS ONE *7*, e48451. https://doi.org/10.1371/journal.pone.0048451.

154. Desai, T.J., Brownfield, D.G., and Krasnow, M.A. (2014). Alveolar progenitor and stem cells in lung development, renewal and cancer. Nature *507*, 190–194. https://doi.org/10.1038/nature12930.

155. Martins, L.R., Sieverling, L., Michelhans, M., Schiller, C., Erkut, C., Grünewald, T.G.P., Triana, S., Fröhling, S., Velten, L., Glimm, H., et al. (2024). Single-cell division tracing and transcriptomics reveal cell types and differentiation paths in the regenerating lung. Nat Commun *15*, 2246. https://doi.org/10.1038/s41467-024-46469-4.

156. Salwig, I., Spitznagel, B., Vazquez-Armendariz, A.I., Khalooghi, K., Guenther, S., Herold, S., Szibor, M., and Braun, T. (2019). Bronchioalveolar stem cells are a main source for regeneration of distal lung epithelia in vivo. The EMBO Journal *38*, e102099. https://doi.org/10.15252/embj.2019102099.

157. Quantius, J., Schmoldt, C., Vazquez-Armendariz, A.I., Becker, C., Agha, E.E., Wilhelm, J., Morty, R.E., Vadász, I., Mayer, K., Gattenloehner, S., et al. (2016). Influenza Virus Infects Epithelial Stem/Progenitor Cells of the Distal Lung: Impact on Fgfr2b-Driven Epithelial Repair. PLOS Pathogens *12*, e1005544. https://doi.org/10.1371/journal.ppat.1005544.

158. Boyd, D.F., Allen, E.K., Randolph, A.G., Guo, X.J., Weng, Y., Sanders, C.J., Bajracharya, R., Lee, N.K., Guy, C.S., Vogel, P., et al. (2020). Exuberant fibroblast activity compromises lung function via ADAMTS4. Nature *587*, 466–471. https://doi.org/10.1038/s41586-020-2877-5.

159. Iwasaki, A., and Pillai, P.S. (2014). Innate immunity to influenza virus infection. Nat Rev Immunol *14*, 315–328. https://doi.org/10.1038/nri3665.

160. El Agha, E., and Thannickal, V.J. The lung mesenchyme in development, regeneration, and fibrosis. J Clin Invest *133*, e170498. https://doi.org/10.1172/JCI170498.

161. Yang, W., Bai, X., Li, H., Li, H., Fan, W., Zhang, H., Liu, W., and Sun, L. (2022). Influenza A and B Virus-Triggered Epithelial–Mesenchymal Transition Is

Relevant to the Binding Ability of NA to Latent TGF-β. Frontiers in Microbiology *13*.

162. Liu, X., Lai, C., Wang, K., Xing, L., Yang, P., Duan, Q., and Wang, X. (2015). A Functional Role of Fibroblast Growth Factor Receptor 1 (FGFR1) in the Suppression of Influenza A Virus Replication. PLOS ONE *10*, e0124651. https://doi.org/10.1371/journal.pone.0124651.

163. Wang, K., Lai, C., Li, T., Wang, C., Wang, W., Ni, B., Bai, C., Zhang, S., Han, L., Gu, H., et al. (2018). Basic fibroblast growth factor protects against influenza A virus-induced acute lung injury by recruiting neutrophils. Journal of Molecular Cell Biology *10*, 573–585. https://doi.org/10.1093/jmcb/mjx047.

164. Fysikopoulos, A., Seimetz, M., Hadzic, S., Knoepp, F., Wu, C.-Y., Malkmus, K., Wilhelm, J., Pichl, A., Bednorz, M., Tadele Roxlau, E., et al. (2021). Amelioration of elastase-induced lung emphysema and reversal of pulmonary hypertension by pharmacological iNOS inhibition in mice. Br J Pharmacol *178*, 152–171. https://doi.org/10.1111/bph.15057.

165. Seimetz, M., Parajuli, N., Pichl, A., Veit, F., Kwapiszewska, G., Weisel, F.C., Milger, K., Egemnazarov, B., Turowska, A., Fuchs, B., et al. (2011). Inducible NOS Inhibition Reverses Tobacco-Smoke-Induced Emphysema and Pulmonary Hypertension in Mice. Cell *147*, 293–305. https://doi.org/10.1016/j.cell.2011.08.035.

166. Yu, G., Wang, L.-G., Han, Y., and He, Q.-Y. (2012). clusterProfiler: an R package for comparing biological themes among gene clusters. OMICS *16*, 284–287. https://doi.org/10.1089/omi.2011.0118.

167. Wolf, F.A., Angerer, P., and Theis, F.J. (2018). SCANPY: large-scale single-cell gene expression data analysis. Genome Biology *19*, 15. https://doi.org/10.1186/s13059-017-1382-0.

168. Sun, X., Perl, A.-K., Li, R., Bell, S.M., Sajti, E., Kalinichenko, V.V., Kalin, T.V., Misra, R.S., Deshmukh, H., Clair, G., et al. (2022). A census of the lung: CellCards from LungMAP. Dev Cell *57*, 112-145.e2. https://doi.org/10.1016/j.devcel.2021.11.007.

169. Bergen, V., Lange, M., Peidli, S., Wolf, F.A., and Theis, F.J. (2020). Generalizing RNA velocity to transient cell states through dynamical modeling. Nat Biotechnol *38*, 1408–1414. https://doi.org/10.1038/s41587-020-0591-3.

170. ShinyGO: a graphical gene-set enrichment tool for animals and plants | Bioinformatics | Oxford Academic https://academic.oup.com/bioinformatics/article/36/8/2628/5688742.

171. Hao, Y., Hao, S., Andersen-Nissen, E., Mauck, W.M., Zheng, S., Butler, A., Lee, M.J., Wilk, A.J., Darby, C., Zager, M., et al. (2021). Integrated analysis of multimodal single-cell data. Cell *184*, 3573-3587.e29. https://doi.org/10.1016/j.cell.2021.04.048.

172. Jin, S., Guerrero-Juarez, C.F., Zhang, L., Chang, I., Ramos, R., Kuan, C.-H., Myung, P., Plikus, M.V., and Nie, Q. (2021). Inference and analysis of cell-cell communication using CellChat. Nat Commun *12*, 1088. https://doi.org/10.1038/s41467-021-21246-9.

173. Zabihi, M., Khadim, A., Schäfer, T.M., Alexopoulos, I., Bartkuhn, M., El Agha, E., Vazquez-Armendariz, A.I., and Herold, S. (2024). An Optimized Protocol for the Generation of Alveolospheres from Wild-Type Mice. Cells *13*, 922. https://doi.org/10.3390/cells13110922.

174. Chu, X., Lingampally, A., Moiseenko, A., Kheirollahi, V., Vazquez-Armendariz, A.I., Koepke, J., Khadim, A., Kiliaris, G., Shahriari Felordi, M., Zabihi, M., et al. (2022). GLI1+ cells are a source of repair-supportive mesenchymal cells (RSMCs) during airway epithelial regeneration. Cell. Mol. Life Sci. *79*, 581. https://doi.org/10.1007/s00018-022-04599-2.

175. Khadim, A., Kiliaris, G., Vazquez-Armendariz, A.I., Procida-Kowalski, T., Glaser, D., Bartkuhn, M., Malik, T., Chu, X., Moiseenko, A., Kuznetsova, I., et al. (2025). Myofibroblasts emerge during alveolar regeneration following influenza-virus-induced lung injury. Cell Reports *44*, 115248. https://doi.org/10.1016/j.celrep.2025.115248.

176. Tsukui, T., Sun, K.-H., Wetter, J.B., Wilson-Kanamori, J.R., Hazelwood, L.A., Henderson, N.C., Adams, T.S., Schupp, J.C., Poli, S.D., Rosas, I.O., et al. (2020). Collagen-producing lung cell atlas identifies multiple subsets with distinct localization and relevance to fibrosis. Nat Commun *11*, 1920. https://doi.org/10.1038/s41467-020-15647-5.

177. Tsukui, T., Sun, K.-H., Wetter, J.B., Wilson-Kanamori, J.R., Hazelwood, L.A., Henderson, N.C., Adams, T.S., Schupp, J.C., Poli, S.D., Rosas, I.O., et al. (2020). Collagen-producing lung cell atlas identifies multiple subsets with distinct localization and relevance to fibrosis. Nat Commun *11*, 1920. https://doi.org/10.1038/s41467-020-15647-5.

178. Xie, T., Liang, J., Liu, N., Huan, C., Zhang, Y., Liu, W., Kumar, M., Xiao, R., D'Armiento, J., Metzger, D., et al. Transcription factor TBX4 regulates myofibroblast accumulation and lung fibrosis. J Clin Invest *126*, 3063–3079. https://doi.org/10.1172/JCI85328.

179. El Agha, E., Moiseenko, A., Kheirollahi, V., De Langhe, S., Crnkovic, S., Kwapiszewska, G., Szibor, M., Kosanovic, D., Schwind, F., Schermuly, R.T., et al. (2017). Two-Way Conversion between Lipogenic and Myogenic Fibroblastic Phenotypes Marks the Progression and Resolution of Lung Fibrosis. Cell Stem Cell *20*, 261—-273.e3. https://doi.org/10.1016/j.stem.2016.10.004.

180. Mayr, C.H., Sengupta, A., Asgharpour, S., Ansari, M., Pestoni, J.C., Ogar, P., Angelidis, I., Liontos, A., Rodriguez-Castillo, J.A., Lang, N.J., et al. (2024). Sfrp1 inhibits lung fibroblast invasion during transition to injury-induced myofibroblasts. European Respiratory Journal *63*. https://doi.org/10.1183/13993003.01326-2023.

181. Park, J., Ivey, M.J., Deana, Y., Riggsbee, K.L., Sörensen, E., Schwabl, V., Sjöberg, C., Hjertberg, T., Park, G.Y., Swonger, J.M., et al. (2019). The Tcf21 lineage constitutes the lung lipofibroblast population. American Journal of Physiology-Lung Cellular and Molecular Physiology *316*, L872—-L885. https://doi.org/10.1152/ajplung.00254.2018.

182. Frontiers | Validation of a Novel Fgf10Cre–ERT2 Knock-in Mouse Line Targeting FGF10Pos Cells Postnatally https://www.frontiersin.org/journals/cell-and-developmental-biology/articles/10.3389/fcell.2021.671841/full.

183. Al Alam, D., El Agha, E., Sakurai, R., Kheirollahi, V., Moiseenko, A., Danopoulos, S., Shrestha, A., Schmoldt, C., Quantius, J., Herold, S., et al. (2015). Evidence for the involvement of fibroblast growth factor 10 in lipofibroblast formation during embryonic lung development. Development (Cambridge, England) *142*, 4139–4150. https://doi.org/10.1242/dev.109173.

184. Kheirollahi, V., Wasnick, R.M., Biasin, V., Vazquez-Armendariz, A.I., Chu, X., Moiseenko, A., Weiss, A., Wilhelm, J., Zhang, J.-S., Kwapiszewska, G., et al. (2019). Metformin induces lipogenic differentiation in myofibroblasts to reverse lung fibrosis. Nature Communications *10*, 2987. https://doi.org/10.1038/s41467-019-10839-0.

185. Nelson, N.C., and Kugler, M.C. (2024). Exploring a complex constellation of signaling pathways. eLife *13*, e105095. https://doi.org/10.7554/eLife.105095.

186. Boucherat, O., Nadeau, V., Bérubé-Simard, F.-A., Charron, J., and Jeannotte, L. (2014). Crucial requirement of ERK/MAPK signaling in respiratory tract development. Development *141*, 3197–3211. https://doi.org/10.1242/dev.110254.

187. Chaudhry, F.N., Michki, N.S., Shirmer, D.L., McGrath-Morrow, S., Young, L.R., Frank, D.B., and Zepp, J.A. (2024). Dynamic Hippo pathway activity underlies mesenchymal differentiation during lung alveolar morphogenesis. Development *151*, dev202430. https://doi.org/10.1242/dev.202430.

188. Chandran, R.R., Adams, T.S., Kabir, I., Gallardo-Vara, E., Kaminski, N., Gomperts, B.N., and Greif, D.M. (2024). Dedifferentiated early postnatal lung myofibroblasts redifferentiate in adult disease. Front. Cell Dev. Biol. *12*. https://doi.org/10.3389/fcell.2024.1335061.

189. Buechler, M.B., Pradhan, R.N., Krishnamurty, A.T., Cox, C., Calviello, A.K., Wang, A.W., Yang, Y.A., Tam, L., Caothien, R., Roose-Girma, M., et al. (2021). Cross-tissue organization of the fibroblast lineage. Nature *593*, 575–579. https://doi.org/10.1038/s41586-021-03549-5.

190. Selman, M., and Pardo, A. (2021). Fibroageing: An ageing pathological feature driven by dysregulated extracellular matrix-cell mechanobiology. Ageing Research Reviews *70*, 101393. https://doi.org/10.1016/j.arr.2021.101393.

191. Ren, L.-L., Miao, H., Wang, Y.-N., Liu, F., Li, P., and Zhao, Y.-Y. (2023). TGF-β as A Master Regulator of Aging-Associated Tissue Fibrosis. Aging and disease *14*, 1633–1650. https://doi.org/10.14336/AD.2023.0222.

192. Cassandras, M., Wang, C., Kathiriya, J., Tsukui, T., Matatia, P., Matthay, M., Wolters, P., Molofsky, A., Sheppard, D., Chapman, H., et al. (2020). Gli1+ mesenchymal stromal cells form a pathological niche to promote airway progenitor metaplasia in the fibrotic lung. Nat Cell Biol *22*, 1295–1306. https://doi.org/10.1038/s41556-020-00591-9.

193. Po, A., Silvano, M., Miele, E., Capalbo, C., Eramo, A., Salvati, V., Todaro, M., Besharat, Z.M., Catanzaro, G., Cucchi, D., et al. (2017). Noncanonical GLI1 signaling promotes stemness features and in vivo growth in lung adenocarcinoma. Oncogene *36*, 4641–4652. https://doi.org/10.1038/onc.2017.91.

194. Li, C., Lee, M.K., Gao, F., Webster, S., Di, H., Duan, J., Yang, C.-Y., Bhopal, N., Peinado, N., Pryhuber, G., et al. (2019). Secondary crest myofibroblast PDGFRα controls the elastogenesis pathway via a secondary tier of signaling networks during alveologenesis. Development *146*, dev176354. https://doi.org/10.1242/dev.176354.

195. Jones, D.L., Morley, M.P., Li, X., Ying, Y., Zhao, G., Schaefer, S.E., Rodriguez, L.R., Cardenas-Diaz, F.L., Li, S., Zhou, S., et al. (2024). An injury-induced mesenchymal-epithelial cell niche coordinates regenerative responses in the lung. Science *386*, eado5561. https://doi.org/10.1126/science.ado5561.

196. Fang, Y., Chung, S.S.W., Xu, L., Xue, C., Liu, X., Jiang, D., Li, R., Korogi, Y., Yuan, K., Saqi, A., et al. (2025). RUNX2 promotes fibrosis via an alveolar-to-pathological fibroblast transition. Nature, 1–10. https://doi.org/10.1038/s41586-024-08542-2.

197. Moiseenko, A., Vazquez-Armendariz, A.I., Kheirollahi, V., Chu, X., Tata, A., Rivetti, S., Günther, S., Lebrigand, K., Herold, S., Braun, T., et al. (2020). Identification of a Repair-Supportive Mesenchymal Cell Population during Airway Epithelial Regeneration. Cell Reports *33*. https://doi.org/10.1016/j.celrep.2020.108549.

198. Buch, T., Heppner, F.L., Tertilt, C., Heinen, T.J.A.J., Kremer, M., Wunderlich, F.T., Jung, S., and Waisman, A. (2005). A Cre-inducible diphtheria toxin receptor mediates cell lineage ablation after toxin administration. Nat Methods *2*, 419–426. https://doi.org/10.1038/nmeth762.

199. Okuyama, M., Kayama, H., Atarashi, K., Saiga, H., Kimura, T., Waisman, A., Yamamoto, M., and Takeda, K. (2010). A novel *in vivo* inducible dendritic cell ablation model in mice. Biochemical and Biophysical Research Communications *397*, 559–563. https://doi.org/10.1016/j.bbrc.2010.05.157.

200. Hung, C.F., Chow, Y.-H., Liles, W.C., Altemeier, W.A., and Schnapp, L.M. (2017). Ablation of Pericyte-Like Cells in Lungs by Oropharyngeal Aspiration of

Diphtheria Toxin. Am J Respir Cell Mol Biol *56*, 160–167. https://doi.org/10.1165/rcmb.2016-0083MA.

201. Ruedl, C., and Jung, S. (2018). DTR-mediated conditional cell ablation—Progress and challenges. European Journal of Immunology *48*, 1114–1119. https://doi.org/10.1002/eji.201847527.

202. Kramann, R., Schneider, R.K., DiRocco, D.P., Machado, F., Fleig, S., Bondzie, P.A., Henderson, J.M., Ebert, B.L., and Humphreys, B.D. (2015). Perivascular Gli1+ Progenitors Are Key Contributors to Injury-Induced Organ Fibrosis. Cell Stem Cell *16*, 51–66. https://doi.org/10.1016/j.stem.2014.11.004.

203. Danopoulos, S., Bhattacharya, S., Mariani, T.J., and Alam, D.A. (2020). Transcriptional characterisation of human lung cells identifies novel mesenchymal lineage markers. European Respiratory Journal *55*. https://doi.org/10.1183/13993003.00746-2019.

204. Doherty, D.F., Roets, L., and Krasnodembskaya, A.D. (2023). The Role of Lung Resident Mesenchymal Stromal Cells in the Pathogenesis and Repair of Chronic Lung Disease. Stem Cells *41*, 431–443. https://doi.org/10.1093/stmcls/sxad014.

205. Hein, R.F.C., Wu, J.H., Holloway, E.M., Frum, T., Conchola, A.S., Tsai, Y.-H., Wu, A., Fine, A.S., Miller, A.J., Szenker-Ravi, E., et al. (2022). R-SPONDIN2+ mesenchymal cells form the bud tip progenitor niche during human lung development. Developmental Cell *57*, 1598-1614.e8. https://doi.org/10.1016/j.devcel.2022.05.010.

206. Nasri, A., Foisset, F., Ahmed, E., Lahmar, Z., Vachier, I., Jorgensen, C., Assou, S., Bourdin, A., and De Vos, J. (2021). Roles of Mesenchymal Cells in the Lung: From Lung Development to Chronic Obstructive Pulmonary Disease. Cells *10*, 3467. https://doi.org/10.3390/cells10123467.

207. Ojo, O., Lagan, A.L., Rajendran, V., Spanjer, A., Chen, L., Sohal, S.S., Heijink, I., Jones, R., Maarsingh, H., and Hackett, T.L. (2014). Pathological changes in the COPD lung mesenchyme – Novel lessons learned from *in vitro* and *in vivo* studies. Pulmonary Pharmacology & Therapeutics *29*, 121–128. https://doi.org/10.1016/j.pupt.2014.04.004.

208. Rangarajan, S., Bone, N.B., Zmijewska, A.A., Jiang, S., Park, D.W., Bernard, K., Locy, M.L., Ravi, S., Deshane, J., Mannon, R.B., et al. (2018). Metformin reverses established lung fibrosis in a bleomycin model. Nature Medicine *24*, 1121–1127. https://doi.org/10.1038/s41591-018-0087-6.

209. Li, Y., Jiang, D., Liang, J., Meltzer, E.B., Gray, A., Miura, R., Wogensen, L., Yamaguchi, Y., and Noble, P.W. (2011). Severe lung fibrosis requires an invasive fibroblast phenotype regulated by hyaluronan and CD44. Journal of Experimental Medicine *208*, 1459–1471. https://doi.org/10.1084/jem.20102510.

210. Samarelli, A.V., Tonelli, R., Heijink, I., Martin Medina, A., Marchioni, A., Bruzzi, G., Castaniere, I., Andrisani, D., Gozzi, F., Manicardi, L., et al. (2021).

Dissecting the Role of Mesenchymal Stem Cells in Idiopathic Pulmonary Fibrosis: Cause or Solution. Front. Pharmacol. *12*. https://doi.org/10.3389/fphar.2021.692551.

211. Ligresti, G., Raslan, A.A., Hong, J., Caporarello, N., Confalonieri, M., and Huang, S.K. (2023). Mesenchymal cells in the Lung: Evolving concepts and their role in fibrosis. Gene *859*, 147142. https://doi.org/10.1016/j.gene.2022.147142.

212. Kheirollahi, V., Wasnick, R.M., Biasin, V., Vazquez-Armendariz, A.I., Chu, X., Moiseenko, A., Weiss, A., Wilhelm, J., Zhang, J.-S., Kwapiszewska, G., et al. (2018). Metformin induces lipogenic differentiation in myofibroblasts to reverse mouse and human lung fibrosis. bioRxiv, 401265. https://doi.org/10.1101/401265.

213. Meyer, N.J., Gattinoni, L., and Calfee, C.S. (2021). Acute respiratory distress syndrome. The Lancet *398*, 622–637. https://doi.org/10.1016/S0140-6736(21)00439-6.

214. Bowdish, M.E., Barkauskas, C.E., Overbey, J.R., Gottlieb, R.L., Osman, K., Duggal, A., Marks, M.E., Hupf, J., Fernandes, E., Leshnower, B.G., et al. A Randomized Trial of Mesenchymal Stromal Cells for Moderate to Severe Acute Respiratory Distress Syndrome from COVID-19. Am J Respir Crit Care Med *207*, 261–270. https://doi.org/10.1164/rccm.202201-0157OC.

215. Jindal, K., Adil, M.T., Yamaguchi, N., Yang, X., Wang, H.C., Kamimoto, K., Rivera-Gonzalez, G.C., and Morris, S.A. (2024). Single-cell lineage capture across genomic modalities with CellTag-multi reveals fate-specific gene regulatory changes. Nat Biotechnol *42*, 946–959. https://doi.org/10.1038/s41587-023-01931-4.

216. Wang, H., He, L., Li, Y., Pu, W., Zhang, S., Han, X., Lui, K.O., and Zhou, B. (2022). Dual Cre and Dre recombinases mediate synchronized lineage tracing and cell subset ablation in vivo. J Biol Chem *298*, 101965. https://doi.org/10.1016/j.jbc.2022.101965.

217. Guo, W., Zhang, X., Li, L., Shao, P., Liang, C., Zhang, H., Liu, K., Wang, S., Peng, Y., Luo, J., et al. (2024). JAK/STAT signaling maintains an intermediate cell population during prostate basal cell fate determination. Nat Genet *56*, 2776–2789. https://doi.org/10.1038/s41588-024-01979-1.

218. Zhao, H., Liu, Z., Chen, H., Han, M., Zhang, M., Liu, K., Jin, H., Liu, X., Shi, M., Pu, W., et al. (2024). Identifying specific functional roles for senescence across cell types. Cell *187*, 7314-7334.e21. https://doi.org/10.1016/j.cell.2024.09.021.

219. Zhong, W., Zhang, X., Zeng, Y., Lin, D., and Wu, J. (2021). Recent applications and strategies in nanotechnology for lung diseases. Nano Res. *14*, 2067–2089. https://doi.org/10.1007/s12274-020-3180-3.

220. Shiraishi, K., Shah, P.P., Morley, M.P., Loebel, C., Santini, G.T., Katzen, J., Basil, M.C., Lin, S.M., Planer, J.D., Cantu, E., et al. (2023). Biophysical forces

mediated by respiration maintain lung alveolar epithelial cell fate. Cell *186*, 1478-1492.e15. https://doi.org/10.1016/j.cell.2023.02.010.

11.Acknowledgment

Reflecting on this transformative journey, I am profoundly moved by Will Durant's words, "*Education is a progressive discovery of our own ignorance*." This pursuit of knowledge has been a humbling odyssey, one that has continually revealed the vast, uncharted territories of what I have yet to understand. As I stand at the threshold of this milestone, I am acutely aware that it is not by my effort alone that I have arrived here. The unwavering support, wise guidance, and boundless encouragement of mentors, colleagues, and loved ones have illuminated my path. With deepest gratitude, I honor their invaluable contributions that have made this doctoral journey—and the completion of this thesis—not just possible, but profoundly meaningful.

First and foremost, I offer my deepest gratitude to my PhD supervisor, Prof. Elie El Agha, whose visionary guidance, unwavering support, and steadfast belief in my potential have been the foundation of this thesis. Your mentorship pushed me beyond limits, inspiring both my academic growth and passion for discovery. I am equally grateful to Prof. Saverio Bellusci and Prof. Victor J. Thannickal—Prof. Thannickal, though our time was brief, your profound influence reshaped my research philosophy, while Prof. Bellusci's kindness, generous time, and constant support have been pivotal in shaping me into a stronger scholar and person. Your collective wisdom and encouragement have left an indelible mark on my journey.

I sincerely thank Prof. Marek Bartkuhn for his generous time, expert guidance, and patient mentorship, which have deeply shaped my understanding of bioinformatics and empowered me to tackle complex datasets. I am also sincerely thankful to Hannah Hofmann and Kerstin Goth, whose invaluable technical support has been the backbone of this work. I also cherish the camaraderie and collaboration of my colleagues in the lab — the shared moments of brainstorming, problem-solving, and even the occasional setbacks have all enriched this journey, making it both rewarding and transformative. A special and heartfelt thank you goes to Dr. Irina Kuznetsova, whose kindness, wisdom, patience, and willingness to share her expertise have been a guiding light. As Maya Angelou beautifully put it, "*People will forget what you said, people will forget what you did, but people will never forget how you made them feel.*"

To my family, your love and support have been my foundation. Thank you for your endless encouragement and for always believing in me. This milestone would not have been possible without you. Your unwavering faith has given me the strength to persevere, even in the darkest of nights.

Finally, to all those who have contributed to this work, whether directly or indirectly, I extend my heartfelt thanks. This thesis is a testament to the collective effort and support of many individuals, and I am deeply grateful for each and every one of you.

Thank you!